MEDOW - Multi-terminal DC Grid for Offshore Wind, Final report

Cutululis, Nicolaos Antonio

Publication date:
2018

Document Version
Publisher's PDF, also known as Version of record

Multi-terminal DC Grid for Offshore Wind

MEDOW

Final report

Department of Wind Energy
E Report 2018

MEDOW
MULTI-TERMINAL DC GRID FOR OFFSHORE WIND

DTU Wind Energy
Department of Wind Energy

Authors: Nicolaos A. Cutululis (editor)

Title: Multi-Terminal DC Grid for Offshore Wind – Final ReportFinal report

8

Project no.:

317221

Sponsorship:

European Union

Pages: 138

Tables: 9

References: 191

Technical University of Denmark
Department of Wind Energy
Frederiksborgvej 399
Building 118
4000 Roskilde
Denmark
Telephone

niac@dtu.dk
www.vindenergi.dtu.dk

The research leading to these results received funding from the People Programme (Marie Curie Actions) of the European Union's Seventh Framework Programme FP7/2007-2013/ under REA grant agreement no. 317221, project title MEDOW.

Preface

The MEDOW consortium is made up of eleven partners, five universities and six industrial organisations that, between them, possess expertise on the manufacture, design, operation, and control of multi-terminal DC grids.

A DC grid based on multi-terminal voltage-source converter is a newly emerging technology, which is particularly suitable for the connection of offshore wind farms. Multi-terminal DC grids will be the key technology for the European offshore 'Super Grid'.

This project recruited twelve doctoral-level early-stage researchers (ESRs) and five postdoctoral experienced researchers (ERs). In addition to their individual scientific projects, all fellows benefited from interdisciplinary and intersectoral education, which included internships and secondments, a variety of training modules as well as transferable skills courses and active participation in workshops and conferences.

MEDOW offered a development path to researchers across Europe in the area of DC grids, in addition to fostering greater ties between industry and academia in this key development area.

The project also carried out a number of outreach activities which aimed to create awareness among the general public of the research work carried out by the project and its implications for citizens, as well as to introduce school and university students to science, research and innovation.

The project was co-ordinated by Cardiff University (UK).

Title: Multi-terminal DC Grid for Offshore Wind

EU programme: FP7-PEOPLE-2012-ITN

Contract type: Initial Training Network (ITN)

Grant Agreement number: 317221

Start date: 01 April 2013

End date: 31 March 2017

Contact: Professor Jun Liang, LiangJ1@cardiff.ac.uk

Roskilde, 2018

Nicolaos Antonio Cutululis

Content

1. Introduction 6

2. Connection of offshore wind power to DC grids 7

2.1 Optimal wind power transfer through DC grids- Marc Cheah 7

2.2 Control of multi-terminal VSC-HVDC systems for offshore wind power plant- 20

Muhammad Raza 20

2.3 Control and operation of wind power plants connected to DC grids- Kevin Schönleber 30

2.4 Coordinated control of wind power plants in offshore HVDC grids- Jayachandra N. Sakamuri 40

3. Investigation of voltage source converters for DC grids 51

3.1 Operation of DC grids with various types of voltage source converters- Jorge Gonçalves .. 51

3.2 Modular Multilevel Converters for power system applications- Abel Ferreira 63

4. Relaying protection 72

4.1 Distance protection of networks supplied from Multi-Terminal DC Grids- Mohammad Meraj Alam 72

4.2 Solid-state HVDC circuit breakers and fault clearing in multi-terminal HVDC grid- Ataollah Mokhberdoran 84

5. Interactive AC/DC grids 90

5.1 Investigation of impact between AC and DC grids– Alejandro Bayo Salas 90

5.2 Interaction of HVDC grids and AC power systems: operation and control– Robert H. Renner 102

5.3 Control of DC grids to improve stability of AC Grids- Tibin Joseph 115

5.4 Analysis and protection of HVDC systems subject to AC and DC faults– Gen Li 130

1. Introduction

A DC grid based on multi-terminal voltage-source converter is a newly emerging technology, which is particularly suitable for the connection of offshore wind farms. Multi-terminal DC grids will be the key technology for the European offshore 'Super Grid'.

In the project, DC power flow, DC relaying protection, steady state operation, dynamic stability, fault-ride through capability, and impacts of DC grids on the operation of AC grids and power market were studied. Systematic comparison of DC grid topologies and stability control strategies was carried out, and DC grids for offshore wind power transmission and onshore AC grid interconnection were investigated. Operation and control were evaluated using various simulation platforms and experimental test rigs. The outcomes of the project are expected to contribute to integrating offshore wind power into the onshore AC grids in European countries and for the European Super Grid.

The overall objective of the research was to find comprehensive solutions to the key techniques of DC grids for integrating renewable power, and to remove the barriers of the interconnection of AC and DC grids. There are 12 scientific objectives (O1~O12) under four research work packages (WP1~WP4):

WP1: Connection of offshore wind power to DC grids:
O1: Design and analyse the topologies of offshore DC grids
O2: Determine steady state operation characteristics
O3: Develop dynamic control systems for offshore DC grids

WP2: Investigation of voltage source converters for DC grids:
O4: Design and compare various voltage source converters
O5: Investigate power flow control in DC grid
O6: Develop tools for analysing and simulating converter stations

WP3: Relaying protection:
O7: Analyse DC grid faults
O8: Develop DC protection algorithms and post-fault restoration schemes
O9: Investigate AC protection with DC grids

WP4: Interactive AC/DC grids:
O10: Develop simulation and experimental platforms for the integrated DC/AC system.
O11: Investigate impact between AC and DC grids
O12: Validate integrated DC/AC systems using simulation and experimental platforms

The main results of the 12 ESRs trained in the MEDOW project are presented in this report. The report structure follows the project structure, with each following chapter presenting the results obtained within one of the work packages.

2. Connection of offshore wind power to DC grids

2.1 Optimal wind power transfer through DC grids- Marc Cheah

The first HVDC-connected Offshore Wind Power Plants (OWPPs) were built in Germany and are based on Point-to-point (P2P) links [1]. However, in other areas with planned long distance OWPPs, such as UK [2] or US [3], more complex topologies are proposed with offshore interconnection between OWPPs. The interconnection of OWPPs increases reliability, maximizes wind power transfer, addresses intermittency of wind and increases trading capability between countries. In [4] these advantages are presented and different designs are evaluated in terms of economic benefits. The increase of reliability with multi-terminal DC (MTDC) grids was studied in [5]–[7] and AC interconnections were analysed in [8]. Also, minimization of power losses in DC grids with offshore wind integration was addressed in [9]–[11].

In this study, topologies based on AC and DC interconnections between OWPPs are evaluated in terms of power losses minimization and reliability. Power losses of VSCs and AC and DC components are reduced with an optimal active and reactive power scheduling and an optimal voltage operation in the AC and DC offshore grids. Reliability is analysed with Capacity Outage Probability Tables (COPTs) to calculate the total availability of each topology. An example of a cost-benefit analysis with real wind speed data is used to evaluate the best interconnection topology. The additional interconnection investment is compared against the total operational energy savings from the power losses reduction and the increase of availability.

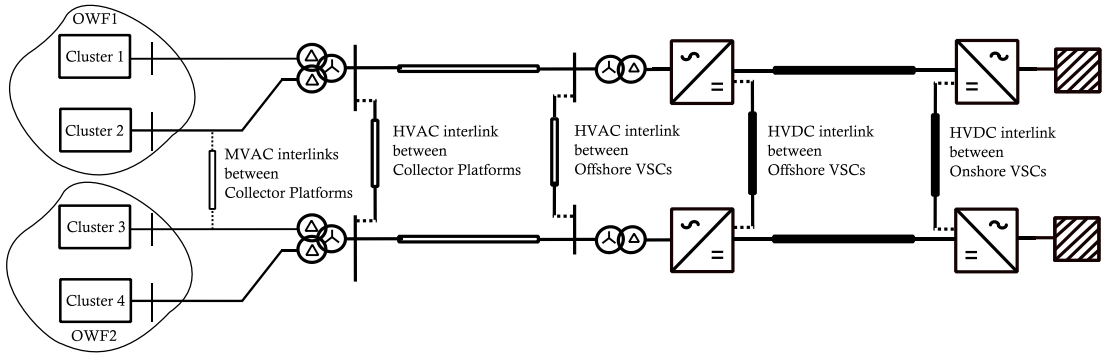

Figure 1: Interconnection options between OWPPs

2.1.1. Interconnection Options

Figure 1 shows the possible interconnections between two OWPPs. HVDC interlink between onshore VSCs is not considered because it is mainly used for energy trading between two countries or to increase the transmission capacity between two areas in the same country. MVAC interlinks between collector platforms are not analysed neither, because MVAC cables are less suitable as an alternative export route due to limitations in number of interlink cables, current rating and excessive power losses compared to equivalent HVAC cables. Therefore, the interconnection topologies analysed in this study are: (i) HVDC interlink between offshore VSCs, (ii) HVAC interlink between offshore VSCs and (iii) HVAC interlink between collector platforms.

2.1.1.1 Power Losses Analysis

An Optimal Power Flow (OPF) is used to minimize the power losses of each topology. The objective function includes the power losses of cables, transformers, HVDC converters and WT converters. The variables to optimize are the AC voltages and angles at the offshore HVDC converters, the DC voltages at the onshore HVDC converters, the active power schedule of the HVDC converters and the reactive power schedule of the offshore HVDC converters and the WT converters. The network equations and the current limits of converters, cables and transformers are the constraints for the OPF. The contribution that active power, reactive power, and voltages have on the total power losses reduction is analysed with additional constraints. Also, power losses are analysed in different operational points and interlink cable lengths.

2.1.1.2 Reliability Analysis

The total availability of each topology is calculated using a COPT-based risk model. This reliability model considers the failure rate and mean time to repair of AC and DC cables, AC and DC breakers, transformers, VSCs and VSC reactors. The general block diagram of the reliability model is shown in Figure 2, where the blocks S1 - S5 represent the equivalent reliability model of different elements. Figure 3 shows an example of a detailed reliability model for the topology with HVAC interconnector between offshore VSCs.

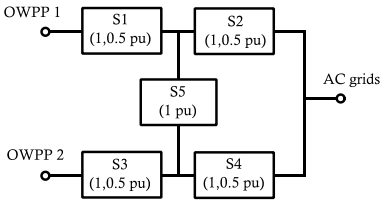

Figure 2: General reliability model for interconnected topologies

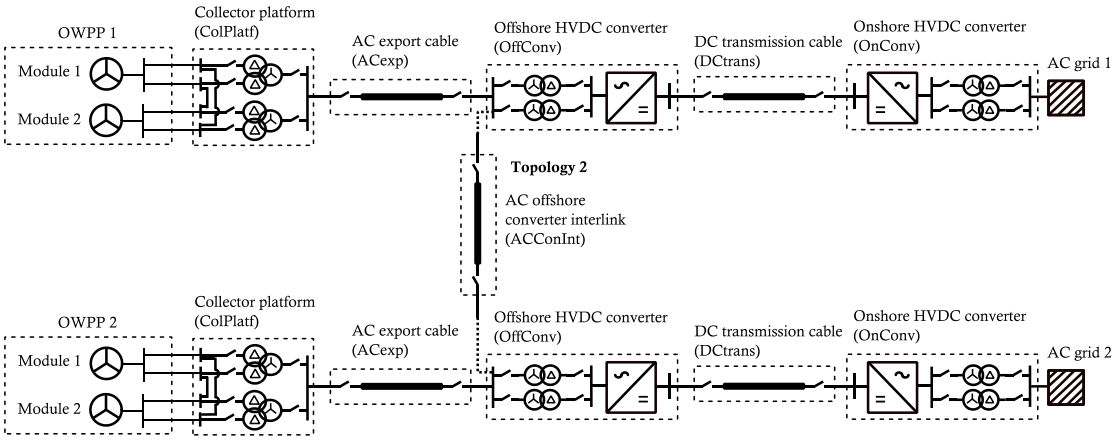

Figure 3: Detailed reliability model for topology with HVAC interlink

2.1.1.3 Cost-Benefit Analysis Results

An example of a cost-benefit analysis is used to evaluate the profit of the interconnector topologies. The two OWPPs have an identical configuration with a rated power equal to 492 MW. The wind generation is based on 1 year wind speed data from FINO 1 [12] and the effect that the distance between the OWPPs have on the wind speed is represented with the cross-correlation model in [13]. The energy cost of offshore wind is considered £120/ MWh [8] and the component costs are from the ETYS 2015 [14].

Table 1 shows the annual energy savings from the availability increase and power losses reduction when interconnectors are used. HVAC interlink between collector platforms provides the highest savings compared to the base case without interlink. However, the HVAC interlink between offshore HVDC converters shows similar results. It is observed that most of the savings are from the availability increase and power losses minimization represents only 10 % of the total savings. Table 2 shows the results of the cost-benefit analysis considering a standard discount rate of 6 % [8]. All the options have a positive NPV for a 25 years investment, but the lowest payback period is for the HVAC interlink between collector platforms.

Table 1: Annual average of undelivered energy and energy losses with their associated savings compared to the base case

	Base Case (no interlink)	**HVDC - Off. Platform**	**HVAC – Off. Platform**	**HVAC – Col. Platform**
Undelivered Energy (%)	1.4	1.1	0.68	0.63
Savings from availability increase (£M)	-	1.33	2.77	2.95
Energy losses (%)	5.79	5.75	5.72	5.71
Savings from power losses reduction (£M)	-	0.16	0.25	0.29

Table 2: Results of cost-benefit analysis

	HVDC - Off. Platform	**HVAC – Off. Platform**	**HVAC – Col. Platform**
Interconnector investment (£M)	28.26	10.78	10.78
Annual savings (£M)	1.49	3.02	3.24
Payback period (years)	10	5	4
Net Present Value for 25 years (£M)	8.29	27.86	30.57

2.1.1.4 Summary

This study compared three interconnection topologies between OWPPs: (i) HVDC interlink between offshore HVDC converters, (ii) HVAC interlink between offshore HVDC converters and (iii) HVAC interlink between

collector platforms. A power losses and reliability analysis were used to evaluate the benefits of the different interconnected options. HVAC interlink between collector platforms is the best option to reduce power losses and increase availability of the OWPPs. However, for long distances between OWPPs HVDC interlink is the only possible option due to an excessive increase of power losses and unavailability.

Optimal P schedule with interconnectors can provide a significant reduction in power losses compared to optimal Q schedule or voltage, if the power generations or the transmission system characteristics of the OWPPs are sufficiently different. The total availability is highly dependent on the wind generation level, the interlink capacity and the transmission capacity. Also, the DC cable availability has a significant contribution to the total availability. Therefore, the estimation of the total availability is highly dependent on the failure rate and mean time to repair values of the DC cable. A cost-benefit analysis is presented to compare the interconnection topologies based on the total savings from power losses reduction and availability increase. All topologies have a payback period equal or lower than 10 years.

2.1.2 Inertia Emulation in Offshore Wind Power Plants

2.1.2.1 Introduction

The inertial response or fast frequency response is responsible for containing the frequency during the first seconds after a power imbalance in an AC grid. A power system with low inertia will have a higher Rate of Change of Frequency (RoCoF) and require additional energy to contain the frequency within operational limits, than a power system with high inertia [15], [16]. This increase in the rate of change of frequency may result in unintended tripping of distributed generators with loss of mains relays. Also, the actions required to contain the frequency would need to take place more rapidly to avoid and excessive frequency reduction that could activate load shedding or even cause loss of synchronism.

Two methods are reported in the literature for provision of inertial response from Wind Turbines [17]–[20]. These are: (i) kinetic energy from WT rotating mass; and (ii) additional active power from WTs operating in deloaded condition. The advantage of using kinetic energy is that the WTs do not have to operate below maximum power extraction and the power is delivered more rapidly. Variable speed WTs are not sensitive to frequency variations in the grid and they do not provide natural inertial response as conventional synchronous generators. In addition, large OWPPs connected through HVDC decouple the offshore grid from the onshore grid. Supplementary controls can be implemented in the WT converters and the HVDC converters to emulate inertial response and release kinetic energy stored in the rotating mass of the WTs.

In this study, control strategies for inertia emulation in OWPPs are compared based on the options already presented in academia and industry. In general, two main options can be defined: Synthetic Inertia (SI) and Temporary Overproduction (TO). The two strategies are compared according to their implementation and MATLAB simulations, where the RoCoF and the maximum frequency deviation are evaluated. Also, a number of solutions are presented to limit the recovery power of the WTs after the kinetic energy has been released. A Hardware-in-the-Loop (HIL) experimental test is used to demonstrate Inertial Emulation with TO in a HVDC-connected OWPP.

2.1.2.2 Inertia Emulation Strategies

2.1.2.2.1 Synthetic Inertia

This strategy mimics the inertial response of conventional synchronous generators. Figure 4a shows the general implementation of SI, which is based on a PD controller. In summary, the following combinations for SI are found in the literature: (i) PD controller without washout filter [21]–[24], (ii) PD controller with washout filter [25], [26] and (iii) proportional controller with washout filter [26]–[28].

2.1.2.2.2 Temporary Overproduction

This strategy provides additional power for a specific period of time. The additional power is independent of the RoCoF, hence TO does not amplify noise of the frequency measurement. The additional power can be implemented as a step or a proportional function [29], [30]. In this study, the control scheme presented in Figure 4b is used to implement TO as a step function.

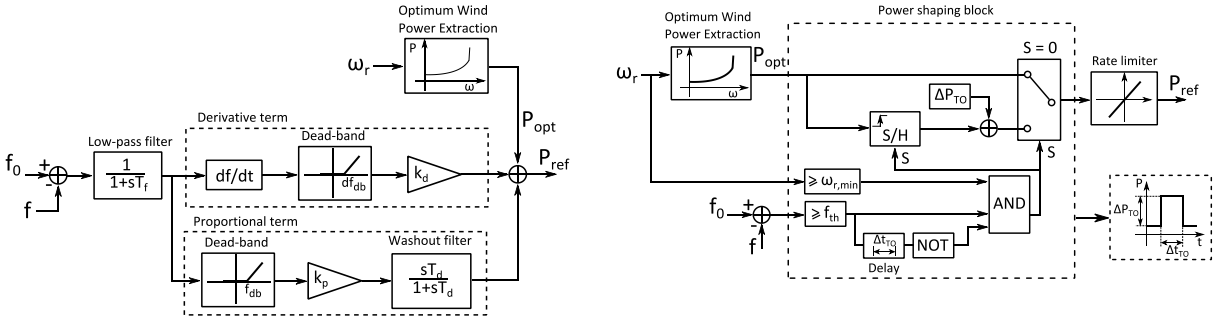

(a) Synthetic Inertia (b) Temporary Overproduction

Figure 4: Control scheme of Inertia Emulation strategies

2.1.2.3 Experimental Test Rig

Inertia Emulation from HVDC-connected OWPPs is tested in an experimental rig. The experiment considers an OWPP connected through a HVDC Point-to-point system. In [31] a similar experiment is presented for a MTDC system using the same experimental rig, but the test was focus on the coordinated control scheme of the MTDC grid. Figure 5 shows the general diagram of the hardware-in-the-loop (HIL) set-up. The main components are: WT test rig, VSC test rig, DC Network cabinet, real time simulator and grid simulator. The WT test rig, VSC test rig and DC Network cabinet represent scaled-down elements of a real system. The real time simulator represents a model of the onshore AC grid, which is interfaced to the VSC test rig with a grid simulator.

2.1.2.4 Results

IE of WTs is implemented as TO, based on the step function in Figure 4b. A communication-free control scheme using DC voltage as an intermediate signal artificially couples the offshore and onshore frequencies. Two different case studies are considered:

- TO: frequency support without reducing the impact of recovery period.
- TO-R: frequency support reducing the impact of recovery period. This is achieved limiting the recovery power at 2 % of pre-disturbance power.

Figure 6 shows the experimental results comparing TO and TO-R. The recovery power limitation reduces significantly the second frequency dip on the onshore frequency, as shown in Figure 6d. The onshore frequency variation is successfully transferred to the offshore grid as shown in the DC voltage (Figure 6b) and

offshore frequency (Figure 6c) results. The WT rotor speed initially decreases to release the kinetic energy from the rotational mass and recovers the initial value after the inertial response service has ended. The rotor speed recovery is slower in TO-R because the recovery power is limited.

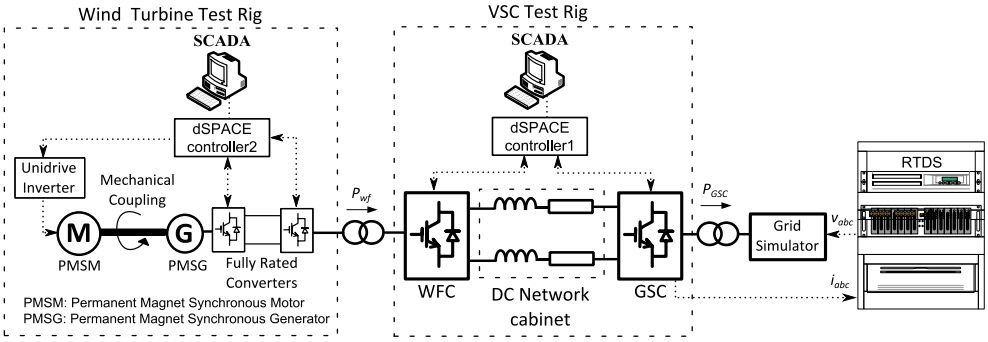

Figure 5: General diagram of the HIL set-up

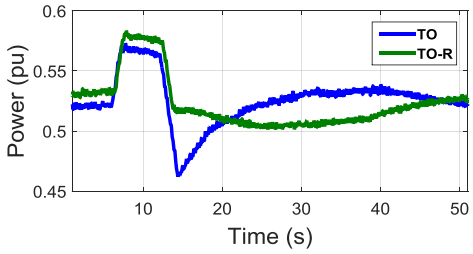

(a) Active power from WFC

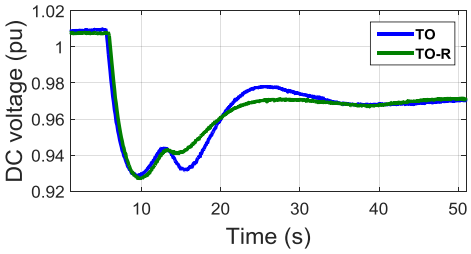

(b) DC voltage at WFC

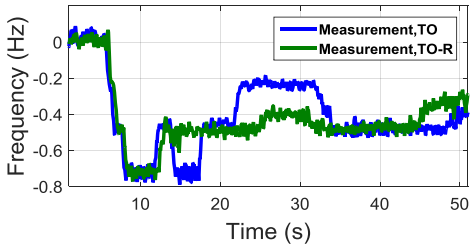

(c) Offshore frequency

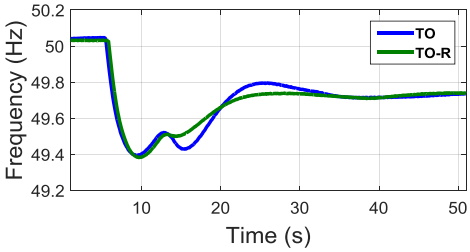

(d) Onshore frequency

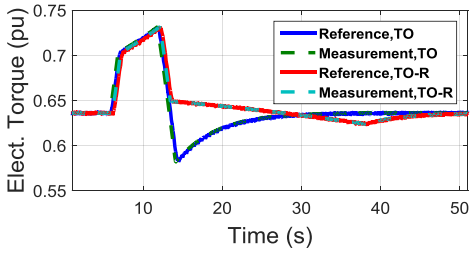

(e) WT electrical torque

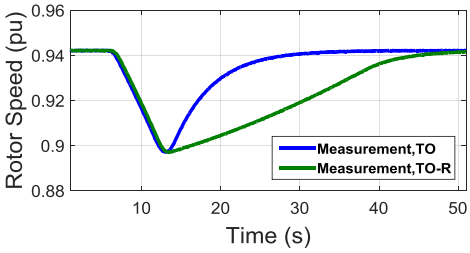

(f) WT rotor speed

Figure 6: Experimental results of Inertia Emulation using TO and comparing case without recovery period reduction (TO) and with reduction (TO-R).

2.1.2.5 Summary

This study analysed two main options for Inertia Emulation in OWPPs: Synthetic Inertia and Temporary Overproduction. SI strategies are based on different combinations of PD controllers and TO can be implemented with a step or proportional function. Considering the current system operator requirements for WT inertial response, the parameter tuning in TO is more convenient than in SI. Also, TO is more robust against frequency measurement noise than SI, but it provides a constant additional power independently of the frequency deviation, unless a proportional function is used. The PD and P controllers with washout filter and the TO can be tuned to have a similar performance in terms of RoCoF and maximum frequency deviation. The recovery power can generate a second frequency dip, which is especially important in TO. The impact of recovery power can be reduced if the recovery period is delayed or the recovery power is limited.

A HIL experimental test was used to demonstrate Inertia Emulation with TO in an OWPP connected through a HVDC point-to-point link. A communication-free strategy was chosen to couple artificially the onshore and offshore frequencies. Two case studies were compared to test the effectiveness of limiting the WT recovery power.

2.1.3 Electrical Resonance Stability in HVDC-connected Offshore Wind Power Plants

2.1.3.1 Introduction

Electrical interactions between offshore HVDC converter control and series resonances have been identified by CIGRE Working Groups B3.26 [32] and B4.55 [33] as potential causes of instability in HVDC-connected Offshore Wind Power Plants (OWPPs). In HVDC-connected OWPPs, the long export ac cables and the power transformers located on the offshore HVDC substation cause series resonances at a frequency range of 100 ~ 1000 Hz [32]–[34], i.e. at harmonic frequencies. Moreover, the offshore grid is a poorly damped system directly connected without a rotating mass or resistive loads [32], [35]. The typical control of an offshore HVDC converter [36] could further reduce the total damping at the resonant frequencies until the system becomes unstable.

This study analyses and discusses the impact that harmonic series resonances have on the voltage stability of HVDC-connected OWPPs. An impedance-based representation is used to identify resonances and to assess stability considering the effect of the offshore converters. The resonance stability of an OWPP is determined using an alternative approach to the positive-net-damping criterion [37]. This has been reformulated to evaluate the net-damping for electrical series resonances and to provide a clear relation between electrical resonances of the OWPP and stability. Analytical expressions of the harmonic series resonances are obtained and the total damping of the OWPP is used to characterize conditions of stability. The effect that the HVDC converter control parameters and the OWPP configuration have on stability is shown using examples.

2.1.3.2 Impedance-based Representation of an HVDC-connected OWPP

Figure 7a shows the configuration of an HVDC-connected OWPP. Figure 7b shows an impedance-based model of the HVDC-connected OWPP suitable for the analysis of electrical resonances and stability. The ac cables of the export and collector system are modelled as single π sections with lumped parameters and the transformers are modeled as RL equivalents. The VSCs are represented by equivalent circuits, which include

the frequency response of the controller. The offshore VSC is represented by a Thévenin equivalent as it controls the ac voltage of the offshore grid [36], [38]; however, Norton equivalents are used to represent the WT VSCs since they control current [38], [39].

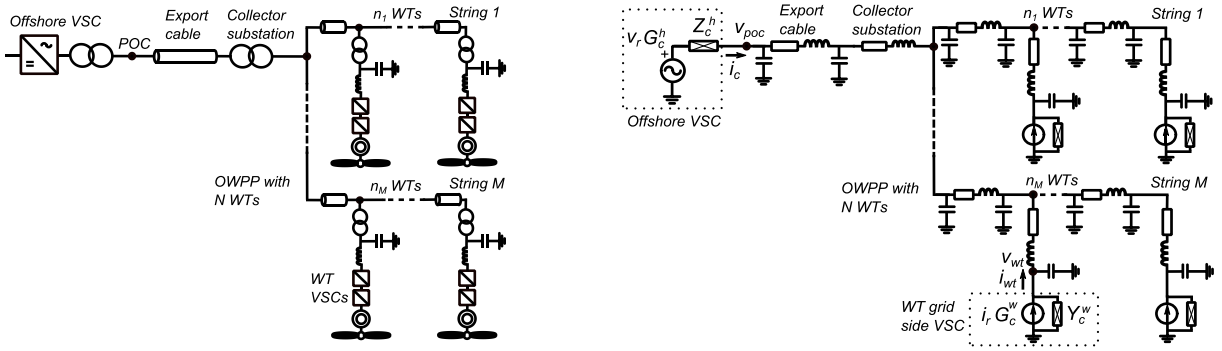

(a) General scheme (b) Impedance-based model

Figure 7: HVDC-connected OWPP

2.1.3.3 Stability Analysis

The stability analysis of the HVDC-connected OWPP is studied based on the following closed-loop transfer function in *s*-domain:

$$T(s) = \frac{1/Z_g(s)}{1+Z_c^h(s)/Z_g(s)} \quad \textbf{Equation 1}$$

where Z_g is the equivalent impedance of the offshore grid and Z_c is the HVDC converter impedance. Also, the equivalent impedance from the voltage source $\mathbf{v_r}G_c^h$ in Figure 7b is expressed as:

$$Z_{eq}^h = Z_c^h + Z_g \quad \textbf{Equation 2}$$

A variation to the positive-net-damping criterion given in [37], [40] is here employed to analyse system stability. The criterion has been reformulated to evaluate electrical resonance stability. Therefore, positive-net-damping criterion is defined as:

$$R_T(\omega_{res}) > R_g(\omega_{res}) + R_c^h(\omega_{res}) \quad \textbf{Equation 3}$$

where resistance R_T represents the total damping of the system, resistance R_c^h the HVDC converter damping and resistance R_g the offshore grid damping. From Equation 3 the offshore HVDC VSC is asymptotically stable if the total damping of the system, R_T, is positive in the neighbourhood of an electrical series resonance.

2.1.3.4 Results

The modified positive-net-damping criterion was applied to analyse the impact of electrical series resonances in the voltage stability of an HVDC-connected OWPP. The effects of the offshore HVDC converter control and the OWPP configuration are considered in the study. The system is analysed in no-load operation and when WTs are connected.

Figure 8 shows an example of an unstable case in no-load operation due to the ac voltage control of the offshore HVDC converter. The intersection between Z_c^h and Z_g approximately determines the series resonant frequency. When the system is unstable the resonant frequency is located in the negative-resistance region of Z_c^h, as shown in Figure 8a. Following the Nyquist criterion, the Nyquist curve encircles $(-1,0)$ in clockwise direction and the open loop system does not have unstable poles. Therefore, the system is unstable because the total number of zeros with positive real part is 1. In Figure 8c, the voltage at POC shows oscillations at 296 Hz due to the resonance instability identified in Figure 8a.

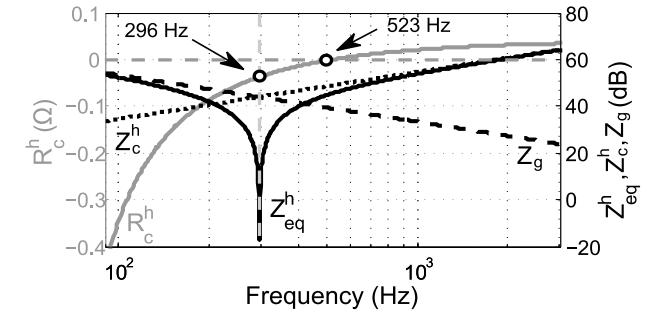

(a) Frequency response: $R_c^h, Z_{eq}^h, Z_c^h, Z_g$.

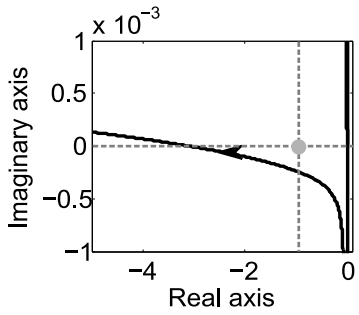

(b) Nyquist curve of Z_c^h/Z_g (only positive frequencies)

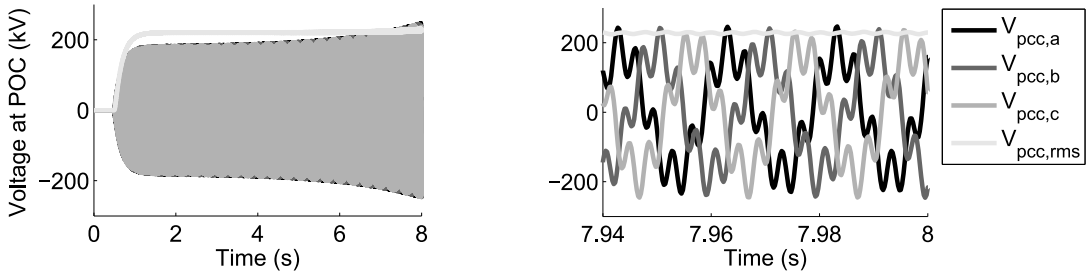

(c) Instantaneous and RMS voltages at POC. Step change is applied at 1 s.

Figure 8: Unstable example in no-load operation with PI gains of ac voltage control equal to $\boldsymbol{k_{p,v} = 0.01}$ and $\boldsymbol{k_{i,v} = 4.6}$ and export cable length equal to $\boldsymbol{l_{cb} = 10\ km}$

Figure 9 describes an example where the ac voltage control is designed to have a fast dynamic response (*e.g.* $k_{p,v} = 1$ and $k_{i,v} = 500$) and the number of WTs decreases from 80 to 24. When the number of WTs reduces to 24 the offshore converter becomes unstable since the resonance lies in the negative-resistance region, as shown in Figure 9a. Also, the Nyquist curve agrees with the positive-net-damping criterion as shown in Figure

9b. In Figure 9c the instantaneous voltages at POC show oscillations at 449 Hz when the number of WTs is reduced at 1 s; this is due to the resonance instability identified in Figure 9a.

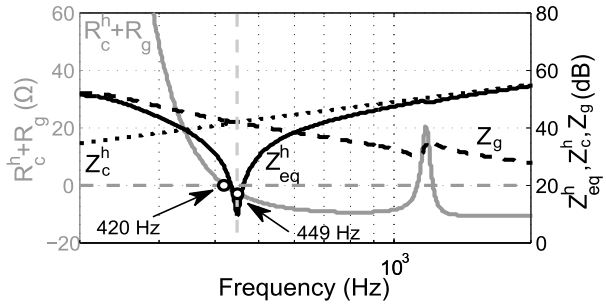

(a) Frequency response of $R_c^h + R_g, Z_{eq}^h, Z_c^h$ and Z_g.

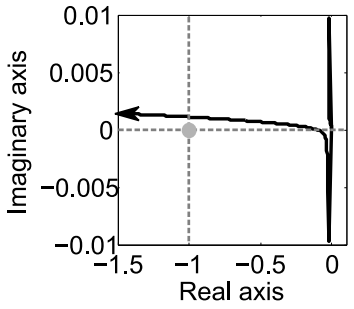

(b) Nyquist curve of Z_c^h/Z_g (only positive frequencies)

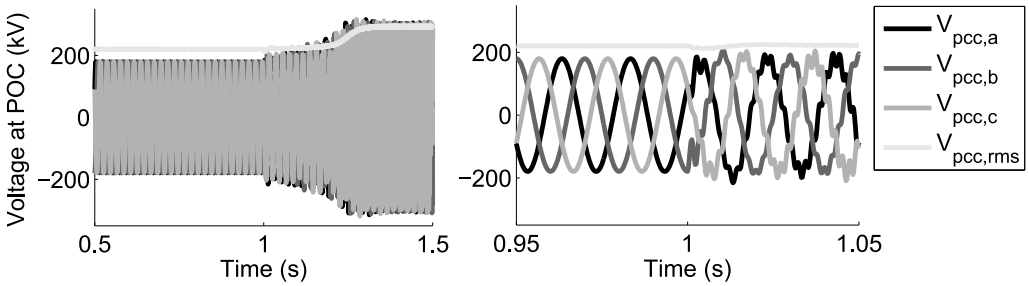

(c) Instantaneous and RMS voltages at POC when the number of WTs is reduced from 80 to 24 at 1 s.

Figure 9: Unstable example when 24 WTs are connected, $\boldsymbol{k_{p,v} = 1}$ and $\boldsymbol{k_{i,v} = 500}$.

2.1.3.5 Summary

This study described the impact of harmonic series resonances in the voltage stability of an HVDC-connected OWPP. The positive-net-damping criterion was reformulated to define the conditions of stability of an HVDC-connected OWPP as a function of the ac voltage control parameters of the HVDC converter and the configuration of the OWPP. The modified criterion was evaluated for electrical series resonances based on the phase margin condition. Expressions of the harmonic resonance were derived from simplified VSC and cable models.

As a result, the electrical resonance instabilities were analysed for different operational conditions. In no-load operation the risk of detrimental resonance interaction increases, because the resonance has poor damping and is located at the lowest frequency. The connection of WTs moves the resonance to higher frequencies and increases the total damping. If the HVDC converter control is designed to have a fast dynamic response, the converter reduces the total damping at the resonance frequency.

2.1.4 References

[1] TenneT, “About offshore projects Germany.” [Online]. Available: http://www.tennet.eu/our-grid/offshore-projects-germany/about-offshore-projects-in-germany/. [Accessed: 12-Sep-2016].

[2] National Grid, “Offshore Development Information Statement 2010,” 2010.

[3] J. Lin, “Integrating the First HVDC-Based Offshore Wind Power into PJM System—A Real Project Case Study,” *IEEE Trans. Ind. Appl.*, vol. 52, no. 3, pp. 1970–1978, May 2016.

[4] J. De Decker and P. Kreutzkamp, “Offshore Electricity Grid Infrastructure in Europe,” 2011.

[5] S. Wang, J. Liang, and J. Ekanayake, “Optimised topology design and comparison for offshore transmission,” in *2012 47th International Universities Power Engineering Conference (UPEC)*, 2012, pp. 1–6.

[6] C. MacIver, K. R. W. Bell, and D. P. Nedic, “A Reliability Evaluation of Offshore HVDC Grid Configuration Options,” *IEEE Trans. Power Deliv.*, vol. 31, no. 2, pp. 810–819, Apr. 2016.

[7] A. Beddard and M. Barnes, “Availability analysis of VSC-HVDC schemes for offshore windfarms,” in *6th IET International Conference on Power Electronics, Machines and Drives (PEMD 2012)*, 2012, pp. E13–E13.

[8] K. Nieradzinska, C. MacIver, S. Gill, G. A. Agnew, O. Anaya-Lara, and K. R. W. Bell, “Optioneering analysis for connecting Dogger Bank offshore wind farms to the GB electricity network,” *Renew. Energy*, vol. 91, pp. 120–129, Jun. 2016.

[9] M. Aragüés-Peñalba, A. Egea-Àlvarez, S. G. Arellano, and O. Gomis-Bellmunt, “Droop control for loss minimization in HVDC multi-terminal transmission systems for large offshore wind farms,” *Electr. Power Syst. Res.*, vol. 112, pp. 48–55, Jul. 2014.

[10] J. Cao, W. Du, H. F. Wang, and S. Q. Bu, “Minimization of Transmission Loss in Meshed AC/DC Grids With VSC-MTDC Networks,” *IEEE Trans. Power Syst.*, vol. 28, no. 3, pp. 3047–3055, Aug. 2013.

[11] A. Abdel-Khalik, “Optimum power transmission-based droop control design for multi-terminal HVDC of offshore wind farms,” *IEEE Trans. Power Deliv.*, vol. 28, no. 3, pp. 3401–3409, 2013.

[12] Bundesamt fuer Seeschifffahrt und Hydrographie, “FINO1 - Forschungsplattformen in Nord- und Ostsee Nr. 1.” [Online]. Available: http://www.fino1.de/en/. [Accessed: 12-Sep-2016].

[13] G. Giebel, “On the Benefits of Distributed Generation of Wind Energy in Europe,” Universität Oldenburg, 2000.

[14] National Grid, “Electricity Ten Year Statement 2015 - Appendix E,” 2015.

[15] National Grid, “System Operability Framework 2015,” no. November, p. 34, 2015.

[16] P. Tielens and D. Van Hertem, “The relevance of inertia in power systems,” *Renew. Sustain. Energy Rev.*, vol. 55, pp. 999–1009, Mar. 2016.

[17] K. V. Vidyanandan and N. Senroy, “Primary frequency regulation by deloaded wind turbines using variable droop,” *IEEE Trans. Power Syst.*, vol. 28, no. 2, pp. 837–846, May 2013.

[18] P. Tielens, M. Reza, A. Marinopoulos, and J. Driesen, “Frequency support by wind power plants in isolated grids with varying generation mix,” in *2012 IEEE Power and Energy Society General Meeting*, 2012, pp. 1–8.

[19] J. F. Conroy and R. Watson, “Frequency Response Capability of Full Converter Wind Turbine Generators in Comparison to Conventional Generation,” *IEEE Trans. Power Syst.*, vol. 23, no. 2, pp. 649–656, May 2008.

[20] H. Ye, W. Pei, and Z. Qi, “Analytical Modeling of Inertial and Droop Responses From a Wind Farm for

Short-Term Frequency Regulation in Power Systems," *IEEE Trans. Power Syst.*, pp. 1–10, 2015.

[21] G. Ramtharan, N. Jenkins, and J. Ekanayake, "Frequency support from doubly fed induction generator wind turbines," *IET Renew. Power Gener.*, pp. 3–9, 2007.

[22] I. Moore, "Inertial Response from Wind Turbines," Cardiff University, 2012.

[23] J. Licari and J. Ekanayake, "Coordinated inertia response from permanent magnet synchronous generator (PMSG) based wind farms," *J. Natl. Sci. Found. Sri Lanka*, vol. 43, no. 4, 2015.

[24] F. Hafiz and A. Abdennour, "Optimal use of kinetic energy for the inertial support from variable speed wind turbines," *Renew. Energy*, vol. 80, pp. 629–643, 2015.

[25] J. Morren and S. De Haan, "Ridethrough of wind turbines with doubly-fed induction generator during a voltage dip," *Energy conversion, ieee …*, vol. 20, no. 2, pp. 435–441, 2005.

[26] J. Van de Vyver, J. D. M. De Kooning, B. Meersman, L. Vandevelde, and T. L. Vandoorn, "Droop Control as an Alternative Inertial Response Strategy for the Synthetic Inertia on Wind Turbines," *IEEE Trans. Power Syst.*, vol. PP, no. 99, pp. 1–10, 2015.

[27] K. Clark, N. W. Miller, and J. J. Sanchez-Gasca, "Modeling of GE wind turbine-generators for grid studies," 2010.

[28] L. Ruttledge and D. Flynn, "Emulated Inertial Response From Wind Turbines: Gain Scheduling and Resource Coordination," *IEEE Trans. Power Syst.*, vol. 31, no. 5, pp. 3747–3755, Sep. 2016.

[29] J. Brisebois and N. Aubut, "Wind farm inertia emulation to fulfill Hydro-Québec's specific need," in *2011 IEEE Power and Energy Society General Meeting*, 2011, pp. 1–7.

[30] M. Asmine and C.-É. Langlois, "Field measurements for the assessment of inertial response for wind power plants based on Hydro-Québec TransÉnergie requirements," *IET Renew. Power Gener.*, vol. 10, no. 1, pp. 25–32, Jan. 2016.

[31] O. Daniel Adeuyi, "Grid Connection of Offshore Wind Farms through Multi-Terminal High Voltage Direct Current Networks," Cardiff Univeristy, 2016.

[32] Working Group B3.36, "Special Considerations for AC Collector Systems and Substations Associated with HVDC - Connected Wind Power Plants," 2015.

[33] Working Group B4.55, "HVDC Connection of Offshore Wind Power Plants," 2015.

[34] M. Bradt, B. Badrzadeh, E. Camm, D. Mueller, J. Schoene, T. Siebert, T. Smith, M. Starke, and R. Walling, "Harmonics and resonance issues in wind power plants," in *2011 IEEE Power and Energy Society General Meeting*, 2011, pp. 1–8.

[35] C. Buchhagen, C. Rauscher, A. Menze, and J. Jung, "BorWin1 - First Experiences with harmonic interactions in converter dominated grids," in *International ETG Congress 2015; Die Energiewende - Blueprints for the new energy age*, 2015, pp. 1–7.

[36] H. Liu and J. Sun, "Voltage Stability and Control of Offshore Wind Farms With AC Collection and HVDC Transmission," *IEEE J. Emerg. Sel. Top. Power Electron.*, vol. 2, no. 4, pp. 1181–1189, Dec. 2014.

[37] L. Harnefors, "Proof and Application of the Positive-Net-Damping Stability Criterion," *IEEE Trans. Power Syst.*, vol. 26, no. 1, pp. 481–482, Feb. 2011.

[38] X. Wang, F. Blaabjerg, and W. Wu, "Modeling and Analysis of Harmonic Stability in an AC Power-Electronics-Based Power System," *IEEE Trans. Power Electron.*, vol. 29, no. 12, pp. 6421–6432, Dec. 2014.

[39] L. Harnefors, M. Bongiorno, and S. Lundberg, "Input-Admittance Calculation and Shaping for Controlled Voltage-Source Converters," *IEEE Trans. Ind. Electron.*, vol. 54, no. 6, pp. 3323–3334, Dec. 2007.

[40] G. Stamatiou and M. Bongiorno, “Stability Analysis of Two-Terminal VSC-HVDC Systems using the Net-Damping Criterion,” *IEEE Trans. Power Deliv.*, pp. 1–1, 2016.

2.2 Control of multi-terminal VSC-HVDC systems for offshore wind power plant- Muhammad Raza

2.2.1 Introduction

In first half of the year 2016, offshore wind power plants with the combine capacity of 511 MW were installed in European seas. In 2016, it is expected to connect offshore energy of total capacity of 4.2 GW with the grid when under construction wind power plants will be fully commissioned. The statistic shows the ambition of EU states to achieve the threshold of 40 GW of offshore wind power by the end of 2020. In order to manage the enormous amount of offshore energy into the grid, the European Wind Energy Association (EWEA) proposed a 20 year offshore network development master plan which provides gradual approach to plan offshore grid in the North and Baltic Seas. The proposed transnational offshore grid will provide benefit to European countries such as access to offshore wind energy, enhance the ability to trade electricity, and smooth the wind energy variability on the markets.

Most of the wind power plants currently installed in the North Sea are close to shore. Wind turbines will move into deeper water and further from the shore as the technology grows. Existing operational wind power plants are built not further than 20 km from the shore and not more than 20 m deep, but in future it will be installed at the distance greater than 60 km and in depth more than 60 m. Most of the offshore wind power plants are connected with the onshore grid via AC cable. This is suitable for short distances and low power transmission, but with the increase in distance, submarine AC cable generates higher capacitive reactive power which limit the active power flow capability of the cable. The use of high voltage direct current (HVDC) technology is essential for the offshore grid to overcome the AC cable limitation. However, the cost of the HVDC converter station is higher than AC substation but the cost of DC cables is lower than AC cables. Further, the HVDC converter station have higher losses, but lower losses per km than AC system. Thus, there is a trade off in the use of DC versus AC transmission system. Based on the length verse power constraints, it can be proposed that the offshore nodes must be located near wind power plant cluster to minimize the number of nodes per country, but wind power plant near coast must be directly connected with AC cable to onshore grid. The principle of the future offshore transmission network will depend on three basic components.

- Lines/Branches: Transmission capacity is limited by submarine cable characteristics
- Offshore nodes: The offshore platform will serve as a common connection point for different offshore wind power plants as well as interconnector between TSOs
- Onshore nodes: It is the connection points between offshore and onshore electrical network

There are two basic types of HVDC transmission links i.e. line commutated converter (LCC) and voltage source converter (VSC) HVDC transmission system. The LCC-HVDC transmission system widely used at voltage of up to 800 kV operating over 6 GW per line. However, LCC-HVDC have some disadvantages compare to VSC-HVDC such as inability to connect to weak grid, and complex switching system for bi-directional operation. The VSC-HVDC transmission is considered to be a favorable system for offshore grid due to it distinguish feature such as compact size, modular development of the system, ability to provide dynamic voltage support to AC voltage hereby can be used for black start, and simple power reversal principle which based on current direction. Furthermore, the multi-terminal application of VSC-HVDC transmission system enables the development of meshed DC grids. A HVDC transmission system based on VSC exists mostly in point-to-point configuration, and the research on multi-terminal DC node is in early stages. Although most of the VSC technology already exist in principle, but there are several technical aspects of VSC HVDC transmission which

requires to be addressed such as the forming of the offshore AC grid and its control, the short-circuit control of the wind turbines and the VSCs connected with offshore AC hub, an MTDC system, integration of offshore AC grid with offshore DC grid, power distribution, offshore grid codes, etc. Thus, the aim of the research was to:

"Design and develop the control system of voltage source converter (VSC) for high voltage direct current (HVDC) transmission systems to interconnect offshore wind power plants in multi-terminal grid configuration".

Different scenarios to interconnect wind power plants, offshore nodes and onshore nodes are demonstrated in Figure 10. Such an offshore grid can act as a mediator among several wind power plants and different countries grids. The offshore wind power plants cluster/hub close to shore are connected with AC cable to shore and neighbour countries via HVDC cable. Offshore node is a substation that is formulated by connecting several wind power plant at a common point that are at short distance with each other. If distance between hub to hub or hub to onshore substation is greater than 60 km then they are connected via HVDC transmission system. This report will highlight the possible control schemes and its characteristics for such an integrated offshore grid.

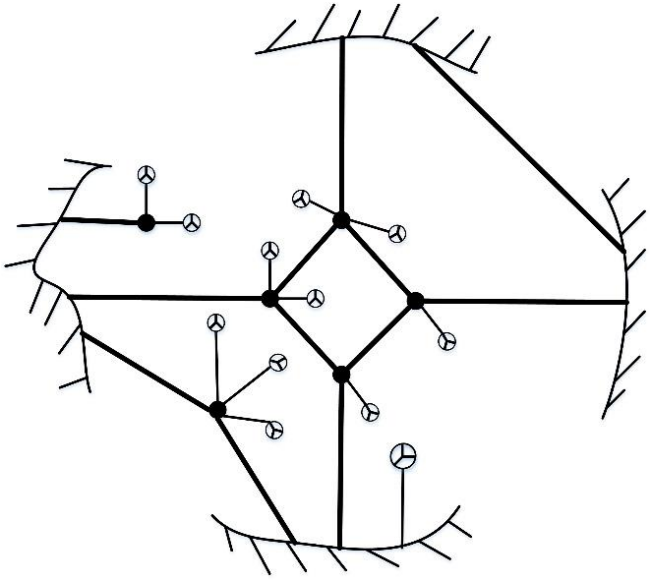

Figure 10: Mesh offshore grid: different scenarios of interconnecting offshore wind farms, offshore substation, and onshore substation.

2.2.2 Offshore Grid Concepts

The future offshore mesh grid can be realized as shown in Figure 11. There are two sets of VSCs converter in the system. First, the offshore converter that are linking offshore AC system to DC system and secondly, the onshore converters that are linking the DC network with the onshore AC network. The offshore converters have responsibility to form the offshore grid which means it must energized the network and impose the frequency on the network. The onshore converters requires to balance the power in the DC network. The onshore converters are synchronized with the grid frequency and injects available DC power.

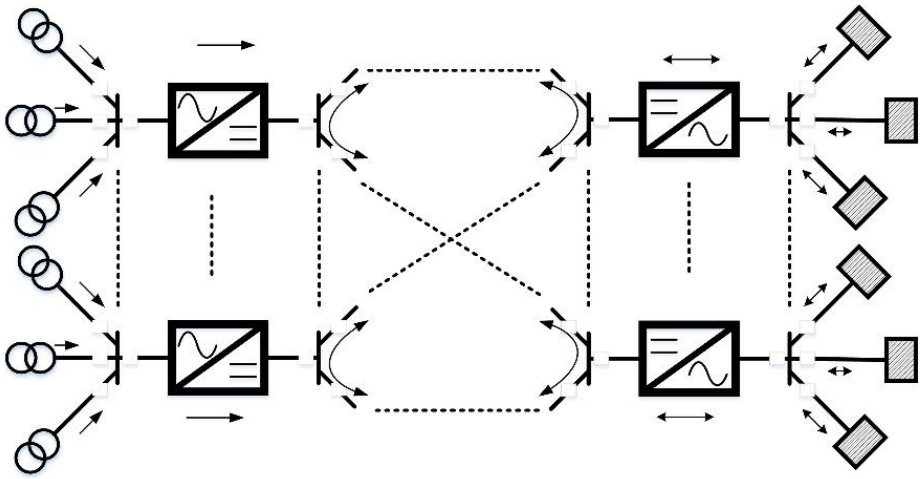

Figure 11: Mesh AC/DC Offshore grid.

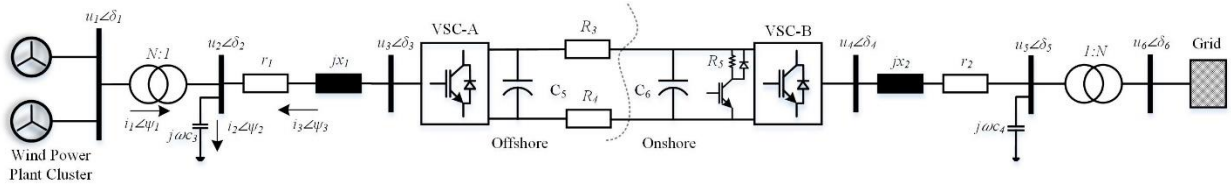

Figure 12: Offshore farms integration with onshore grid using VSC-HVDC transmission system in point-to-point configuration.

The basic transmission configuration of a VSC-HVDC system to interconnect offshore wind farm with the onshore grid is a point-to-point configuration as illustrated in Figure 12. In such configuration, the capacity of the wind power generation is equal to the capacity of the VSC and connected to only one onshore grid. The protection schemes is based on the conventional method i.e. AC circuit breaker on AC network, and DC chopper installed at onshore substation for DC fault. This configuration is limited from the prospective of trade and the size of the wind farm is limited up to VSC capacity [41], [43].

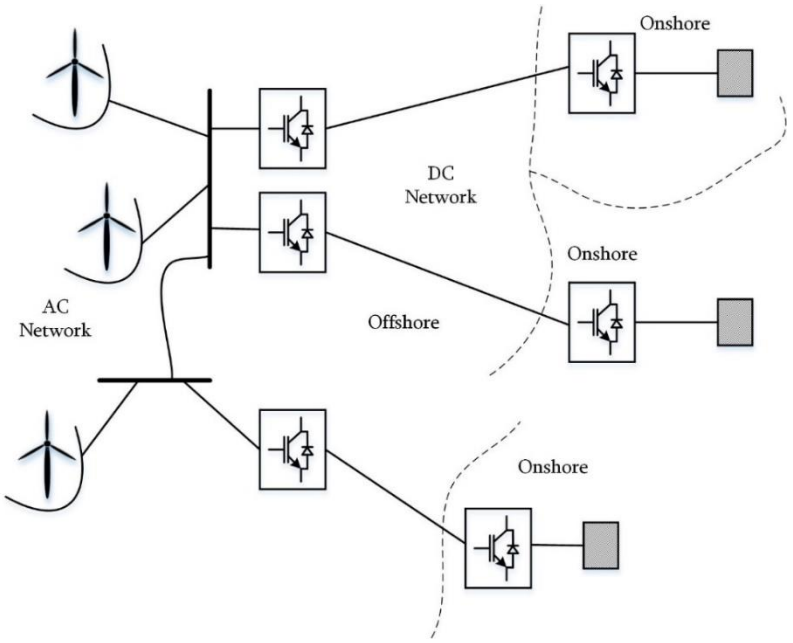

Figure 13: Offshore AC network interconnected with multiple onshore grids using VSC-HVDC transmission system.

The concept of point-to-point VSC-HVDC transmission system can be extended for the development of an offshore grid. An example of an offshore is illustrated in Figure 13, in which three wind farms are connected with three onshore grids [42]. The DC connection is in point-to-point configuration therefore it does not required addition protection schemes. Offshore AC network is controlled via more than one VSC system. The VSC systems act as the slack sources in the network hereby provides redundancy for continues operation in case of failure in one transmission system. The power in the offshore AC network is now balanced by multiple VSC. The offshore network usually contain only static devices and does not have any inertia. Nowadays, most of the wind farms contains synchronous machine with fully rated converters hereby isolate the offshore network from the wind turbine inertia. The disadvantage of not having inertia in the system is the link between frequency and the network power which does not exists, and the power balancing and sharing must be achieved via communication among VSC systems which requires extra communication cables and introduce delays in the control schemes [47]. With the application of frequency and voltage droop scheme, the communication signal can be avoided and power can be share via only local measurements. The frequency and voltage droop equations are Equation 4 and Equation 5.

$$\omega_{ref} = \omega_0 - k_f(P - P_0) \quad \textbf{Equation 4}$$

$$u_{ref} = u_0 + k_u Q \quad \textbf{Equation 5}$$

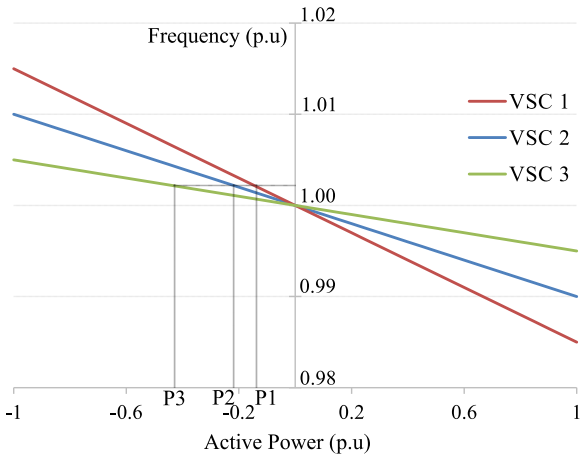

Figure 14: Frequency droop with different gains and same active power set-points

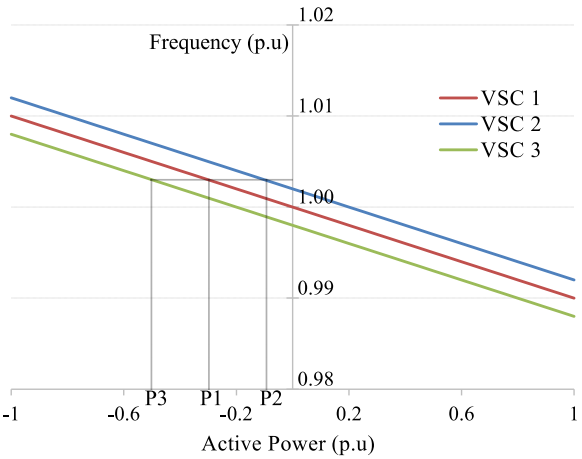

Figure 15: Frequency droop scheme having same slope but different active power set-points

The different principle of power sharing between VSCs using frequency droop scheme are illustrated in Figure 14 and Figure 15. There are two strategy to share the active power, firstly sharing by assigning different droop gains, and secondly by assigning different active power set-points. In first strategy, the active power flow direction through all VSCs would be same at all wind power in-feed however the rate of change of imposed frequencies by each VSCs would be different as illustrated in Figure 16. In a stable system, imposed frequencies by each VSCs will converge to the same equilibrium point however their dynamic behaviour would be significantly varies from each other. The main advantage of this schemes is that the active power will not be exchanged from one VSC to another with the wind energy variation. This can be observed from Figure 17. The VSCs transfer energy to onshore only that is generated by the wind farms [44], [46].

In the second strategy, active power is shared by assigning different active power set-points and having same droop gains in all VSCs. The frequency and active power response is illustrated in Figure 18 and Figure 19. It can be observed that the transient response in the frequencies of VSCs are almost identical and possess high damping compare to previous strategy. However, it can be notices from the active power response that at no wind power infeed energy is transferred from one VSCs to another. This can be regarded as an energy trade between two onshore grids via offshore AC network, but it has lower efficiency and unnecessary active power loss that occurs in the offshore converters. It is preferable to use multi-terminal DC network instead for energy transfer between onshore grids. The advantage of having offshore AC network is that the offshore hub capacity can be higher than the power capacity of one VSC-HVDC transmission system and larger wind farms can be installed.

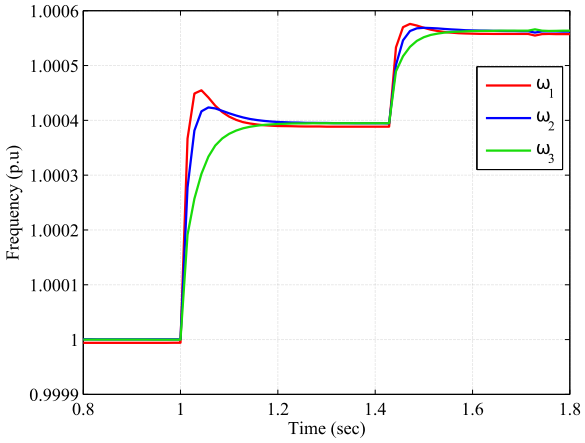

Figure 16: Frequency response at different gains

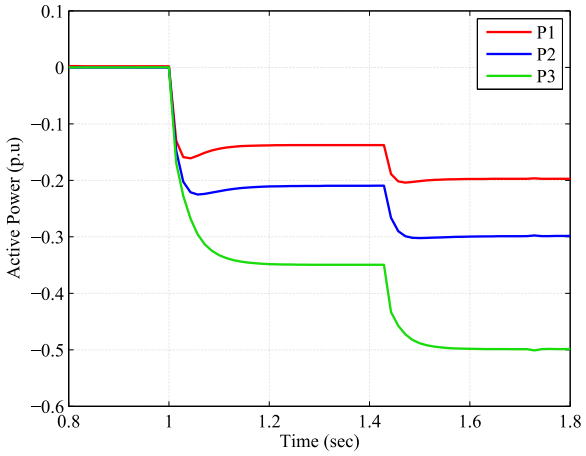

Figure 17: Active power sharing at different droop gains

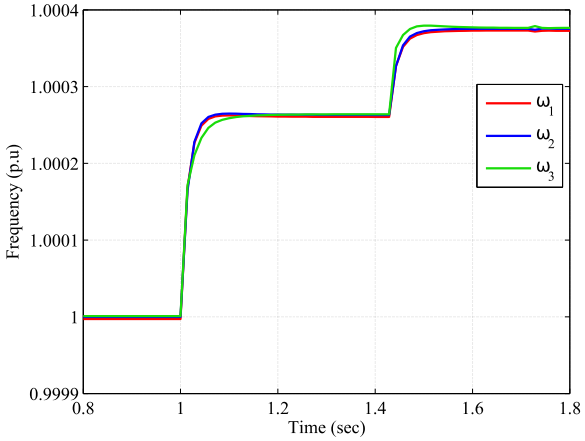

Figure 18: Frequency response at different active power set-points

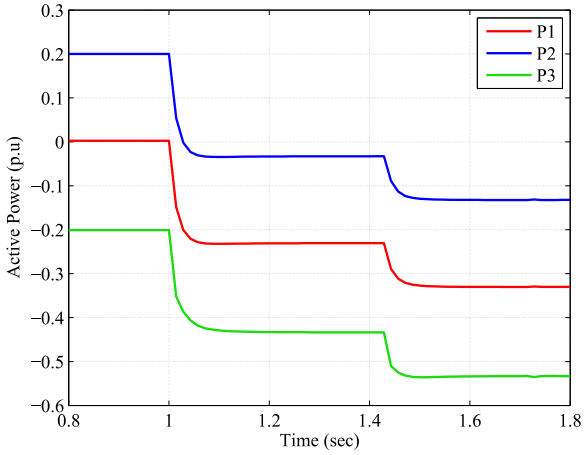

Figure 19: Active power sharing using set-points

For an offshore AC network, it is important to have frequency coordination and active power reduction schemes in the wind generation system in case failure of one transmission system [48]. Furthermore, the reactive power sharing between VSCs in the offshore is achieved by assigning appropriate voltage droop gains. Since, the VSCs are controlling different busbars in the network and the reference voltages applied by the VSCs do not converge at the same equilibrium points thus there is no significant difference between reactive power sharing via droop gains or reactive power set-points. The application of voltage droop requires addition voltage stability criteria in order to control the reactive power sharing as well as to keep the network long term voltage stability [46]. In addition, the voltage droop schemes enables additional degree of control on the reactive power management in the offshore AC network which improves the losses in the network [45], [49]. Whereas traditionally, it was mainly achieved by wind turbines reactive power set-points.

A multi-terminal VSC-HVDC transmission system is preferable in order to enhance the trade between different countries for long distances. A configuration of MTDC transmission is illustrated in Figure 20. The offshore DC hub is suitable if the wind farms are located far from each other. Different configuration can be employed such

as radial, radial-ring, star, meshed etc. However, the complexity in the DC system varies according to the DC fault protection scheme.

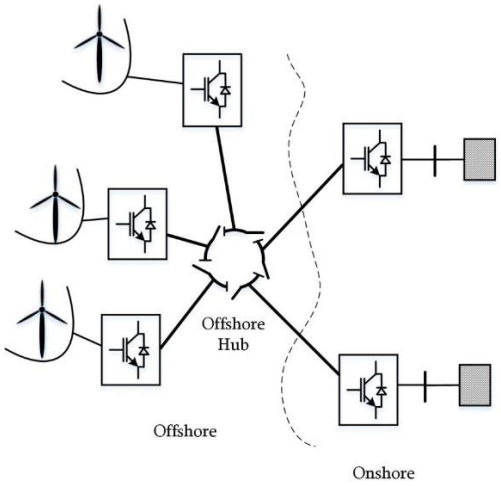

Figure 20: Multi-Terminal VSC-HVDC transmission system configuration.

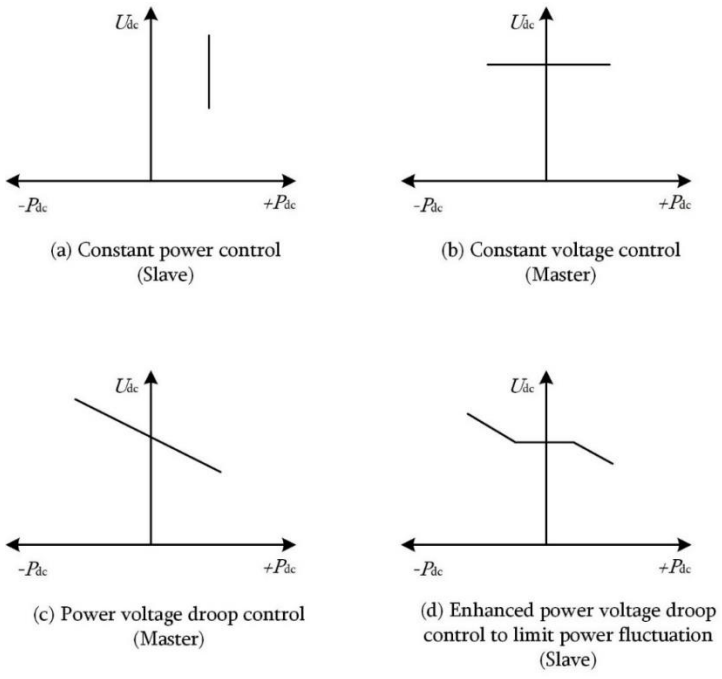

Figure 21: Control scheme for MT-VSC-HVDC transmission systems

The DC voltage in the MTDC system is controlled by onshore converters. The control principle for onshore side converter is illustrated in Figure 21. The most common control scheme is the Master-Slave principle in which one offshore converter control the DC voltage called as Master converter, and the remaining offshore

converters are operated in constant power control known as Slave converters. In such control principle, a communication signal is required among onshore converters in case of failure in master converter. In such case, one of the slave converter has to be operated as master converter in order to continue the operation. Master-slave control method inherent power flow limitation that is only one converter is balancing the power in the DC network, this means that theoretically the capacity of the master converter should be equal or greater than the sum of all the slave converters.

An alternative method of power sharing is the droop control, in which all the converters collaborate to balance the power according to the sharing factor. The droop principle is illustrated in Figure 21c. In case of imbalance in power, the controllers adjust the injection in a proportional manner. Converter adjust the deviation according to their droop gains and control the individual converter contribution in the power balancing. The droop control provides the slack source redundancy in the network, however, the power fluctuation in-feed in the onshore grid is proportional to the wind variation.

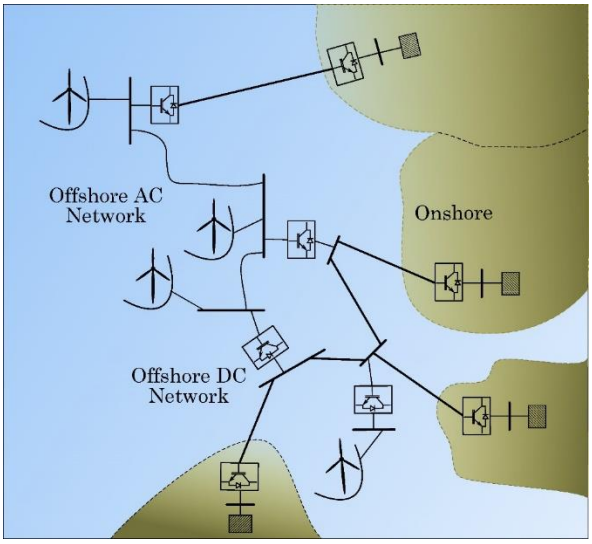

Figure 22: Combine solution of offshore AC network and MTDC transmission system.

The power fluctuation can be reduced by enhancing the droop principle as illustrated in Figure 21d. In this scheme, one onshore converter is designated as master converter controlling solely DC voltage and other onshore converters are operating in constant power control mode within the DC voltage limits. As soon as these DC voltage limits violated, converters start operating with the principle of droop to balance the voltage.

A combine solution of an offshore AC network and offshore DC hub can be introduced as illustrated in Figure 22 to utilize the characteristic of both configurations. Such configuration can enhance the trade between countries as well as provide better integration of offshore wind farms located far from onshore grids.

2.2.3 Summary

The objective of this research was to derive information and recommendations for future wind power plant projects. The results could be useful for developers, planners and operators, as well as to national and European authorities. The analysis in this research will allow assessing:

- Information and recommendations for future wind power plant projects.
- Beneficial for pre-project planning and realization of offshore wind power plants.
- Assessing the consequences and solutions for the offshore electrical power system with respect to voltage control, reactive power and transient behaviour.
- Proposed scenarios for calculation opportunities and risk of certain configurations of offshore wind station and the connection to the onshore grid.
- Explore the possibilities for connecting the wind farms to the onshore grid, including the option of an offshore grid extension.
- Demonstrate the possibilities for reliable technical solution for wind power generation and integration.
- Provide the industry with validated design tools and standards.
- Tools for optimal wind power station design and control.
- Concepts for an optimal interconnection of electricity grid from offshore to onshore and insight in transient behaviour.
- Choice of optimal wind farm electrical lay-outs.

2.2.4 Author Publications

[41] M. Raza and O. Gomis-Bellmunt, “Dynamic modelling and implementation of VSC-HVDC system: A grid connected offshore wind farm application” in 3rd International conference on smart grid and green IT system, (Barcelona, Spain), pp. 53-62, 2014.

[42] M. Raza and O. Gomis-Bellmunt, “Multi-infeed control of VSC-HVDC transmission system for offshore wind power plant integration”, in 13th International Workshop on Large-Scale Integration of Wind Power into Power Systems as well as on Transmission Networks for Offshore Wind Power Plants, (Berlin), pp. 376-381, Nov 2014.

[43] M. Raza and O. Gomis-Bellmunt, “Control design strategy to enhance the fault ride through capability of VSC-HVDC transmission system interconnecting offshore wind power plant”, in EWEA Annual Conference and Exhibition 2015, (Paris, France), Nov 2015.

[44] M. Raza and O. Gomis-Bellmunt, “Control system of voltage source converter to interconnect offshore AC hub with multiple onshore grids”, 4th International Conference on Renewable Energy Research and Application, (Palermo, Italy), Nov 2015

[45] M. Raza, Carlos Collados, and O. Gomis-Bellmunt, “Reactive power management in an offshore ac network having multiple voltage source converters”, 16th IEEE International Conference on Environment and Electrical Engineering, Florence, Italy, 7-10 June 2016

[46] M. Raza, K. Schönleber, and O. Gomis-Bellmunt, “Droop control design of multi-VSC system for offshore network to integrate wind energy”, Energies-Journal of MDPI, vol. 9, no. 10, p. 826, Oct

[47] M. Raza, and O. Gomis-Bellmunt, “Small signal stability analysis of offshore ac network having multiple voltage source converters”, IEEE Transactions on Power Delivery (in review process)

[48] M. Raza, and O. Gomis-Bellmunt, “Short Circuit Analysis of an Offshore AC Network having Multiple VSCs Imposing Frequency”, IEEE Transactions on Power System (in review process)

[49] M. Raza, and O. Gomis-Bellmunt, “Reactive power management in an offshore ac network having multiple voltage source converters”, IEEE Transactions on Industry Applications (in review process)

2.3 Control and operation of wind power plants connected to DC grids- Kevin Schönleber

2.3.1 Introduction and objectives

The research project “Control and operation of wind power plants connected to DC grids” was conducted by Early Stage Researcher Kevin Schönleber at the industrial partner Alstom Renovables España S.L. (now General Electric Renovables España S.L.). Being a manufacturer for offshore wind turbines (WTs), among others, there is a special interest in the grid integration of these systems. Specifically, when very remote offshore wind power plants (WPPs) are to be connected to the main grids, high-voltage direct current (HVDC) technology is the technical-economical choice. Moreover, HVDC technology using voltage-source converters (VSCs) is the state-of-the-art solution for this application. The HVDC transmission might be a point-to-point connection in the simplest embodiment, but multi-terminal and meshed structures which were investigated within the MEDOW project could evolve in the future. Regardless of the HVDC connection (point–to–point, multi–terminal or meshed), the offshore ac grid formed by the WPPs and the offshore VSC-HVDC operates asynchronously to the main grids, is characterized by extensive submarine cabling and ultimately interfaced by multiple power converters. Several challenges are addressed in this project to enhance the operation and control of those offshore ac grids.

The focus was laid on the offshore ac grid where full power converter based WTs are linked to an offshore VSC– HVDC. Due to this configuration, studies regarding the operation and control of these grids might be bounded by the respective dc links of the WT converter and the offshore VSC- HVDC. Figure 23 draws a generic offshore ac grid connected via HVDC transmission to the main grid.

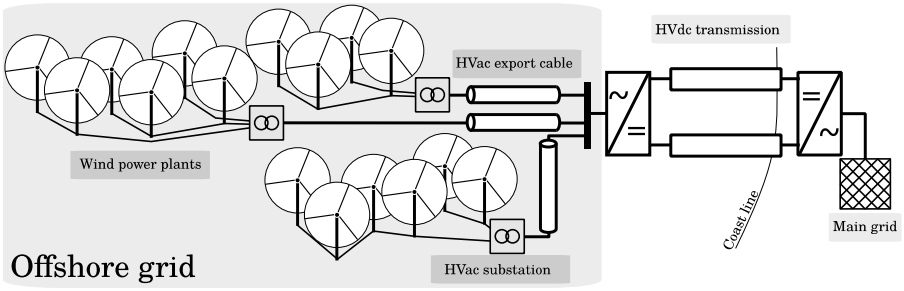

Figure 23: Schematic of offshore grid formed by several WPPs connected to a point-to-point HVdc transmission scheme.

The main objectives of the work are outlined as follows:

- Analysis and recommendation of reactive power dispatch strategies for the offshore grid of HVDC – connected WPPs. The particularities of such systems must be thoroughly addressed (decoupled operation, multiple converters, and reactive power requirements due to submarine cables).
- Analysis and proposition of reactive power/voltage control in HVDC –connected WPPs clusters. Here, the actual operator boundaries for operation and control play a crucial role for the operation and control framework deployment.
- Proposition of control method and suitable current injection during fault ride through (FRT) of unbalanced faults by the grid–forming offshore VSC– HVDC.

- Analysis of FRT strategies by the grid-connected WT converters during unbalanced faults in the offshore grid.

To sum up, two main topics of interest were covered: first, enhancement of normal operation through reactive power control and second, FRT operation of HVDC -connected WPPs.

2.3.2 Methodology

The theory implicated and highlighted in the following was applied through computer simulations with Matlab/Simulink and the SimPowerSystems toolbox. Experimental implementation of the investigated strategies was not envisaged during the project. Moreover, the studies on normal operation and steady-state voltage/reactive power control were made through steady-state load flow calculations. For this purpose, the Matlab power systems package MATPOWER is used. The simulations on FRT during electrical faults in the offshore ac grids demanded transient/dynamic simulations in the time domain. In the project, the use of any proprietary models was omitted and own generic models were developed to ease the publication of related results.

2.3.3 Reactive power control in normal operation

Reactive power management in the offshore grid is independent from the main grid when an HVDC transmission link is used. The offshore VSC- HVDC sinks the total active and reactive power and acts as a slack source to the offshore ac grid. Furthermore, it provides the voltage reference to the latter. In this work, reactive power control strategies were proposed with the objective to lower the power losses in the offshore ac grid. Figure 24 concludes the communication paths of the considered strategies whose characteristics are further depicted in Table 3.

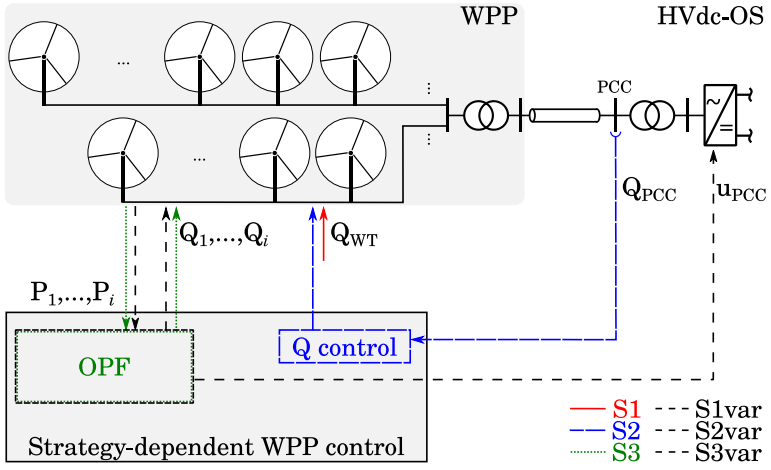

Figure 24: Control scheme for MT-VSC-HVDC transmission systems

Table 3: Characteristics of the considered reactive power control strategies

	S1	S2	S3	S1var	S2var	S3var
Objective	Unity PF WTs	Unity PF VSC–HVdc	min $P_{\text{total}}^{\text{loss}}$			
Communication	Local	Remote				
Q_i set–points	0 Mvar	WPPC	OPF	0 Mvar	OPF	OPF
Q_i distribution	Uniform	Uniform	Variable	Uniform	Uniform	Variable
Q_{PCC} set–point[1]	Power flow	0 Mvar	Power flow			
u_{PCC} set–point	Fixed		Variable			
Average execution time OPF[2]	n/a	n/a	188.8 s	1.9 s	9.8 s	243.9 s

[1] The reactive power at the PCC is determined by the power flow in the offshore grid.
[2] Data is given for the case study.

The six reactive power control strategies consider unity power factor operation by the WTs (strategy S1), unity power factor operation by the offshore VSC- HVDC through dispatch of reactive power set-points by the WPP control (WPPC) (S2), or optimal dispatch of reactive power among all converters (S3). The first two strategies are conventional operation concepts, whereas the latter makes use of optimal power flow (OPF) algorithms. Furthermore, all three strategies are also proposed with a variable reference voltage imposed by the offshore VSC as S1var, S2var, and S3var, respectively. Those latter strategies all rely on a multi-variable OPF aiming to lower the total power losses in the system. To achieve maximum power output system, the total losses assessed in the algorithm consider the power converter losses of the WTs, the offshore grid losses, and ultimately the losses occurring in the offshore VSC (refer to the boundaries depicted to describe the system in Figure 25).

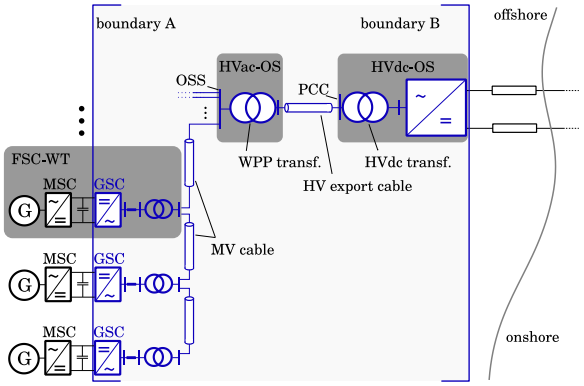

Figure 25: System boundaries for loss assessment

To evaluate the impact of the proposed strategies, the annual energy production (AEP) was identified as key performance indicator (KPI) in this work. Furthermore, wind speed distributions for offshore locations were considered. A wake model was applied to gain the individual power output of each WT for a given WPP defined in the case study.

In the industrial application, several WPPs might be connected to the same offshore ac grid. Such systems imply multi-layered operation and control structures which should be considered for the development of reactive power control strategies. Hitherto, for the application of reactive power control in HVDC -connected WPP cluster an optimization-based strategy was defined. It foresees to communicate reactive power set-points

to the WPPs and a voltage set-point to the offshore VSC. The internal management of each WPP might be made with the strategies S1 to S3 presented earlier.

2.3.4 Fault ride through of unbalanced faults

The operation of the offshore VSC- HVDC is denoted as grid-forming operation mode, contrary to the grid-connecting operation mode used by the WT converters. The grid-forming converter aims to provide the voltage reference and operate as a slack source to the offshore ac grid; however, during faults it is of utmost importance that the converter currents can be limited to avoid damage of the semiconductor devices. Therefore, at least during fault situations a dedicated current controller had been suggested in earlier research. For unbalanced faults, the current might be controlled in symmetrical components to gain full control over positive and negative sequence. The control concept proposed and used for this work is constituted by a voltage control (VC) and current control (CC) which are developed respectively in symmetrical components. The control proposal is sketched in Figure 26.

To improve the current limitation during unbalanced fault situations for the grid-forming VSC- HVDC, an extended saturation method was proposed to maximize the current injection by the converter when two phases are faulted. The controlled fault current by the converter aims to help protection schemes in the decision of fault isolation.

Moreover, four FRT strategies by the WT converters were investigated for fast reactive current provision during unbalanced faults in the offshore grid. The FRT strategies consider mitigation of power converter over-modulation through active or reactive power reduction as well as positive and negative sequence grid support. The strategies are further outlined in Table 4.

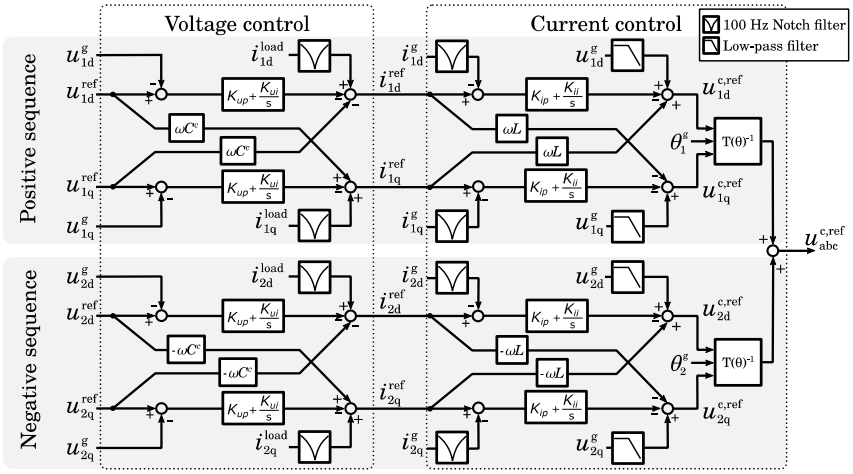

Figure 26: Control concept in symmetrical components for the grid

Table 4: FRT strategies applied by the WT converters and denoted as reference calculation (RC) strategies

RC	Pos. seq. ctrl	Neg. seq. ctrl	OM limitation
RC1	No support	Zero	Yes
RC2	Voltage support	Zero	No
RC3	Voltage support	Zero	Yes
RC4	Voltage support	Voltage support	No

2.3.5 Case studies

2.3.5.1 Reactive power control in normal operation

The analysis on the reactive power control strategies uses the WPP characteristics from the French Fécamp project which is planned to have a rated output of 498 MW composed by 83 WTs of 6 MW each. Figure 27 visualizes the WPP layout. In the case study the WPP is connected by a 10-km-long export cable system to the offshore VSC, whereas the original project is located nearshore and thus ac-connected. Further relevant reference data, including component parameters and voltage levels, are provided in [50].

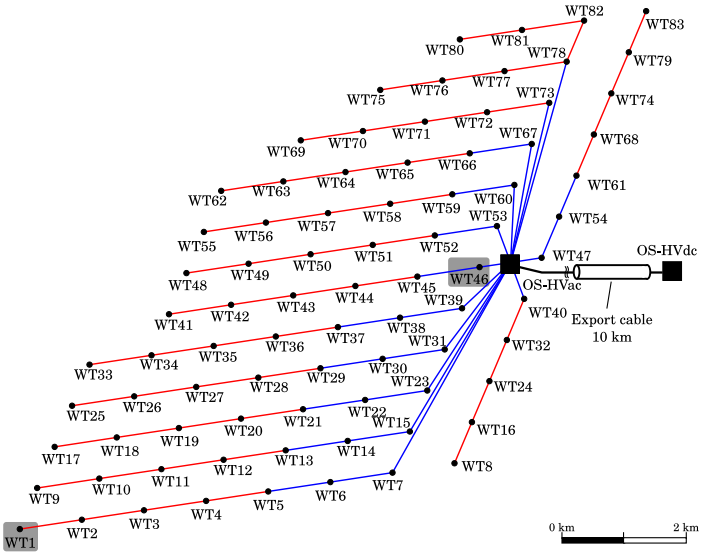

Figure 27: WPP layout and reference data for the reactive power control analysis

2.3.5.2 Fault ride through of unbalanced faults

The FRT strategies, both for the WTs and for the offshore VSC- HVDC, were analysed for unbalanced faults at the 150 kV busbar of a HVDC -connected WPP cluster connecting three parks. The electrical schematic of the system is given in Figure 28. Namely line-to-line (LL) and single-line-to-ground (SLG) faults were applied at fault location FA.

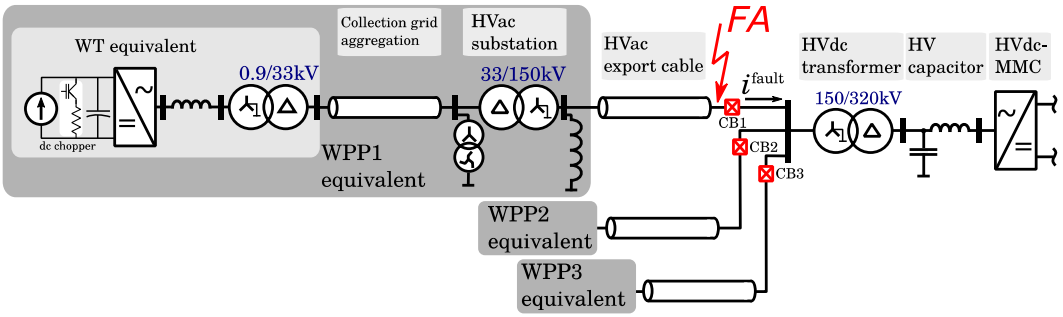

Figure 28: Electrical System of the offshore AC grid for FRT analysis

2.3.6 Results

In the following the results of the case studies are presented. It should be mentioned that more detailed results were disseminated in [50] and [51] for the reactive power control for the normal operation of HVDC -connected WPPs. The work on reactive power control in WPP cluster is currently under review [52]. The studies on FRT of unbalanced faults in the offshore grid is submitted and albeit under review [53]-[54].

2.3.6.1 Reactive power control in normal operation

In the following, a selection of results is presented for the studies of conventional and optimization-based reactive power control strategies in HVDC -connected WPPs. Here, wake effects were not considered and all WTs receive the same wind speed. Figure 29 depicts the relative total system loss to the base strategy S1. The results demonstrate that S2 causes higher losses than S1 for the active power range $0.0 < p < 0.6$ p.u. and less losses for $p > 0.6$ p.u.. As expected, the employment of the OPF algorithm in S3 has the lowest loss values over the whole power range within the strategies with a fixed voltage reference (S1, S2 and S3). The variable strategies S1var to S3var demonstrate that the voltage reference as control variable has an important impact on the power losses. Specifically, in the higher power range for $p > 0.4$ p.u. the variable strategy performs better than its fixed voltage reference counterpart (S1var with respect to S1, etc.). It is remarkable that S1var causes a similar result as S3var although the latter uses a more complex optimization incorporating the individual reactive power set–points of the WTs.

Figure 30 depicts the voltage reference set–point u_{PCC}. For the strategies S1 to S3 u_{PCC} is fixed at 1.0 p.u.. The variable strategies S1var and S2var result in similar voltage profiles as S3var. In the lower power range the system voltage is decreased to reduce the reactive power requirements (and related power losses) and the associated power losses in the converters, whereas for higher powers the increase of the system voltage leads to lower losses.

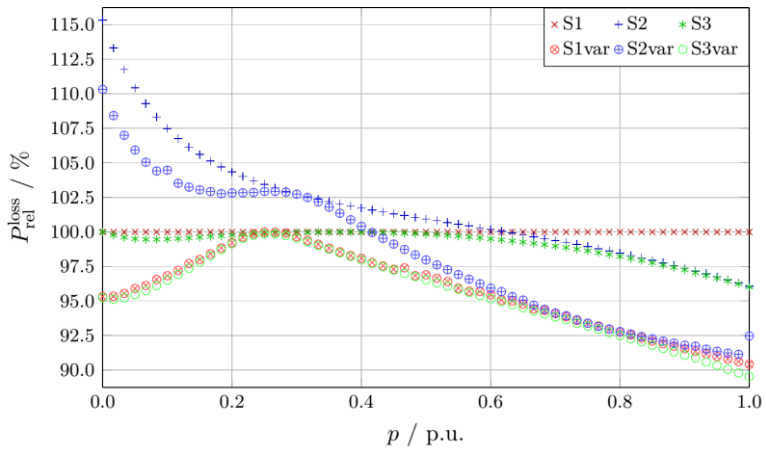

Figure 29: Relative total system losses respective to S! (set equal to 100%)

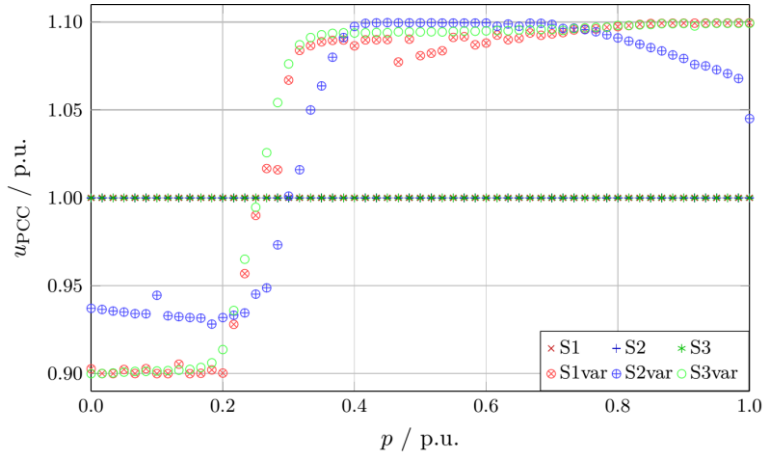

Figure 30: Voltage reference at PCC. For the fixed strategies, the voltage reference is continuously set to 1 p.u., whereas for the variable strategies the OPF determines the respective value.

Table 5 summarizes the AEP, energy losses per year and the economical equivalence thereof per year, when a feed-in tariff of 130 MEUR/year is considered. The results demonstrate, that the variable voltage strategies might increase the AEP and lower the annual energy losses (AEL) and their respective costs.

Table 5: Annual energy losses (AEL) and the monetary equivalent (ME) of the six strategies

	S1	S2	S3	S1var	S2var	S3var
AEP[1] / GWh	1811.37	1812.07	1813.50	1817.69	1815.60	1818.19
AEL[2] / GWh	94.54	93.84	92.41	88.22	90.30	87.72
ME of AEL / M€ yr^{-1}	12.29	12.20	12.01	11.47	11.74	11.40

[1] Refers to the energy injected to the HVdc link on the offshore side.
[2] Refers to the energy losses in the offshore grid, including power converter losses.

For the simulations on HVDC -connected WPP clusters (not shown in this report), the input of the power losses occurring in a WPP under different operating points with respect to active and reactive power are important. The results for the case study WPP considered above are drawn in Figure 31. It is obvious, that a reactive power set-point demanded at the connection point of the WPP consequently increases the internal loss due to the additional converter and grid currents.

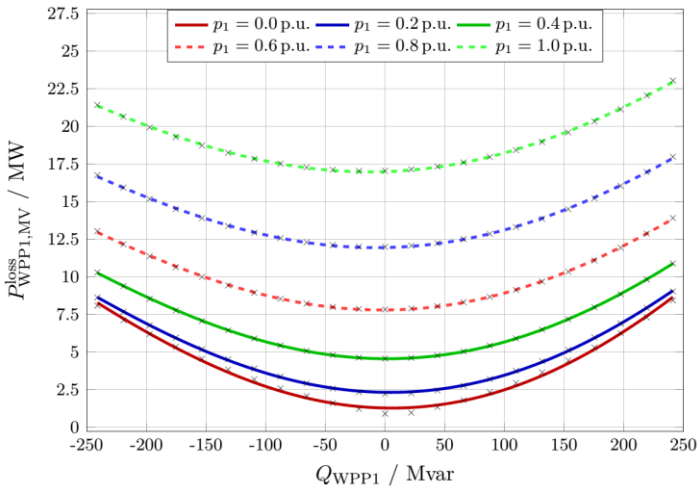

Figure 31: Power losses in the case study WPP under varying operating points

2.3.6.2 Fault ride through of unbalanced faults

The results of the comparison between the normal and extended fault current strategy are depicted in Figure 32. As an example, a SLG fault at the 150 kV busbar causes a situation were two phases appear to be faulted when passed through the HVDC transformer (the current references for these phases rise at the output of the VC during the fault). The WPPs are not connected and thus inject zero current. In the normal saturation scenario activated during the first 250 ms of the fault only one phase reaches the maximum current. In the next 250 ms, the extended fault saturation allows that both phases, b and c, reach the maximum fault current provision by the VSC- HVDC. Intrinsically this increases as well the fault current provision at the fault location. Further results are given in [53].

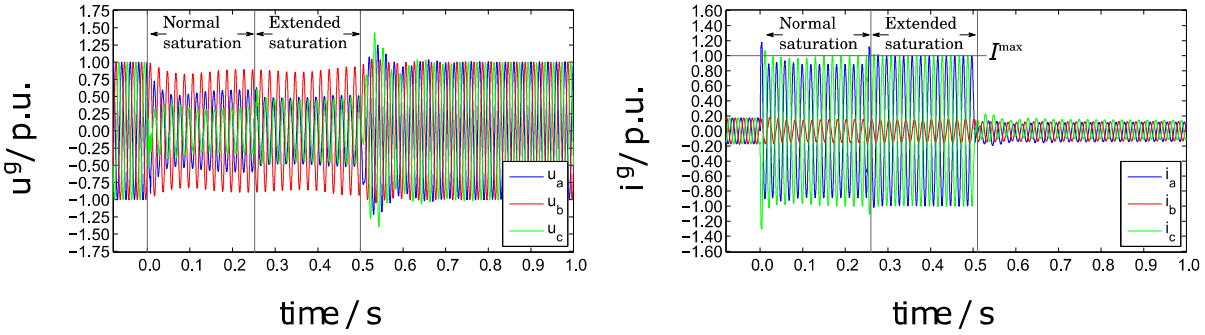

Figure 32: Comparison of normal and extended saturation during a SLG fault at the 150 kV busbar

Besides the control enhancement during unbalanced faults by the offshore VSC- HVDC, four FRT strategies by the WT converters in the offshore grid were analysed. Figure 33 depicts the results for a LL fault for four FRT strategies. For all four cases, the fault is applied for 250 ms. Strategy RC1 shows a good transient behavior for the grid voltage which is decreased in positive and negative sequence component. This behavior results from the over-modulation reduction scheme implemented in the WT converter controls. The third row shows that the current injection by the WPP1 for this strategy is reduced during the fault and ramped up in the post-fault time frame. Compared to the other strategies, over-voltages might be avoided. More detailed results are given in [54]. The strategies RC2 and RC3 cause the highest voltage magnitudes during the fault (refer to Row 1 and Row 2). For these strategies, the negative sequence currents are consequently controlled to zero which is visible by the balanced currents injected by the WPP (Row 3). Strategy RC4 supports the grid voltage in positive and negative sequence which leads to an unbalanced converter response and lower voltage magnitudes compared to the previous cases.

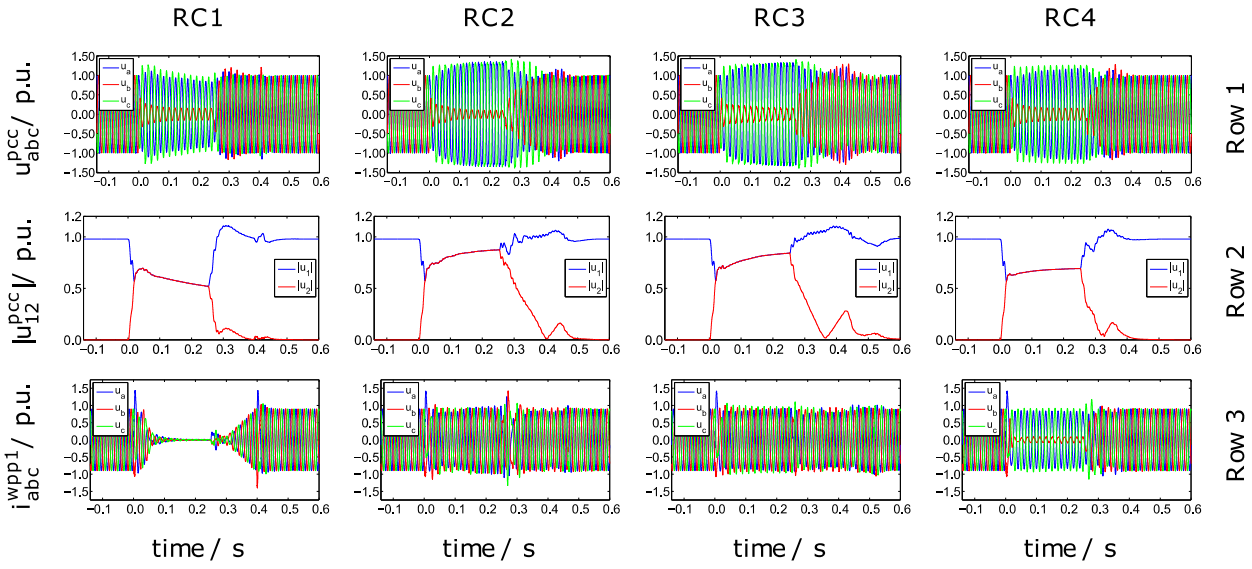

Figure 33: Results for four FRT strategies during a LL fault at the 150 kV busbar

2.3.6.3 Conclusions

The research project treated two main topics regarding the operation and control of HVDC -connected WPPs.

Firstly, the steady-state reactive power and voltage control in the offshore ac grid was investigated. The work envisaged principally the potential power loss reduction through reactive power control in the decoupled offshore ac grid. Therefore, optimization-based reactive power control was proposed which results in a sharing of reactive power between the WT converters and the offshore VSC-H HVDC. The evaluation against conventional strategies, where reactive power is solely provided by the offshore VSC- HVDC or by the WTs, demonstrated reduced power losses which equal 0.8 MEUR per year for a 500 MW reference WPP. The decoupled offshore grid offers additionally the incorporation of the voltage reference in the optimization algorithm. This concept enables further reduction of losses which was also effectively demonstrated for more complex structures, when WPP clusters are operated with the proposed strategies. The reactive power might be shared effectively, if the WPPs are operated at unity power factor and the voltage reference by the offshore VSC- HVDC adapts to the active power injection. Higher collection grid voltages, e.g. 66 kV in the future will increase the need for improved reactive power control in the offshore ac grids of HVDC -connected WPPs and motivate more research in this field.

Secondly, dynamic simulations on the FRT behaviour of the WTs and the offshore VSC were conducted for unbalanced faults in the offshore grid. Therefore, a control method in symmetrical components, comprising voltage and current controllers in positive and negative sequence, was proposed. Besides that, a saturation method which enhances the current provision by the offshore VSC was suggested and tested. It was shown that such a control method successfully rides through unbalanced faults in the offshore grid and furthermore increases slightly the controlled fault current. Moreover, four FRT strategies by the WTs were analysed which use controllers in symmetrical components. Here, over-modulation reduction strategies on either active or reactive current were also considered. The results demonstrate that solely positive sequence grid support might lead to over-voltages during unbalanced faults. Combined positive/negative sequence grid support is advantageous besides controlled active power limitation which also limits the over-voltages.

2.3.7 Publications

[50] K. Schönleber, C. Collados, R.T. Pinto, S. Ratés-Palau, O. Gomis-Bellmunt, Optimization-based reactive power control in HVDC-connected wind power plants, Renew. Energy. 109 (2017) 500–509.

[51] K. Schönleber, S. Ratés-Palau, M. De-Prada-Gil, O. Gomis-Bellmunt, Reactive power optimization in HVDC-connected wind power plants considering wake effects, in: U. Betancourt, T. Ackermann (Eds.), 14th Wind Integr.

[52] K. Schönleber, S. Ratés-Palau, O. Gomis-Bellmunt, Analysis of reactive power strategies in HVDC-connected wind power plant clusters, Under Review.

[53] K. Schönleber, E. Prieto-Araujo, S. Ratés-Palau, O. Gomis-Bellmunt, Analysis of fault ride through in HVDC-connected wind power plants during unbalanced faults, Under Review.

[54] K. Schönleber, E. Prieto-Araujo, S. Ratés-Palau, O. Gomis-Bellmunt, Handling of unbalanced faults in HVDC-connected wind power plants, Under Review.

2.4 Coordinated control of wind power plants in offshore HVDC grids- Jayachandra N. Sakamuri

2.4.1 General Background and Motivation

Due to the depletion of fossil fuels, increased concerns for environmental impact by fossil fuels, and technology developments have encouraged the use renewable sources for electrical power production. The European Union's (EU) Renewable Energy Directive created an overall policy for the generation and promotion of energy from renewable sources in the EU [55]. According to this directive, EU targets to fulfil at least 27% of its total energy needs with renewables by 2030. This shall be achieved through the execution of individual national targets of its member countries. According to the Renewable Energy Projections as published in the National Renewable Energy Action Plans, wind energy has the potential to supply 40.6% of all renewable electricity; whereas offshore wind energy will account for 27% of the total wind energy share [56], [57], which is equal to a total of 40 GW of installed offshore wind energy throughout Europe by 2020. The European Wind Energy Association (EWEA)'s new central scenario expects 320 GW of the wind energy capacity to be installed in the EU in 2030, of which 254 GW of onshore wind and 66 GW of offshore wind [58]. To meet the EU action plan targets, The North Seas Countries' Offshore Grid initiative (NSCOGI) was formed among nine North Sea countries and agreed on closer energy cooperation to enable development of an efficient and economic offshore grid infrastructure for integration of offshore wind energy [59], [60], which also involves selection of technology to transmit offshore wind power: AC or DC.

Due to their distance from the shore and higher installed capacity, the power from the offshore wind power plants (OWPPs) in the North Sea can be transmitted to the shore using voltage source converter (VSC) based high voltage DC (HVDC) transmission systems [61]. Also, Multi-Terminal DC (MTDC) transmission system seems to be a promising solution for interconnecting offshore wind power plants with different onshore AC grids and to lay foundation for future European super grid [62],[63]. Several research projects and researchers have already focused on finding solutions for key challenges for integration of offshore wind power to MTDC grids, for example, TWENTIES, OffshoreDC, Multi-terminal DC grid for offshore wind (MEDOW), to name few projects [64][64]-[66].

This PhD project is a part of the research project funded by EU and it is in a consortium organized by Cardiff University with a project title MEDOW [66], which is a consortium, formed by eleven partners (five universities and six industries). MEDOW has mainly 12 key research objectives under 4 work packages:

WP1 - Connection of Offshore Wind power to DC grids

WP2 - Investigation of voltage source converters for DC grids

WP3 - Relaying protection

WP4 - Interactive AC/DC grids

One of the objectives of MEDOW is to develop coordinated control schemes for effective delivery of ancillary services from OWPPs to AC and DC grids. This has motivated to study the challenges on the control and coordination of OWPPs and MTDC grid for effective operation of the onshore AC grid. Nowadays, the trend is increasing for integrating multiple OWPPs to a common HVDC station [67]-[69], where the offshore AC grid voltage control and reactive power sharing between OWPPs are major concerns. These challenges have

composed the main motivation of the present thesis: "*Coordinated Control of Wind Power Plants in Offshore HVDC grids*".

2.4.1.1 Problem Definition

Traditionally power from OWPPs is transmitted to the main land AC grid through AC cables and the AC cable connections are normally feasible for a transmission distance up to 60 km [70]. AC transmission is not a viable option for increased transmission distance from the shore due to the higher charging current requirement because of cable capacitance which results in higher losses with AC cable. Therefore, VSC-HVDC technology becomes suitable option for grid integration of large OWPPs located far from the shore (>80 km).

The HVDC decoupling from the mainland AC grid makes the offshore AC grid weak and vulnerable to dynamical voltage events due to the limited short circuit power contribution from the HVDC converter and OWPP [71]-[73]. This leads to significant concern for voltage ride through (VRT) capability of OWPPs in the offshore AC grid. Moreover, due to the large available wind resource in the North Sea, many OWPPs are being planned in the close vicinity as clusters and are being connected and considered to be connected to a common HVDC station [67],[69]. The steady state voltage/reactive power control and dispatch strategy of the OWPP cluster connected to the offshore HVDC converter is also important as several OWPPs in close proximity may be connected to the same HVDC converter station, particularly in the growing offshore grid. This requires coordination between them for reactive power and AC voltage control between the clusters of OWPPs in the offshore AC grid.

HVDC Interconnectors to interconnect two synchronous areas are already existing today or being built and since they are, almost all, based on VSC technology. It is very likely that they will then be combined with OWPP connections, transforming it in a MTDC and, why not, in a fully meshed offshore DC grid. The increased penetration of wind power plants (WPPs) into the power system postures several challenges to its operation and stability [62], [63]. Among them, frequency control is one of the important concerns for the transmission system operators (TSOs) along with other system services, for example, fault ride through (FRT) support, reactive power and voltage control. In particular, increased penetration of WPPs replacing conventional synchronous machines leads to the reduced effective inertia of the power systems and that may lead to a lower frequency nadir point, or load shedding, for a large infeed/generation loss in power systems. The primary frequency control today might be too slow for the future power system with much less inertia and then a faster response is needed, creating the need for fast primary frequency control (FPFC) [65]. Therefore, WPPs including OWPPs are required participate in frequency control to limit the frequency nadir [65] i.e. FPFC of the power system. Moreover, the impact of wind speed on the OWPPs power output and the corresponding impact on frequency control also have to be analyzed.

The primary frequency control today might be too slow for the future power system with much less inertia and then a faster response is needed, creating the need for fast primary frequency control (FPFC) [65].

Another challenge with the OWPPs in the HVDC/MTDC system is that they do not respond to the frequency events in the associated onshore AC grid due to the power electronic interfaces in the form of converters inside the WTs and HVDC transmission system. Therefore suitable methods have to be developed to make sure that onshore AC grid frequency events are available to the OWPPs controllers so that they can participate in frequency control.

Considering the above points, the attention in this thesis is directed towards two main research challenges resulted due to OWPPs integration to HVDC /MTDC transmission systems.

- Coordinated AC voltage/reactive power control in cluster of OWPPs connected through common HVDC station.

- Onshore AC grid frequency control from OWPPs in MTDC grid: Methods for frequency control, Impact of wind speed on the frequency control.

2.4.1.2 Thesis Objectives and Limitations

The main objectives of this PhD work can be described as:

- To better understand the AC voltage and reactive power control in the offshore AC grid with the cluster of OWPPs connected to common offshore VSC-HVDC station, and study the reactive power contribution from WTs within the cluster for symmetrical faults at different locations of the offshore AC grid.

- To develop coordinated control schemes for reactive power and AC voltage control in the offshore AC grid composed of cluster of OWPPs connected to common offshore VSC-HVDC station to improve the steady state and dynamical performance of the offshore AC grid.

- To analyze the different methods for frequency control from OWPPs connected through MTDC grids, with and without depending on the communication channels to replicate the onshore AC grid frequency events at offshore AC grid. To study other possible active power balance control services from OWPPs to AC and DC grids (DC voltage control, fault ride through support)

- To study the impact of wind speed on the OWPPs active power output and the corresponding impact on frequency control from OWPPs in MTDC grid.

- To demonstrate the proof of concept of frequency control methods for OWPPs in MTDC grid and the impact of wind speed on the frequency control using a laboratory scaled 3-terminal DC grid test set up.

The main limitations of the study are:

- The study is focused on using root-mean-square (RMS) simulation models; therefore the electromagnetic transient phenomena are discarded.

Only impact of symmetrical faults in the offshore AC grid is considered. The asymmetrical faults and their impact on the offshore AC grid voltage profile and on the coordinated voltage control schemes are not considered.

2.4.2 Thesis Contributions and Main Results

The main contributions of the study performed in this thesis are given below.

1) Three methods for reactive power and AC voltage control in the cluster of OWPPs connected to common HVDC station: (1) Voltage droop control method (2) Coordinated Reactive Power Control Scheme (3) Coordinated Voltage Control Scheme, have been proposed and compared. Methods are proposed to improve steady state reactive power distribution to avoid excessive voltage at WTs and voltage ride through capability of the offshore AC grid with cluster of WPPs connected to common HVDC station.
2) Two methods for frequency control: (1) Communication based, (2) Coordinated control, from OWPPs in MTDC grid have been presented. These methods are validated by time domain simulations using DIgSILENT PowerFactory and performing tests on a 3-terminal laboratory scaled test set up. The impact of wind speed on the frequency control form OWPPs in MTDC grid have been verified with the time domain simulations and experimental tests.
3) The main results of the study have been disseminated in the form of presentations and publications international conference and reputed journals and they are given in next section.

2.4.2.1 List of Publications

The following lists of conference and journal publications are the major contributions to make this report. These papers are included in the appendices and are referenced at appropriate places in the report as needed.

Journal Publications:

J1 Ömer Göksu, Jayachandra N. Sakamuri, C. Andrea Rapp, Poul Sørensen, Kamran Sharifabadi, “Cluster Control of Offshore Wind Power Plants Connected to a Common HVDC Station”, Energy Procedia, Volume 94, Sep 2016, Pages 232-240, ISSN 1876-6102

J2 Jayachandra N. Sakamuri. Rather Z.H., Cutululis N.A., Rimez J., “Coordinated Voltage Control in Offshore HVDC Connected Cluster of Wind Power Plants ", *IEEE Trans. on Sustainable Energy*, vol.7, pp.1592-1601, Oct 2016.

J3 Jayachandra N. Sakamuri., Altin M, Hansen A.D., Cutululis N.A., “Coordinated Frequency Control from Offshore Wind Power Plants Connected to multi terminal DC System Considering Wind Speed Variation ", *IET Rene. Power Generation, Special Issue: Active Power Control of Renewable Energy Generation Systems,* Available Online Aug 2016

J4 Jayachandra N. Sakamuri, Joan Sau, Eduardo Prieto, Oriol Gomis, Altin M, Hansen A.D., Cutululis N.A., “Experimental Validation of Frequency Control from Offshore Wind Power Plants in Multi Terminal DC Grid", *Under Review at CIGRE Science & Engineering*.

J5 Jayachandra N. Sakamuri, Joan Sau, Eduardo Prieto, Oriol Gomis, Altin M, Hansen A.D., Cutululis N.A., “Impact of Release of OWPP Kinetic Energy Support on DC voltage in MTDC Grids", *Under Review at IEEE Trans of Power Delivery*.

Conference Publications:

C1 Jayachandra N. Sakamuri, Rather Z.H., Cutululis N.A., Rimez J., “Dynamic Reactive Power Control in Offshore HVDC Connected Wind Power Plants ", *Proc.t 14th Wind Integration Workshop*, Brussels, 2015.

C2 Jayachandra N. Sakamuri, Rather Z.H., Cutululis N.A., Rimez J., “A New Coordinated Voltage Control Scheme for Offshore AC Grid of HVDC Connected Offshore Wind Power Plants ", *Proc. CIGRE Canada Conference*, Winnipeg, Canada, 2015.

C3 Jayachandra N. Sakamuri, Das K, Altin M., Hansen A.D., Cutululis N.A., Tielens P. Dirk Van Herterm, “Improved Frequency Control from Wind Power Plants Considering Wind Speed Variation", *Proc. 19th Power System Computation Conference*, Genoa, Italy, 2016.

C4 Jayachandra N. Sakamuri., Hansen A.D., Cutululis N.A., Altin M., Sørensen P.E., “Coordinated Fast Primary Frequency Control from Offshore Wind Power Plants in MTDC System ", *Proc. IEEE Energycon Conference*, Leuven, Belgium, 2016

C5 Jayachandra N. Sakamuri, Altin M, Hansen A.D., Cutululis N.A., Rather Z.H.,, “Coordinated Control Scheme for Ancillary Services from Offshore Wind Power Plants to AC and DC Grids ", *Proc. IEEE PES General Meeting 2016*. (selected as best conference paper)

C6 Jayachandra N. Sakamuri, Joan Sau, Eduardo Prieto, Oriol Gomis, Altin M, Hansen A.D., Cutululis N.A., “Suitable Method of Overloading for Fast Primary Frequency Control from Offshore Wind Power Plants in Multi-Terminal DC Grid", *Accepted for IEEE PowerTech Conference*

2.4.3 Main Results

The simulation and experimental results of fast primary frequency control (FPFC) from OWPPs connected through a 3-terminal DC grid is given in this section. Mainly the impact of release of offshore wind power plant kinetic energy support on DC voltage in MTDC grids is discussed.

2.4.3.1 Simulation Model

A three-terminal DC grid test system with an OWPP, shown in Figure 34, is considered in this paper. The test DC grid interconnects two independent onshore AC grids (AC grid-1 and AC grid-3) and one offshore AC grid having an OWPP. Root mean square (RMS) models for OWPP, VSC-HVDC converters, cables, and transformers have been used for the investigation and implemented in DIgSILENT PowerFactory.

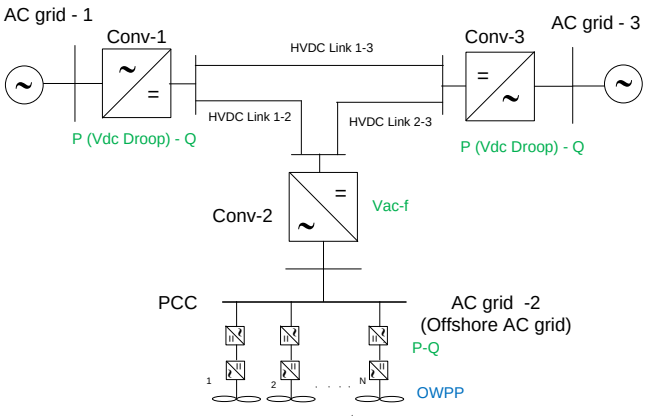

Figure 34: Three-terminal HVDC grid layout

In the following sub sections, a brief description of the onshore and offshore HVDC converter control, OWPP control, and additional controls needed for frequency control are given.

A. Onshore HVDC Converter

The Conv-1 and Conv-3 in Fig. 1 are the onshore HVDC converters, based on VSC technology, connected to AC grid-1 and grid-3, respectively. They share the responsibility of active power balance in the DC grid; hence, they operate in active power control with a DC voltage droop. The Conv-2 in Figure 34, is the offshore HVDC converter is also a VSC connected to the offshore AC grid (i.e. AC grid-2). The main responsibility of this converter is to control the AC voltage and frequency of the offshore AC grid and exchanging the power generated by the OWPP to the DC grid. A supplementary droop controller is added at each of these converters which takes the responsibility of replicating the onshore AC grid frequency at offshore grid in a coordinated manner.

2.4.3.2 Laboratory Scale MTDC Test Set up

The objective of laboratory scaled test set up is to validate the use of DC grid voltage as an equivalent AC grid frequency indicator and also to study the impact of wind speed on the fast primary frequency control. The frequency control test is performed on a three-terminal DC grid laboratory test set up shown in Figure 35. The three-terminal DC grid laboratory scaled test set up is composed of three cabinets, as shown in Figure 35, and a physical emulation of the DC cables. The DC lines (1-2, 1-3 and 2-3) are modelled using the PI equivalent cable. The cable capacitance is included in the VSC capacitance. Each cabinet contains a three-phase 12.5 kVA transformer, the VSC, the control board and the measuring boards. The VSCs are two-level converters based on insulated-gate bipolar transistors (IGBTs) with a nominal power of 5.7 kVA. The nominal AC RMS voltage is 230 V phase to phase. The switching frequency of each converter is 20 kHz and it is controlled using a control board based on a digital signal processor (DSP) F28M35 of Texas Instruments (TI). All the converters are physically connected to the same AC grid of the laboratory, which is 230 V phase-to-phase. The behavior of the OWPP in the AC side of Conv-2 is emulated using a model implemented in LabVIEW in an external controller that receives data from the DC grid and sends the power reference to be injected by Conv-2 in the DC grid. The frequency event in the AC grid of Conv-1 is emulated considering a model of a virtual AC grid implemented in the DSP of the control board of Conv-1.

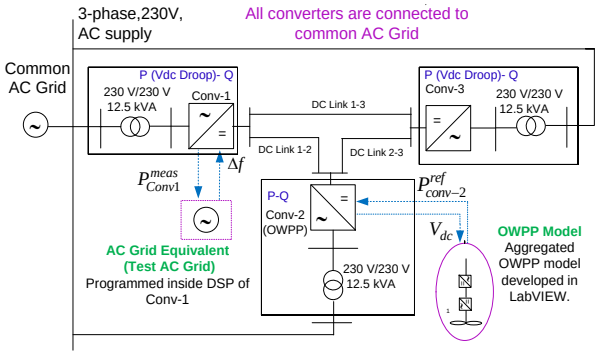

Figure 35: Three-terminal HVDC grid layout

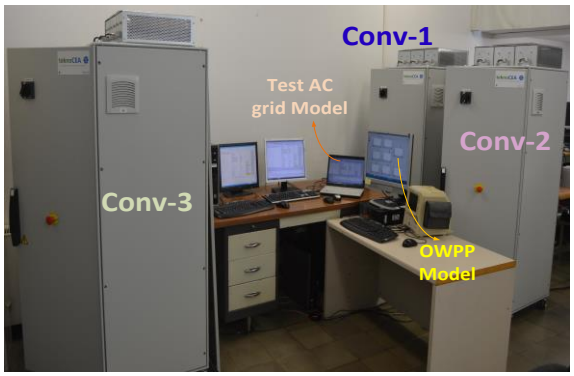

Figure 36: Three-terminal HVDC grid layout

A SCADA system is implemented in LabVIEW using the cRIO 9024 controller of National Instruments (NI) to monitor the variables of the MTDC grid and it also includes the emulation of the OWPP of Conv 2. The OWPP emulation in the cRIO 9024 is communicated with Conv 2 via the Digital to Analog Converter (DAC) and the Analog to Digital Converter (ADC) of its control board. The emulation of the frequency event of AC grid of Conv 1 is implemented by software in the DSP of Conv. 1.

2.4.3.3 Simulation and Experimental Results

The simulation results and corresponding experimental validation of FPFC from OWPPs and other converters in a three-terminal DC grid are presented for three different wind speeds: (1) above rated wind speed (1.1 pu), (2) just below rated wind speed (0.92 pu) and (3) low wind speed (0.7 pu). Here, the results for just below rated wind speeds have been presented. An under frequency event is created at test AC grid by increasing its electrical power output ΔP_l = 0.15 pu at time t = 6s. In all three the test cases, kinetic energy of the OWPP is utilized by overloading the WT for 10 seconds after the initiation of frequency event, i.e. the kinetic energy support of the OWPP is released at time t = 16s. The impact of release of the kinetic energy support from the OWPP on the DC and AC grids is studied and possible mitigation methods are discussed.

Frequency Control at just below rated wind speed (Vw_0.93)

The behavior of the WT for overloading at just below rated speed is interesting because of its dynamics. The simulation and experimental results of frequency control (frequency, DC voltage, and active power) are given in Fig.4.

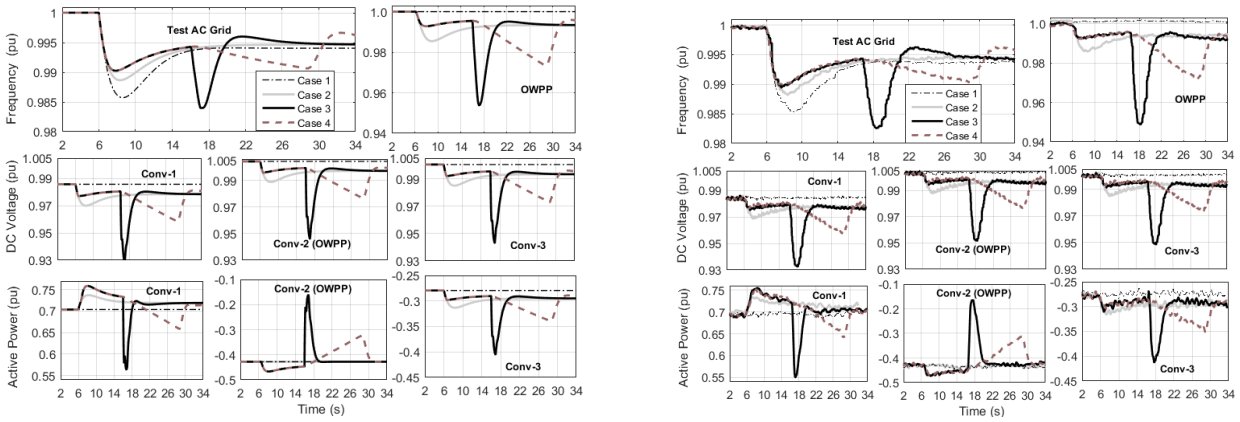

Figure 37: Coordinated frequency control-Vw_0.92 pu - Simulation and experimental results 1). No Support, 2). Support from Conv-3 3). Support from OWPP and Conv-3 4). Support from OWPP and Conv-3 with rate limiter at WT

During the frequency control period, the frequency of the test AC grid is improved with the participation of OWPP and Conv-3 (Case 3) compared to other two cases (Case 1 and 2). However, at end of frequency control period, there is a considerable dip in the DC voltage of the DC grid and frequency of the test AC grid, in case 3 compared to a and b. However, the magnitude of secondary dips are lesser for Case 4 (overloading is released with a rate limiter) compared to Case 3, which is explained a bit later in this section. The reason for these secondary dips is due to the sudden drop in active power output after the release of kinetic energy support from the OWPP. This is understood by the simulation and experimental results of WT dynamics given in Fig. 3. During the frequency control period, the WT power output (P_{out}) is increased above its optimal value (P_{mppt}). Hence, the WT speed (O_{gen}) starts to decrease with the progress of overloading, causing a reduction in the aerodynamic power (P_{aero}), which further reduces the P_{mppt} . The P_{aero} cannot be increased, as done in case of above rated wind speeds, because the pitch is already at its optimal position. This process is continued until the end of frequency control period which results in a considerable reduction of P_{mppt} . For prolonged frequency control period, there is a risk that WT stops producing power at some point. At the end of frequency control period, P_{out} is set back to P_{mppt} , hence results in sudden reduction of active power output of WT (0.9 pu to 0.3 pu). After that, WT starts recovering and reaches its pre-overloading operating point quickly (approximately in 2.5 s). However, the sudden drop in WT, hence OWPP power output burdens the Conv-3 because it increases its power output to maintain the balance in the DC grid.

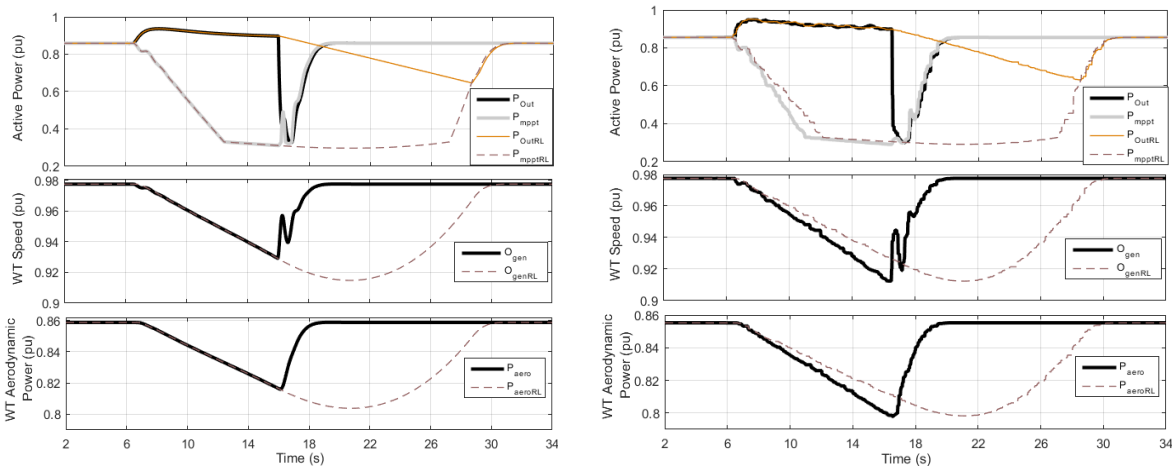

Figure 38: WT Dynamics for Frequency control at Vw_0.92 pu-Simulation and experimental results

This sudden power drop from OWPP has to be avoided to avoid secondary effects on DC grid voltage and frequency of the test AC grids. One possible way is to smoothly releasing the overloading of the OWPP using a rate limiter (RL. At the end of frequency control period, the overloading of the OWPP is released at a rate of 0.025 pu/s instead of using instantaneous release and the corresponding results are given as Case 4 in Figure 37. It can be observed from Figure 38 that the magnitude and rate of secondary dip in frequency an DC voltage are lesser with the rate limiter option (Case 4) compared to the case without rate limiter (Case 3). The corresponding WT dynamics are also smoother, as shown in Fig 5 with subscripts 'RL', for example, WT power output with rate limiter (P_{outRL}), optimal power output with rate limiter (P_{mpptRL}), and WT speed with rate limiter (O_{genRL}).

Therefore, the simulation and experimental results prove that the OWPPs and the other converters in a MTDC grid can participate in frequency control without depending on communication channels between the converters in the DC grid and the DC voltage can be used to transmit the frequency of the affected AC grid between the other AC grids. However, wind speeds play a major role on frequency control. In case of above rated wind speeds, the additional aerodynamic power can be utilized by changing the pitch angle to get the additional energy during the frequency control period. In this case, WT dynamics are smoother and secondary DC voltage and frequency dips due to the release of kinetic energy support from OWPP are reasonable. However, at just below rated wind speed, overloading the wind turbine results in a faster reduction in WT output power, causing significant secondary dips in frequency and DC voltage at the end of frequency control period. Limiting the rate of power release can smoothen the WT dynamics to some extent and minimizes the secondary effects. At lower wind speed, secondary DC voltage and frequency dips are minimal due to less share in the active power output from OWPP compared to the other converters in the DC grid. However, the recovery time after releasing the overloading is longer, thus sufficient time has to be ensured to make the OWPP ready for another frequency event.

2.4.4 References

[55] European Commission, "DIRECTIVE OF THE EUROPEAN PARLIAMENT AND OF THE COUNCIL on the promotion of the use of energy from renewable sources (recast)," November 2016, [Online]. Available: https://ec.europa.eu/energy/sites/ener/files/documents/1_en_act_part1_v7_1.pdf

[56] Energy Research Centre of the Netherlands (ECN), “Renewable Energy Projections as Published in the National Renewable Energy Action Plans of the European Member States Summary report,” ECN, Technical Report Feb 2011, [Online]. Available: http://ledsgp.org/wp-content/uploads/2015/10/renewable-energy-projections.pdf

[57] European Wind Energy Association, “Wind Energy Scenarios for 2020,” Technical Report July 2014, [Online]. Available: https://windeurope.org/fileadmin/files/library/publications/reports/EWEA-Wind-energy-scenarios-2020.pdf

[58] European Wind Energy Association, “Wind Energy Scenarios for 2030,” Technical Report August 2015, [Online]. Available: https://windeurope.org/fileadmin/files/library/publications/reports/EWEA-Wind-energy-scenarios-2030.pdf

[59] Political Declaration on energy cooperation between the North Seas Countries, [Online]. Available: http://www.benelux.int/files/9014/6519/7677/Political_Declaration_on_Energy_Cooperation_between_the_North_Seas_Countries.pdf

[60] EWEA. Wind in power: 2014 European statistics. Technical Report. European Wind Energy Association (EWEA); 2015. [Online] Available: https://windeurope.org/wp-content/uploads/files/about-wind/statistics/EWEA-Annual-Statistics-2015.pdf

[61] ABB AB Grid Systems - HVDC, “HVDC Light - It’s time to connect,” ABB, Ludvika, Technical Report, December[Online] Available: https://library.e.abb.com/public/2742b98db321b5bfc1257b26003e7835/Pow0038%20R7%20LR.pdf

[62] D. Van Hertem, M. Ghandhari , "Multi-terminal VSC HVDC for the European Supergrid: Obstacles," Renewable and Sustainable Energy Reviews, vol 14, pp 3156–3163, Dec 2010

[63] D. Van Hertem, O. Gomis-Bellmunt and J. Liang, HVDC Grids: For Offshore and Supergrid of the Future, IEEE Press Series on Power Engineering, Ed. John Wiley & Sons, 2016.

[64] TWENTIES project, “Final report-short version, June 2013, [Online]. Available: http://www.ewea.org/fileadmin/files/library/publications/reports/Twenties_report_short.pdf

[65] N.A. Cutululis, L. Zeni, W.Z. El-Khatib, J, Holbøll, P.E. Sørensen, G. Stamatiou, O. Carlson, V.C. Tai, K. Uhlen, J. Kiviluoma, T., Lund, “Challenges Towards the Deployment of Offshore Grids: the OffshoreDC Project”. Proceedings of 13th International Workshop on Large-Scale Integration of Wind Power into Power Systems as well as on Transmission Networks for Offshore Wind Power (WIW 2014). Energynautics GmbH, 2014.

[66] Multi-terminal DC grid for offshore wind (MEDOW), [Online]. Available: http://sites.cardiff.ac.uk/medow/

[67] A. Abdalrahman, E. Isabegovic, “ DolWin1 - Challenges of connecting offshore wind farms”, Proc.. IEEE International Energy Conference, Apr 2016

[68] V. C. Tai and K. Uhlen, “Design and Optimisation of Offshore Grids in Baltic Sea for Scenario Year 2030,” EERA DeepWind’2014, Energy Procedia, vol. 53, pp. 124–134, 2014

[69] Siemens SylWin1 Press Release, [online] Available: http://www.siemens.com/press/en/pressrelease/?press=/en/pressrelease/2015/energymanagement/pr2015040192emen.htm&content[]=EM

[70] D. M. Larruskain, I. Zamora1, A. J. Mazon, O. Abarrategui, J. Monasterio, “Transmission and

Distribution Networks: AC versus DC", Proc. Solarec-2005, pp 1–6, 2005.

[71] R. Irnawan, K. Srivastava, M. Reza, "Fault detection in HVDC-connected wind farm with full converter generator", Int. Jounrnal Elect. Power Energy Syst., vol. 64, pp. 833-838, Jan. 2015.

[72] E. Muljadi, N. Samaan, V. Gevorgian, J. Li, and S. Pasupulati, "Short circuit current contribution for different wind turbine generator types," in Power and Energy Society General Meeting, 2010 IEEE, pp. 1 -8, july 2010.

[73] O. Gomis-Bellmunt, , F.Hassan, C.Barker, A. Egea-Alvarez, "Capability curves of a VSC-HVDC connected to a weak AC grid considering stability and power limits". Proc. 11th IET International Conference on AC and DC Power Transmission, ,2015

3. Investigation of voltage source converters for DC grids

3.1 Operation of DC grids with various types of voltage source converters- Jorge Gonçalves

3.1.1 Introduction and objectives

A Direct Current (DC) grid based on multi-terminal Voltage Source Converters (VSCs) is a newly emerging technology, which is particularly suitable for the connection of Offshore Wind Farms. Multi-terminal DC grids will be the key technology to enable a European offshore SuperGrid.

The main objective of this fellow was to investigate VSCs and their compatibility when used in DC grids. Specifically, the objectives for the work within the Work Package and the project were:

- Modelling of 2-level VSC and half-bridge and full bridge Modular Multilevel Converters (MMCs).
- Development of a detailed Modular Multilevel Converter model suitable for the implementation of alternative control objectives.
- Implementation of an electro-thermal model in order to examine the thermal behaviour of semiconductors in Modular Multilevel Converter applications.
- Development of effective active thermal control strategies for Modular Multilevel Converters.
- Establish a control algorithm for the monitoring and management of Sub-Modules State of Health.
- Construction of an experimental platform for the validation of the proposed algorithms and control methodologies.

3.1.1.1 Simulations

The methodology followed in order to attain the proposed objectives consisted in the development of appropriate simulation models of the power electronic converters, followed by the proposal and computer validation of suitable control strategies before the experimental validation of the same. As the simulation models needed to be accessible for other members of the network, which use various software packages according to the type of studies performed, the simulation models for 2-Level VSC and half- and full bridge MMCs were implemented is both PSCAD/EMTDC and Matlab/Simulink using the Plexim PLECS toolbox.

The control loops implemented in the simulation models are shown in Figure 39. The control of a MMC requires not only the typical vector control implemented in the Park reference frame and here named ’VSC Control’, as it is common to all VSC-type topologies, but also dedicated control loops and processes: Circulating Current Suppression, Modulation and Capacitor Voltage Balancing.

Specifically to the work of this ESR within the WP, major attention was dedicated to the model in PLECS as it allowed the implementation of the electro-thermal model of the semiconductors in the detailed switching model of semiconductors, which was not possible on other platforms. Electrical and thermal simulation studies were validated initially in PLECS before the conception, design and assembly of the experimental platform.

The 2-Level VSC topology has been replaced commercially by MMCs, represented in Figure 40, which possess significant technical advantages such as lower losses and harmonic distortion. Consequently, the

models of 2- level VSCs are not included or further discussed in this report as they have been used only for the benchmark of the dynamic performance of different converter topologies but not to achieve the technical objectives of the ESR and the WP. Furthermore, the active thermal control methodologies and the Sub-Module thermal balancing strategy proposed by the fellow are independent of the Modular Multilevel Converter topology, therefore only a half-Bridge MMC configuration was utilised to achieve the initially set objectives and also in the experimental platform.

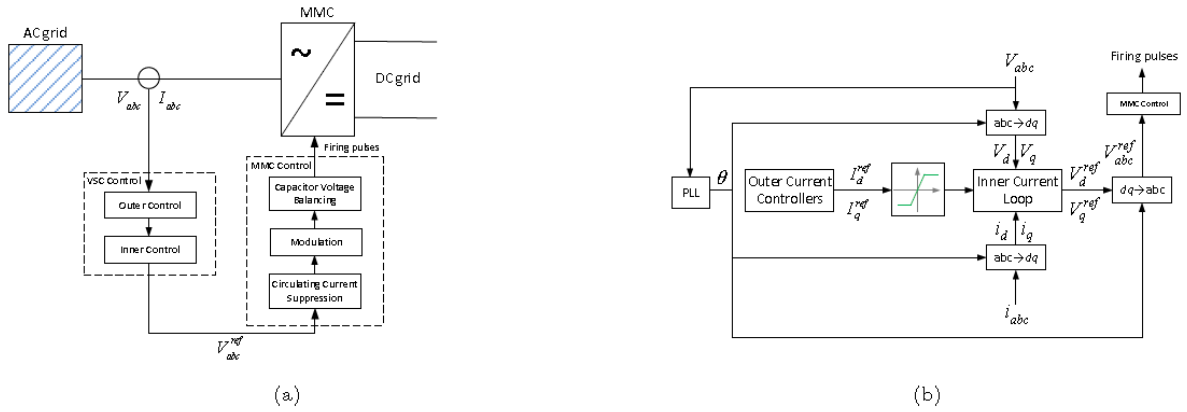

Figure 39: Control Structure of a Modular Multilevel Converter: (a) - General Detailed Control Structure and (b) - Control Structure of a Voltage Source Converter

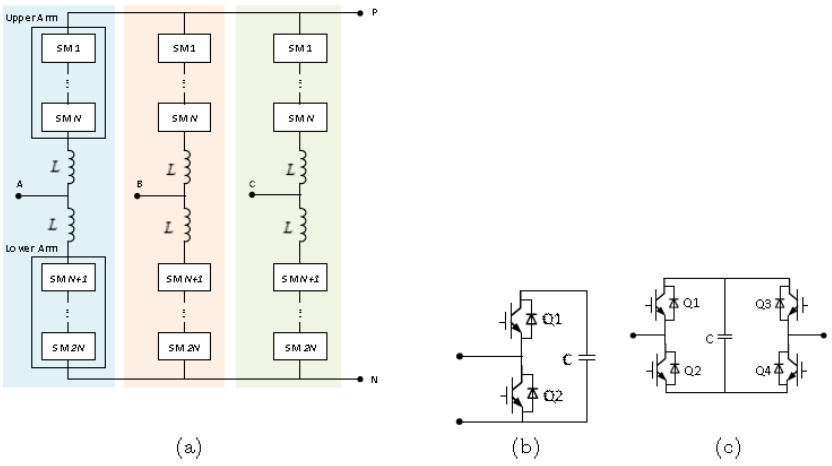

Figure 40: Modular Multilevel Converter: (a) - Topology; (b) - Half-Bridge Sub-Module configuration and (c) - Full Bridge Sub-Module configuration

3.1.1.2 Experimental Platform

The construction of a 3-phase MMC, even with a reduced rating and only a few SMs per arm, is complex, costly and time consuming. In order to understand detailed electro-thermal interaction of the sub-SM level but keeping the system-level phenomena at sight, a reduced-order setup is considered in this work. The proposed setup, shown in Figure 41, allows a detailed study of the operation and control of MMCs, while reducing the complexity of an experimental platform of a complete three-phase of mono-phase MMC. This functionality is achieved at the expense of customised voltage and current control loops that allow the perfect emulation of the typical arm current and SM' capacitor voltages in MMCs.

3.1.2 Simulations and Results

3.1.2.1 Simulation Models

For the MMC topology, simulation models were built for both half-bridge and full bridge sub-module configurations, where the typical multilevel output voltage waveforms and line currents for a point-to-point test system with 10 SMs per arm are shown in Figure 42(a) and the SM capacitor voltages of the upper and lower arms of the three phases are represented in Figure 42 (b). Both voltage are current outputs are fairly sinusoidal, eliminating the need for extensive AC-side filtering as in previous 2-Level VSC applications. The capacitor voltages are balanced through the implementation of a closed loop balancing algorithm with individual voltage feedback, as shown in Figure 41.

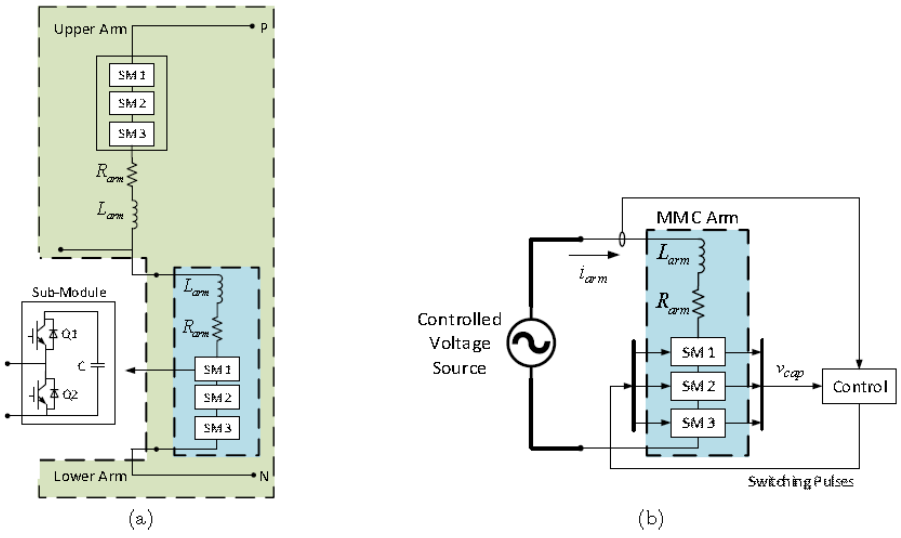

Figure 41: Modular Multilevel Converter Setup: (a) - Complete Phase Leg and (b) - Reduced Arm Setup

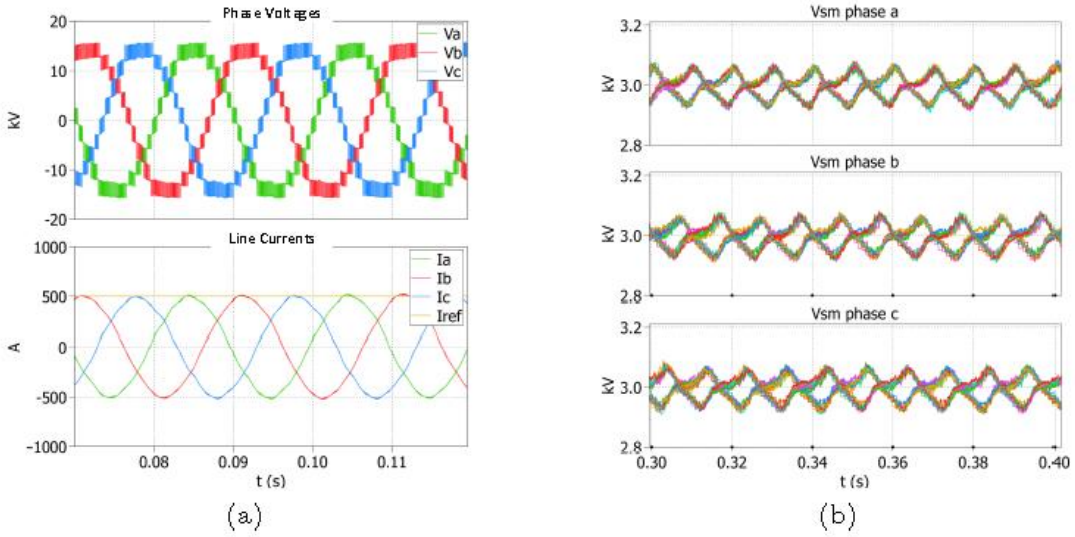

Figure 42: Simulation results for typical electrical quantities in a Modular Multilevel Converter: (a) - Voltage and current output waveforms and (b) - Sub-Module capacitor voltages

3.1.2.2 Experimental Platform

A picture of the complete experimental setup is shown in Figure 43, including the detail of a Sub-Module and the parameters of the MMC Arm are represented in Table 6. The semiconductor modules in each SM are Half-Bridge IGBT Modules FF75R12YT3 commercially available from Infineon. The SMs are liquid cooled as in commercial high power applications, allowing an accurate representation of industrial operating conditions.

The complete system is controlled through a LabVIEW running on a host computer and connected to a National Instrument myRIO board based on a Xilinx FPGA. The FPGA is responsible for the monitoring and control of the electrical quantities in the platform, temperature calculation and data logging.

Table 6: System parameters

Parameter	Value	Unit
Number of Sub-Modules per arm (N)	3	-
Sub-Module Capacitance (C_{SM})	4.7	mF
Arm Inductance (L_{Arm})	3.3	mH
Nominal Sub-Module Voltage ($V_{SM\,nom}$)	50	V
Sub-Module Operating Voltage Limit ($V_{SM\,max}$)	80	V
Nominal Arm Voltage ($V_{Arm\,ref}$)	150	V
Carrier Frequency (f_{sw})	1	kHz
Fundamental Frequency (f_0)	50	Hz
Nominal Coolant Temperature ($T_{Coolant}$)	50	$^{\circ}C$

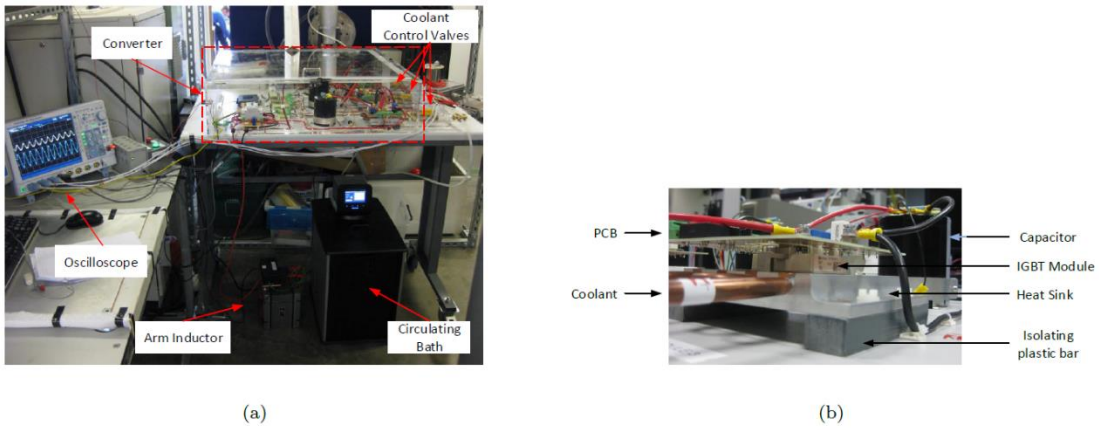

Figure 43: Experimental MMC Setup: (a) Physical assembly and (b) Detail of a sub-model structure

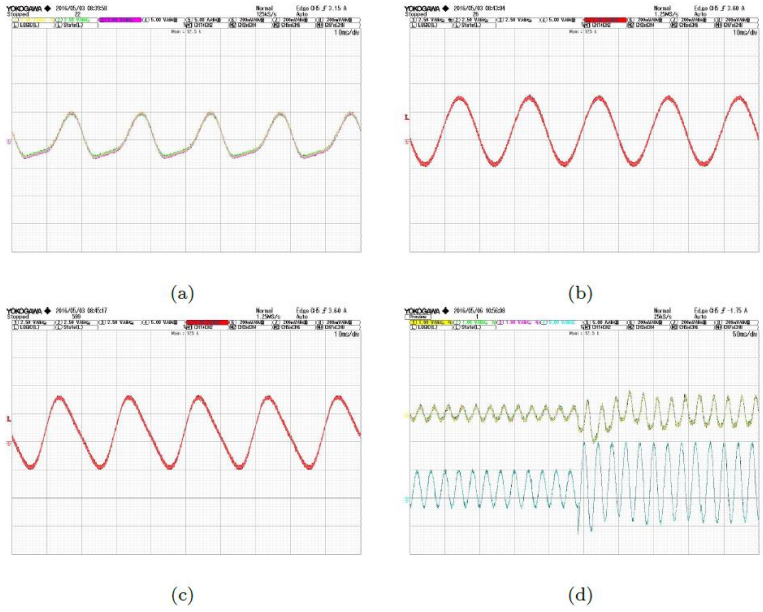

Figure 44: Experimental results of the operation of the Modular Multilevel Converter Arm: (a) Sub-Module voltages; (b) Arm Current without circulating component; (c) Arm Current with circulating component and (d) Response of the Sub-Module capacitor voltages to a step change in the arm current reference.

Figure 44 represents the experimental waveforms for typical electrical quantities in a MMC. Figure 44(a) shows the three capacitor voltages of the sub-modules, which are balanced around a nominal value of 50 V. The arm current, composed by a fundamental 50 Hz frequency component and a dc component is represented in Figure 44(b) and Figure 44(c), with and without circulating current suppression controller enabled. Compared to a three-phase MMC, the reduced-order setup allows a more flexible control with an arbitrary magnitude of any desired harmonic component in the arm current. The response of the capacitor voltages to an arm current step

of 5 A to 10 A s is represented in Figure 44(d) as an example of a dynamic operating condition. As it can be observed, the current magnitude changes promptly and leads to an increase in the capacitor voltage ripple, without changes their average value and therefore remaining the total arm voltage unchanged.

3.1.2.3 Active Thermal Control

The aim of Active Thermal Control strategies is to regulate semiconductors junction temperature and ensure they are kept within safe bounds. As in a MMC the temperature rise is almost entirely due to conduction losses as the low switching frequencies make switching losses small, previous 2-Level thermal control methods acting on the switching frequency are unsuitable. Conduction losses are a function of the current through the IGBTs and diodes in the SMs, therefore the control of the junction temperature in MMCs can only be effectively performed by varying the current magnitude in the SMs, which is, at any moment, common to all the SMs conducting. In this work an additional control loop is proposed to enable the converter control to be sensitive to the junction temperature and ensure that temperature limits are respected at all times by limiting the electrical transmission capability if necessary, i.e. the thermal and electrical limits are defined together and not separately.

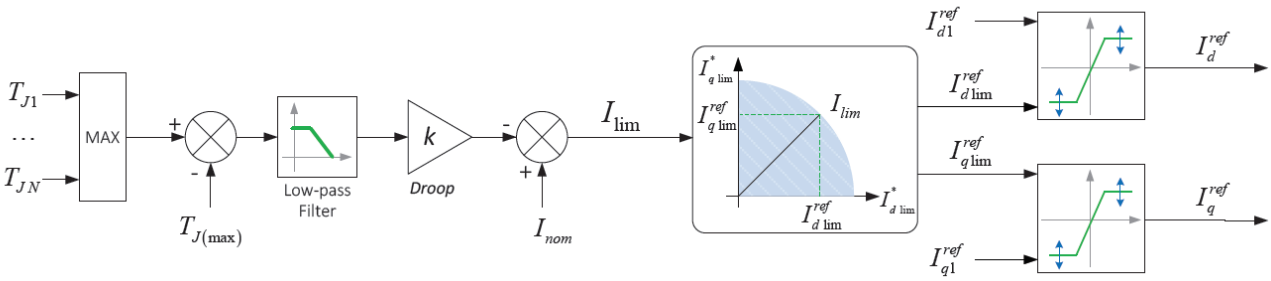

Figure 45: Inclusion of semiconductors temperature in the current control loop of Modular Multilevel Converters.

The proposed control scheme dynamically sets the current limits by following the time behavior of the temperature. The current limit is defined as:

$$I_{lim} = I_{nom} + k \cdot \left(T_{J_{nom}} - T_J\right) \qquad \textbf{Equation 6}$$

Where T_j is the semiconductor temperature estimation, I_{nom} the nominal current limit, i.e. the design current of the system, $T_{J_{nom}}$ is the nominal (threshold) operating temperature of the semiconductors, chosen to take into account their long-term reliability and k is the temperature-current droop constant used to define the decrease in the current limit per unit increase in junction temperature; k is defined so that $I_{lim}T_{Jnom} = 0$.

As represented in Figure 45, the current limit defined by Equation 6 acts directly on the inner current loop of the VSC control, shown in Figure 39, ensuring a fast control of conduction losses and therefore semiconductors

temperature. Only the current limit is modulated and therefore higher level control objectives such as the control of active or reactive power and AC or DC side voltages remain valid. These control objectives are performed through the control of the d- and q- components of the current, I_d^{ref} and I_q^{ref}, respectively, and are adjusted proportionally to their initial magnitudes as the current limit is modulated. As shown in Figure 45 all the individual semiconductor temperatures are fed to the control system and the largest is used as the limiting factor for the dynamic limit control. In both simulation model and experimental setup, a low-pass fillter with a cutoff frequency of 10 Hz was used to remove the temperature fluctuations due to IGBT switching actions but leave the longer-term temperature rises intact. In the experimental setup the temperature information is provided by an embedded thermistor that reflects the semiconductor module baseplate temperature and the junction temperature is calculated from the thermal network provided by the IGBT module datasheet. As the thermal network data is referred from junction to heat sink and not from junction to baseplate, as available from the experimental setup, the temperature dynamics, provided by the thermal capacitances of the thermal network, are not modelled and an instantaneous junction temperature variation is considered. This implies that the only time constant of the junction is provided by the thermistor measurement, which is much slower than the junction. Consequently, an instantaneous temperature variation provides a pessimistic active thermal control framework, ensuring the actual junction temperature will always be below the estimated values.

Current Overload: Figure 46 shows the simulation and experimental results of the response of the proposed active thermal control method represented in Equation 6 to a 30 overload request from 9 A to 15 A. The temperature-current droop was defined as k = 5 A/°C and the nominal current limit was set to $I_{nom} = 13\ A$. The new current order leads to the increase of the junction temperature to a value close to the defined limit of $T_{Jnom} = 100\ °C$. As a consequence, the current limit is decreased and the maximum deliverable current by the converter is limited to 13 A, which can be sustained indefinitely. When the current order is decreased to 10 A, the junction temperature decreases and the current limit increases accordingly.

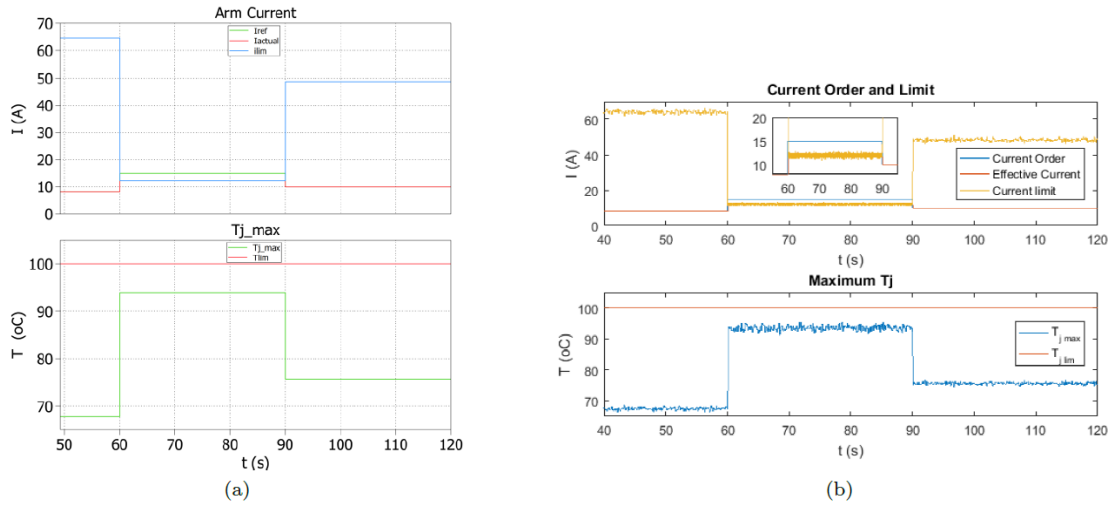

Figure 46: Active thermal control of a Modular Multilevel Converter with an overload request: (a) Simulation Results and (b) Experimental Results.

Cooling system failure: Figure 47 shows the simulation and experimental results of the response of the proposed active thermal control method represented in Equation 6 to a failure in the cooling system of the semiconductor valves. A representative temperature profile of the **coolant** is considered over an extended period to take into account the large thermal time constant of the coolant and cooling system. The profile consists of a temperature ramp-up, representing the temperature increase a result of the cooling system failure, a fixed temperature period representing the action of the redundant cooling pump existing in the converter station, and a ramp down that accounts for the regulation of the coolant temperature back to the nominal operating point, after the redundant pump takes over the function of removing the total heat produced by the semiconductor modules. The duration of each of these three periods is considered to be the same and equal to 300 s. The current order is set to 13 A and remains unchanged throughout the test. As in the previous test, the increase of the junction temperature as a consequence of the cooling system failure leads to the modulation of the current limit. As the junction temperature gets closer to $T_{J_{nom}} = 100\,°\mathrm{C}$, the current limit reaches the nominal value and restrains the effective current delivered by the converter. The current limit is further decreased as the temperature continues to increase and then stabilizes. When the temperature starts to decrease, the current limit increases accordingly and the current delivered by the converter is restored to the set point. Consequently, the proposed active thermal control method can address extreme and unpredictable operating scenarios such as cooling system failures, allowing the safe and continuous operation of the converter by dynamically restraining its transmission capacity, without shutting it down, and keeping its semiconductors temperature within safe operating conditions.

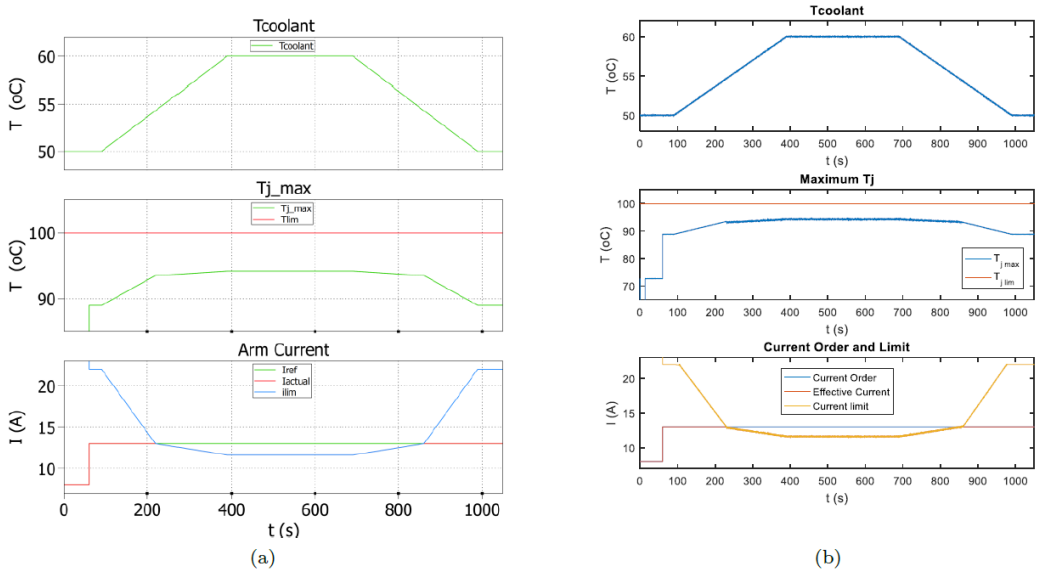

Figure 47: Active thermal control of a Modular Multilevel Converter with a cooling system failure: (a) Simulation Results and (b) Experimental Results.

3.1.2.4 Sub-Module Thermal Regulation

The Sub-Module thermal regulation addresses SM-level thermal imbalances and take corrective measures to correct them. Unlike active thermal control methodologies, which can control the overall maximum and average temperatures in the MMC, eventual semiconductor over-temperatures is SMs are localized and have to be addressed differently.

Although conduction losses are dominant, the localized nature of the SM over-temperature imposes the need for switching loss modulation as a means for temperature regulation. Although notoriously less effectively than conduction loss modulation, and as the low switching frequency cannot be further reduced, SM temperature control can only be performed by modulating its individual capacitor voltage. The effectiveness of capacitor voltage control for individual SM thermal regulation is assess through two case studies: a small and a large disturbance.

Thermal Regulation with Small Disturbance: Two cascaded partial cooling failures occur at SM1 and SM2, at 350 s and 650 s, respectively, using the experimental setup of Figure 43. The restraining of the coolant will lead to a temperature increase with a large time constant, as the partial coolant ow will lead to a small heat absorption from the heat-sink, captured by the accessible temperature measurement in close proximity with the heat sink.

As shown in Figure 48(a), if the thermal balancing is not active, i.e. individual voltage modulation does not occur, when the valve of SM1 is closed, its measured and estimated junction temperatures start to increase. When SM2 valve is partially closed, its measured and estimated junction temperatures increase in a similar manner to SM1. At this point a 5 _C temperature unbalance between SMs 1 and 2 and SM3 exists, both for measured case temperatures and estimated junction temperatures. However if the proposed balancing control is implemented, as represented in Figure 48(b), when the first valve is closed and SM1 temperature starts to increase, its voltage decreases accordingly and the difference to the nominal value of 50 V is equally compensated by SMs 2 and 3. As expected, the large time constant of the cooling imposes a slow response for temperature regulation when compared with voltage and current control functions of the converter.

Although the measured temperatures are different, as seen in the bottom graph of Figure 48 (a), the voltage regulation equalizes the junction temperatures of the three SMs (middle plot). As the individual voltages are below their maximum value, further unbalances can be accommodated.

This is exploited when SM2 also suffers a partial cooling failure similar to SM1. As SM2 temperature increases, its voltage is regulated to a smaller magnitude, similarly to SM1. However, if only SM3 accommodated the additional burden, the thermal unbalance could not be corrected as it would only be transferred to this SM. Therefore, both SMs 1 and 3 participate in the voltage sharing process.

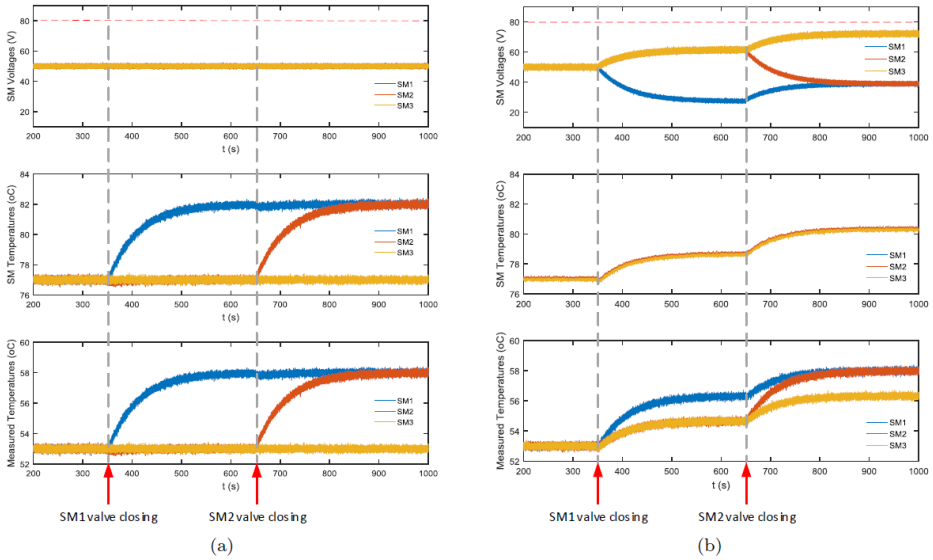

Figure 48: Response of Sub-Modules voltages and temperatures to a 10 °C disturbance: (a) Without thermal regulation and (b) With thermal regulation.

While SM2 temperature increases and its voltage is reduced, SM1 and SM2 voltages will increase until a thermal balance is achieved. As SM1 and SM2 suffered similar partial cooling failures of 5°C, the measured temperatures will tend to the same value, regulating their individual voltages accordingly until a thermal equilibrium is reached. This leaves SM3 with a higher voltage than other SMs but with a lower baseplate temperature as a result of an unobstructed cooling. Nonetheless, junction temperatures are equalized and thermal balancing is achieved.

Results in Figure 48 show that it is possible to keep the converter operating in a stable manner with moderate unbalanced cooling condition for its SMs.

Thermal Regulation with Large Disturbance: In this experiment two cascaded partial cooling failures also occur at SM1 and SM2, at 350 s and 650 s, respectively. However, unlike the previous experiment, cooling failures are different: 5 °C temperature increase for SM1 and 10 °C temperature increase for SM2. Similarly to the previous case, the effect of partial cooling failures of the individual temperatures of the SMs without regulation is shown in Figure 49(a). Without any control action individual SM temperatures differ significantly, especially between SM2 and SM3.

If the proposed balancing control is implemented, as represented in Figure 49(b), when the first valve is closed and SM1 temperature starts to increase, the algorithm sets the individual SM voltages so that a thermal equilibrium is reached, similarly to the previous case as the thermal unbalance is the same. When the cooling valve of SM2 is partially closed, however, the response of the system differs from the previous case as the unbalance is larger. SM2 temperature will initially increase faster, although the algorithm ensures junction temperatures are balanced. Simultaneously, its voltage is diminished and the difference to the nominal value of 50 V compensated by SM3 and SM1, whose voltage was diminished previously as a result of the first partial cooling failure. At approximately 820 s, SM3 voltage reaches the maximum operating limit of 80 V. As its voltage cannot increase further and SM1 voltage increased the necessary amount to ensure a thermal

equilibrium is reached, SM2 voltage is further decreased in order to ensure the arm voltage is set at 150 V. Although SM1 and SM3 reached a thermal equilibrium, SM2 temperature continues to increase, reaching a steady state value slightly higher than the other SMs.

Compared with the results without thermal regulation, thermal temperature of the hottest SM, SM2, is 5_C lower when the thermal balancing algorithm is implemented.

Results in Figure 49(b), especially in the bottom plot show that it is possible to keep the converter operating in a stable manner for a significantly high thermal unbalance of approximately 10_C following a smaller unbalance of 5_C. Globally, a total unbalance of ≈15°C was shared by only three SMs without violating their electrical operating conditions.

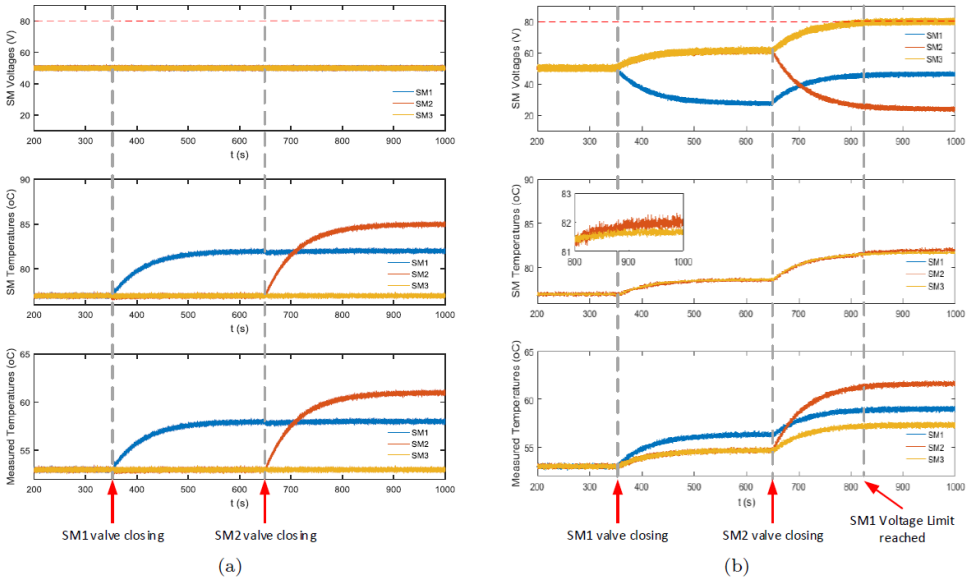

Figure 49: Response of Sub-Modules voltages and temperatures to a 15°C disturbance: (a) - Without thermal regulation and (b) - With thermal regulation.

The experimental voltage measurements results of the voltage regulation for both disturbances that were represented in Figure 48 and Figure 49 can be observed in Figure 50.

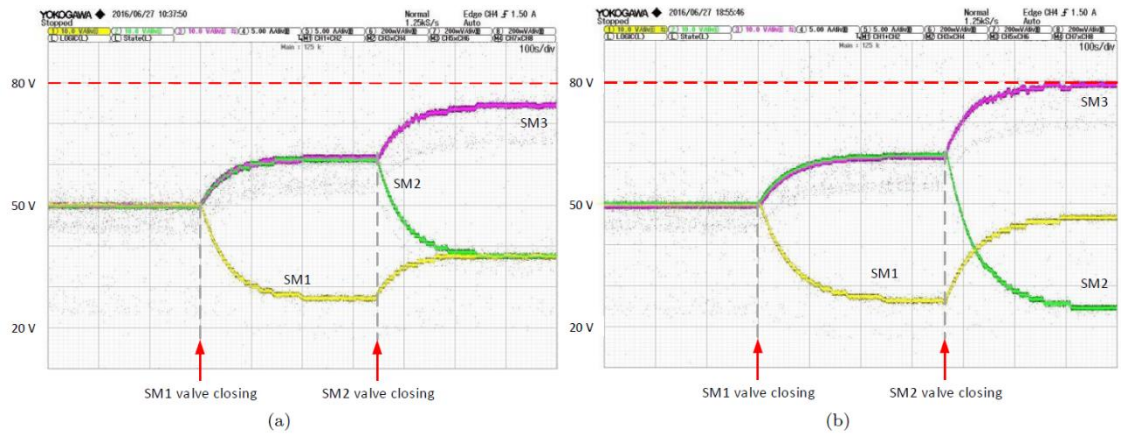

Figure 50: Oscilloscope measurement of Sub-Modules voltages during thermal regulation: (a) Small Disturbance and (b) Large Disturbance. Horizontal scale: 100 s/div; Vertical scale: 10 v/div (-50 V offset).

3.1.3 Summary

The objectives initially set for the ESR within the WP and the overall project were achieved. Specifically, different converter topologies, for 2-Level VSC and half- and full bridge MMCs were implemented in different simulation platforms and benchmarked against results reported in the literature. Due to the high number of semiconductor devices, especially IGBTs and Diodes in recent MMC-based applications, a analysis of semiconductors thermal properties was developed and included on the system-level control of the converter. A method for the active thermal control of MMCs was proposed based on a dynamic rating system cable of coping with abnormal temperature rises and cooling system failures. Extending the application of semiconductors temperature to the system-level, the analysis of the short-term overload capability of semiconductors and its application for an enhanced operation of MMCs was also explored. A thermal control methodology has also been develop to balancing the individual semiconductor temperatures of the Sub-Modules in MMCs, allowing for the total arm voltage to remain constant. Finally, an experimental setup for the investigation of electrical and thermal effects in Modular Multilevel Converters was designed, assembled, tested and used to validate the proposed control strategies to address the initially set objectives.

3.2 Modular Multilevel Converters for power system applications- Abel Ferreira

3.2.1 Introduction

The framework of the research is focused on the investigation of voltage source converters for dc grids, particularly on modular multilevel converter (MMC) performance. Several operating aspects of the MMC were investigated in different chapters of the present document in accordance with the structure pointed out in the Figure 51.

The analysis performed on the MMC for power system applications field, it responds to the following objectives:

Analyze the different **voltage source converter (VSC) topologies proposed by over the years to be applied on the high-voltage dc transmission field (HVdc).** A detailed description of the evolution of the VSC-HVdc topologies is given. Starting from the two-level VSC to the MMC solution, this study shows the trend towards the half-bridge-based MMC systems. This objective is identified on the work structure as the ”Part I: Introduction and literature review”.

Design the control loops for the three-phase-based modular multilevel converters. Due to the converter complexity, first it is emphasized the electric variables that should be con- trolled in order to reach a safe and knowledgeable operation of this power equipment. Then, in accordance with the control requirements of the MMC, the control methodology is de- scribed and mathematically supported. The control approach is then validated during the balanced and unbalanced grid voltage conditions. This goal composes the Part 2 of work, namely the ”Operation and control of the MMC”.

Analysis of the time performance and accuracy of MMC models. The literature reveals that the complexity of the MMC models can be categorized in six groups, from the most to the least accurate. This work analysed two common models and, in addition, it was proposed two converter mathematical models and their features. The validation of those models is accomplished in simulation, by means of steady-state and ac fault behaviour analysis. This task is comprehended in the Part 3 of the thesis, particularly, the ”Performance analysis of the converter”.

Impact analysis of the different strategies followed to rotate the inserted capacitors on the converter performance. The methodology used to balance the energy balance among the capacitors placed in the same stack of the converter greatly affects the converter performance. Therefore, it is studied several cell selection techniques present in the literature. Moreover, it is also proposed and validated a strategy that can further reduce the semiconductor’s power losses and ergo increase the converter efficiency. This task is situated to the Part 3 of the thesis, particularly, the ‘’Performance analysis of the converter”.

Analysis of the semiconductor’s power losses of the MMC. The aim of this work is to describe the power losses produced by the MMC semiconductors over a broad range of steady-state operating conditions. This goal composes the Part IV of thesis, namely the ”Features & applications”.

Analysis of HVdc-design-based half-bridge MMC on the STATCOM operation. In case of a strongly interconnected ac and dc network, the dc transmission grids are expected to be restructured over the time in order to maximize the global power transmission efficiency. Therefore, it is expected that some MMC-terminals can get isolated from the dc grids and, hence, the voltage across their dc poles becomes adaptable. This work investigates the de- grees of freedom of the converter dc poles voltage in terms of the converter control and on its operation performance. Then, a superior performance of the converter is

achievable when- ever its dc voltage value is adjusted. This objective is identified on the thesis structure as the ”Part IV: Features & applications”.

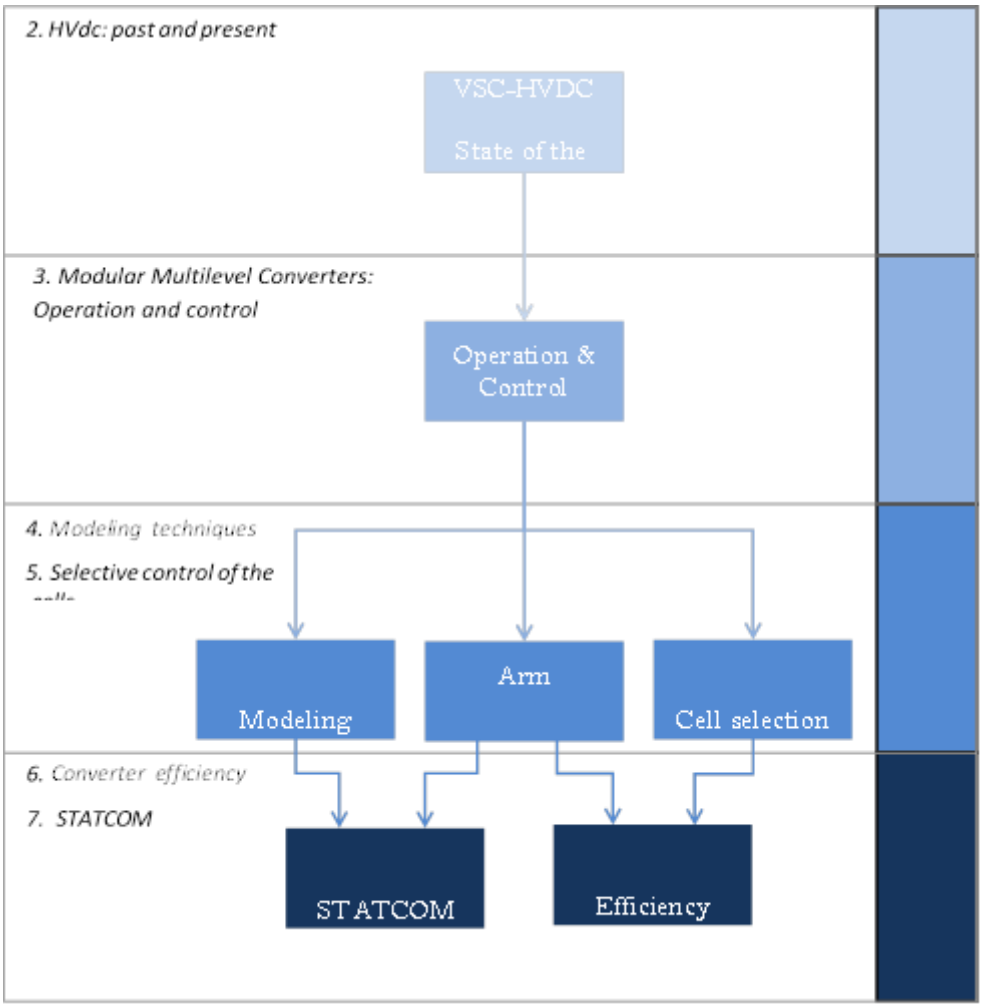

Figure 51: ESR5 work outline

3.2.2 MMC structure

The fourth VSC-HVdc generation is the MMC structure. It was introduced in 2001 on the academia but, it was first commercialized on the HVdc field in 2010 in the *Trans Bay* project. The sketch of the MMC structure is illustrated in Figure 52.

The converter is composed by the series connection of small-scaled power converters designated as submodules (SM) or cells. In opposition to the previous versions of VSC-HVdc projects, on which the semiconductors were aggregated in series, on the original-version of the MMC hundreds of series connected

choppers were used. The series connection of the submodules are typically designated as stacks or the arms of the converter.

The operating principle of this converter structure is the variation of the series-connected number of low-voltage-rated capacitors over the time in each arm, by means of IGBT-based switches present on the SMs. This action intrinsically synthesizes the voltages across the converter arms and legs, which is a required action to manage the voltage at its ac and dc buses.

As the number of capacitors are assembled on the MMC increases, more voltage steps are avail- able at the stack's voltage and accordingly at the converter output. The main achievement of this converter structure is that overcome the challenge of the simultaneous firing the series connection of semiconductor switches, the bottleneck of the previous VSC-HVdc solutions. Moreover, the capacitors and the semiconductor switches of the cells are then designed to withstand only few kV (less than 2 kV), a common voltage rating value in the market. By reason of this structure does not employ capacitors in the dc-link, the voltage between the dc poles is managed accordingly with the inserted number of SM's capacitors on each converter leg. In this view, its modular realization permits a flexible design to the particular characteristics of each HVdc project. Once a SM design is achieved, the adaptation between MMC-HVdc-based projects is done by adjusting the suitable number of SMs assembled in each stack.

Furthermore, due to the fact that each capacitor is responsible to a particular voltage step on the converter arms, a MMC composed by hundreds of SMs generate relatively low harmonic content on its ac voltage. This is particularly important because this VSC requires less ac filters than the previous VSC-HVdc solutions. Furthermore, due to its exceptional output voltage waveform, the average switching frequency of the individual cells is considerably small, particularly, each IGBT commutates between 4 and 8 times (100 to 200 Hz), being responsible to generate up to 1% of total losses, the lowest power losses value achieved by a VSC on the HVdc field.

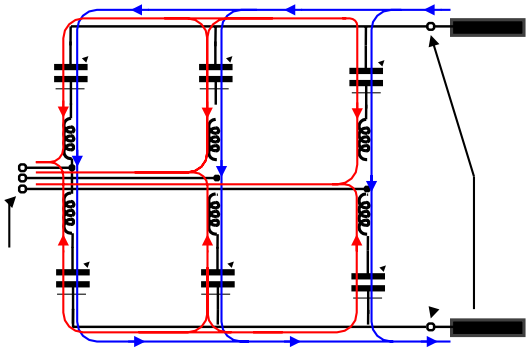

Figure 52: Interactions between the ac and dc sides of the converter.

3.2.3 Operation and control of the MMC

The MMC can operate as a bridge between ac and dc grids, and besides the intrinsic requirements of that feature, it should have additional control algorithms to balance the overall energy storage deviation between the SM's capacitors within the same stack, between its arms and legs. Therefore, it reveals to have an

increased control complexity than the previous VSC-HVdc generations due to its decentralized way to store energy.

To reach a safe operation of the converter, a proper control scheme was proposed for this equipment. Then, besides the standard control loop of the electrical current flow between the converter and its ac grid, additionally, it was also considered the flow of electrical currents that flow between the converter legs to balance the energy storage of the converter among its stacks. To accomplish the controlability of the current that flow on the converter the states of the cells must be permanently revised to maintain the proper power flow between the ac and dc buses of the converter, as emphasized in the Figure 52.

3.2.4 Converter modelling

The introduction of the modular multilevel converters (MMC) supposes a revolution from the electrical point of view because it is composed by a large number of semiconductor's switches. The fact of a HVdc-based converter is characterized by hundreds of electrical nodes, its simulation leads to long simulation periods. Hence, to make the MMC study more affordable, simplified models have been proposed. Depending on the converter analysis that is intended to be carried out, different types of models can be selected.

The MMC models can be classified in respect to their accuracy and inherent computational efforts, introduced by IEEE. The MMC models goes from the type 1 (most accurate) to the type 6 (less accurate). In what concerns the focus of this work, the type 3 and 4 models are the most relevant to be studied. Thus, two literature-based models were studied (TDM and DEM) and compared with two proposed models (SDEM and SDM). The assessment of the simulated models was done in terms of their accuracy and the related simulation lengths retrieved.

The results show that the models proposed are capable to greatly reduce the simulation lengths of the converter, as emphasized in **Figure 53**.

.

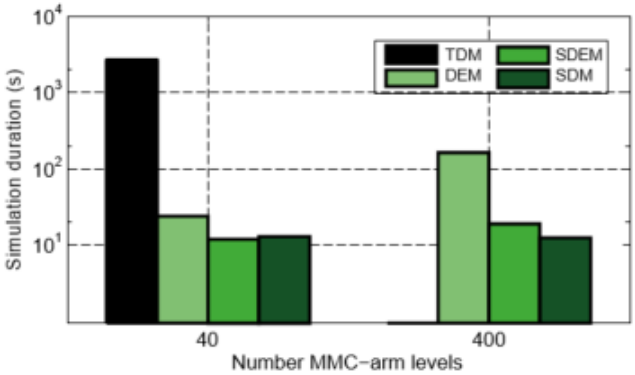

Figure 53: Simulation lengths retrieved by the converter models analyzed.

3.2.5 Selective control of the cells

Once it is defined the required voltage to be applied on the converter arms, the procedure followed to modulate its voltage, as well as, the algorithm embrace to select the suitable capacitors directly impacts on the converter efficiency.

It was reviewed several modulation techniques proposed to be applied on multilevel converters. In addition the impact the injection of zero sequence signals (ZSS) on the arm voltage modulation of the converter was also considered. It was concluded that the presence of the ZSS injection was an higher impact on the converter performance than the methodology followed to modulate the converter arm. The injection of a third harmonic into the modulation, dependently on the amplitude and phase angle chosen for this ZSS, it can increase the linear range of the modulation index or it can minimize the voltage ripple of the capacitors.

Moreover, the injection of the discontinuous ZSS (D-ZSS) on the converter arms modulation can be used to clamp their voltages, as shown in Figure **54**, which can avoid/ eliminate switching events or the semiconductors. Furthermore, by clamping the converter voltages on the intervals that the load stress of the semiconductors is high, it is eliminated the need to rotate the capacitors on the most stressful instants of the semiconductors, improving then the MMC efficiency.

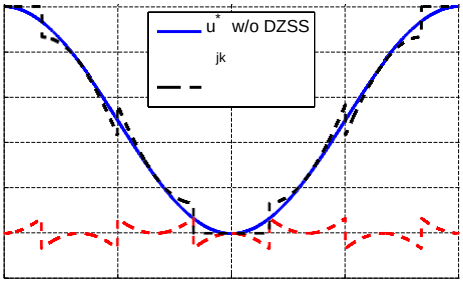

Figure 54: Impact of the DZSS on the normalized arm voltages of the MMC.

The consequent step of modulating the converter arm voltages is the generation of the individual firing signals for the converter switches to synthesize the required arm voltage, in such a way that balances the voltages across the individual capacitors. This is done with the usage of a selective control of the capacitors, which is commonly referred as 'sort & select' algorithm, which is illustrated in Figure **55**. The sorting algorithm ranks the converter capacitors by their voltage $U_{c_{jki}}$. Then, depending on the arm current flow direction i_{jk} being positive/ negative, it is selected the first/ last N^* capacitors of the ranked list. This ensures that the most discharged capacitors would be charged or, in contrast, the most charged capacitor become to discharge. The objective of this algorithm is to balance the energy distribution among the capacitors placed on the same stack.

However, depending on the time instant that the raking list is updated, as well as, the number and procedure followed to select the proper capacitors to be inserted, it greatly impacts on the converter performance. Several literature methods have being compared, and two new hybrid strategies were proposed in order to further curtail the semiconductor's power losses and endorsing the converter with an higher efficiency.

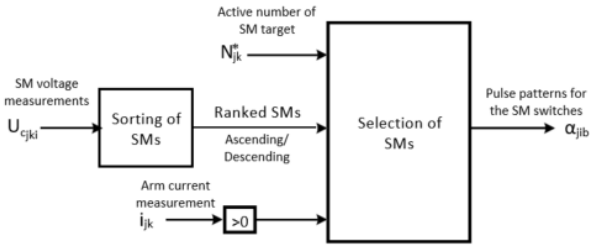

Figure 55: Overall scheme of the classic selection methods.

3.2.6 Converter efficiency

A transversal research question to the current VSC-HVdc solution is its efficiency. Then, it was analysed the ac power flow impact on the converter efficiency, whenever the MMC operate from 0.1 to 1 pu. On the inverter mode of operation, the IGBTs are the devices that mainly guide the arm currents (see Figure 56(a)). In contrast, it was concluded that on the rectifier mode of operation, the diodes are the most stressed semiconductor devices (see Figure 56(b)).

Then, due to the technological features of the diodes and the IGBTs, whenever both are conducting the same magnitude of electrical current, the diodes present lower voltage drop than the IGBTs, which intrinsically generate lower on-state losses than the IGBTs. Thus, as the Figure 56 corroborates, the total losses generated by the MMC on the rectifier are diminished when compared to the inverter modes.

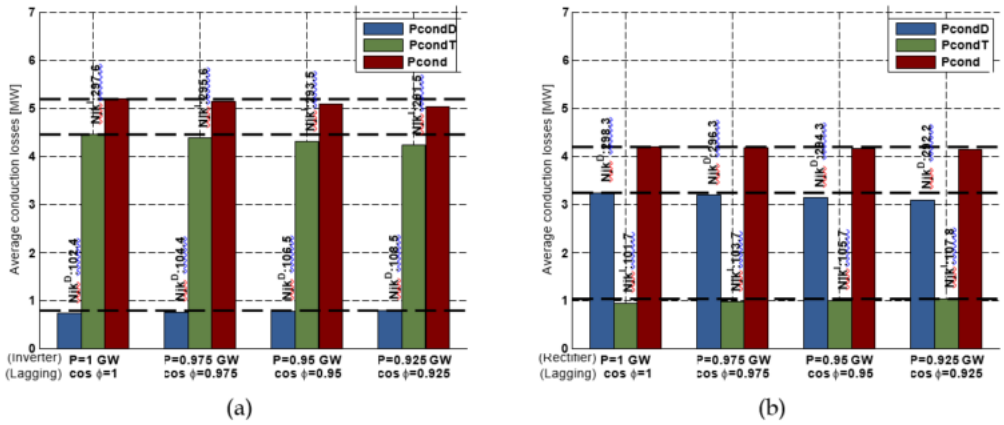

Figure 56: Power losses generated by the MMC semiconductors: (a) inverter and (b) rectifier mode

Moreover, it was also investigated that exist a considerable asymmetric power loss distribution among the upper and lower switches of the half-bridge cell. If it is taken an insight on the operation of one arm (see Figure 57(a)), the arm peak current closely matches with the lower peak of the capacitors insertion index. This means that the higher load of the semiconductors occur at the instant that most of the cells are bypassed (instant t=1.28 s in Figure 57 (b)), then, the current is driven by the lower switches of the cell (IGBT/inverter mode or diode/rectifier mode).

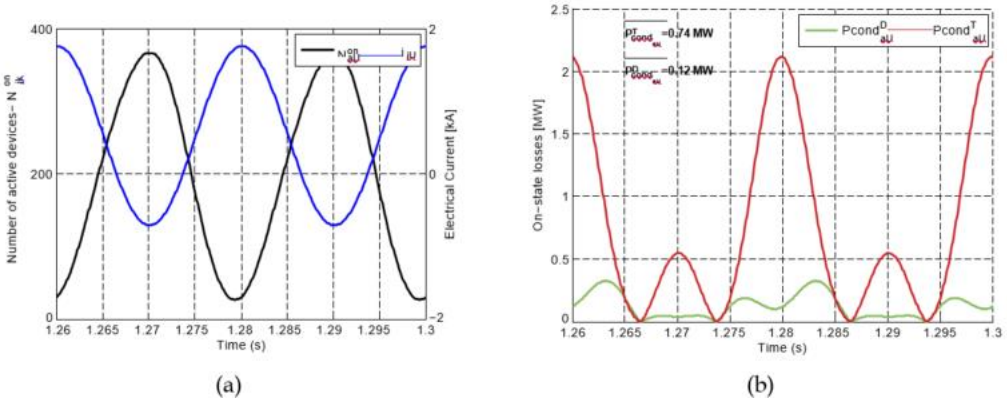

(a) (b)

Figure 57: Power losses generated by the semiconductors assembled in one stack: (a) insertion index vs arm current and (b) on-state losses during the inverter mode

3.2.7 Converter efficiency

In case of a strongly interconnected ac and dc network, the dc transmission grids are expected to be re-structured over the time in order to maximize the power transmission efficiency. In this vision, in some grid configurations, eventually, it is more efficient to transmit power in ac than dc. Therefore, some of the existing HVDC-based MMCs could be sectioned and, consequently, they become isolated from the dc grid. Hence, by endowing those MMC-based dc grid converters with the static synchronous compensation (STATCOM) operating mode, more valuable they become whenever they get split from the correspondent dc grid.

Once the converter becomes slit from a dc grid, its dc voltage target become less-restrictive, and can be changed to guarantee a better performance of the converter. In the converter control perspective, several options are available to modify its dc voltage value, such as, the modification of the individual voltages of the submodules and the mean voltage generated on the converter arms. The converter performance in terms of switching frequency, capacitor's voltage ripple and number of voltage steps in its output was discussed.

The impact of the mean voltage generated on the converter arms (k factor). As well as, the amplitude of the stack voltage U_{jk}^{Σ} were studied and the results were normalized in respect of the converter nominal conditions and are illustrated in Figure 58. Observing the impact of both factor, although some values generate the same DC voltage, it is clear that the converter performance is affected in different ways. It is evident that the reduction of the mean voltage of the arms has a significant impact on the switching frequency and voltage ripple reduction Figure 58. In opposition, by reducing the energy storage of the converter, it is significantly increased the number of voltage levels produced in each stack, which directly increases the power quality of the converter, with the cost of increasing the switching frequency of the converter Figure 58. Furthermore, if the converter can safely withstand higher voltage amplitude than $U_{jk}^{\Sigma} = 640\ kV$ in the respective arms, it is also an interesting option. Besides enabling a higher storage, this action also reduces the average switching frequency of the converter due to the capacitor's voltage increase.

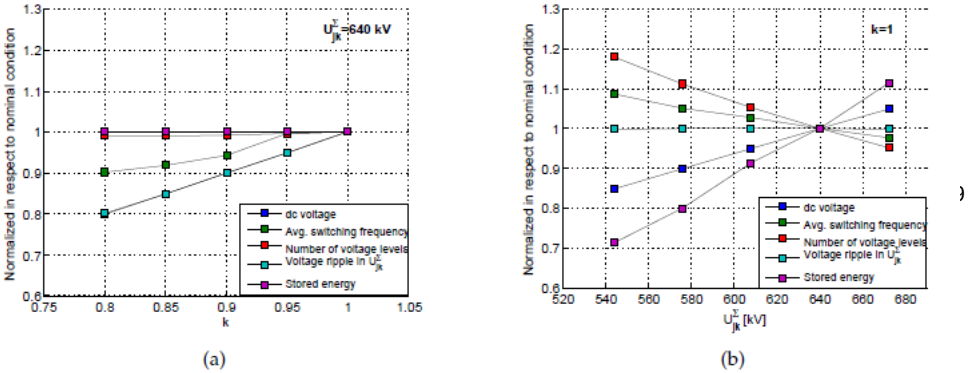

(a) (b)

Figure 58: Impact of the DZSS on the normalized arm voltages of the MMC.

Under the circumstances, on one way, the *k* factor can be used to increase the converter efficiency, as well as, the reduction of the voltage ripple of the capacitors. On the other hand, the energy storage of the converter can be handled in such a way that increased the number of voltage leve3ls on the arms, which translates to the increase of the power quality of the converter. However this option compromises the average switching frequency of the converter. Finally, depending on the converter performance required, the appropriate solution should be used.

3.2.8 Conclusions

Several studies for improving the operation of the modular multilevel converters systems have been investigated in this work. Moreover, the degrees of freedom of this technological solution were investigated, such as the requirements for the electrical variables control, the flexibility allowed on the converter voltages synthetization, its efficiency and its applications as the STATCOM mode. These fields were then explored and the main findings throughout the work was disseminated in the following international publications:

Journal papers:

J1 Abel Ferreira, Carlos Collados, Oriol Gomis-Bellmunt, ”Modulation Techniques applied to Medium Voltage Modular Multilevel Converters for Renewable Energy Integration”, submitted to Elsevier Renewable and Sustainable Energy Reviews, Jan., 2016.

J2 Abel Ferreira, Oriol Gomis-Bellmunt, ”Modular Multilevel Converter losses model for HVDC applications”, submitted to Elsevier Electrical Power System Research, Mar., 2016.

Conference papers:

C1 Abel Ferreira, Oriol Gomis-Bellmunt, Miquel Teixido´ , ”Modular multilevel converter modeling and controllers design”, European Conference on Power Electronics and Applications (EPE’14-ECCE Europe), Lappeenranta (FIN), 2014.

C2 Abel Ferreira, Rodrigo Teixeira-Pinto, Oriol Gomis-Bellmunt, Miquel Teixido´ , ”Elimination of MMC Differential Currents via a feedback LTI control sys- tem”, International Conference on Power Electronics (ICPE’15-ECCE Asia), Seoul (KOR), 2015.

C3 Abel Ferreira, Carlos Collados, Oriol Gomis-Bellmunt, Miquel Teixido´ , ”Modular multilevel converter electrical circuit model for HVdc applications”, European Conference on Power Electronics and Applications (EPE’15-ECCE Europe), Geneva (CHE), 2015.

C4 Abel Ferreira, Oriol Gomis-Bellmunt, Miquel Teixido´ , ”Grid power flow impact on the on-state losses of the modular multilevel converter”, International Conference on AC and DC Power transmission (IET’16-ACDC), Beijing (CHI), 2016.

C5 Abel Ferreira, Oriol Gomis-Bellmunt, Miquel Teixido´ , ”Comparison of Cell Selection Methods for Modular Multilevel Converters”, IEEE International Conference on Environment and Electrical Engineering (IEEE EEEIC’16), Florence (ITA), 2016.

C6 Abel Ferreira, Oriol Gomis-Bellmunt, Miquel Teixido´ , ”HVDC-based modular multilevel converter in the STATCOM operation mode”, European Con- ference on Power Electronics and Applications (EPE’16-ECCE Europe), Karlsruhe (GER), 2016.

C7 Abel Ferreira, Oriol Gomis-Bellmunt, Miquel Teixido´ , ”Adaptive discontinuous zero sequence signal for modular multilevel converter applications”, European Conference on Power Electronics and Applications (EPE’16-ECCE Europe), Karlsruhe (GER), 2016.

C8 Antonio Martins, Filipe Pereira, Vitor Sobrado, Adriano Carvalho, Abel Ferreira, ”Design and implementation of a microgeneration system including storage”, International Conference on Compatibility and Power Electronics (CPE), Lisbon (POR), 2015.

C9 Antonio Martins, Joao Faria, Abel Ferreira, ”FPGA-based Implementation of a Fundamental Frequency Modulation Algorithm for Cascaded H-Bridge Inverters”, IEEE International Conference on Environment and Electrical Engineer- ing (IEEE EEEIC’16), Florence (ITA), 2016.

4. Relaying protection

4.1 Distance protection of networks supplied from Multi-Terminal DC Grids- Mohammad Meraj Alam

4.1.1 Objective

The main goal of this Project work is to investigate the impacts of Voltage Source Converter (VSC)–High voltage DC (HVDC) system on the distance protection of transmission lines following the network guidelines for HVDC connections of reactive current support during the fault using mathematical, offline simulation and real time simulation methods. The effect of the converter dynamics, fault location, fault resistance, limitation strategies of the converter, fault types and grid codes on the distance relay is also studied by analyzing the apparent impedance trajectory on RX plane and performing a closed loop test in Real Time Digital Simulator (RTDS). The distance relay is assessed during symmetrical and asymmetrical faults on a transmission line connected to VSCHVDC.

Furthermore, the research proposes a novel solution to the problem faced by the distance relays in the form of adaptive reach settings selection algorithm when the network consists of VSC-HVDC system. The proposed solution has been tested and validated in a closed loop using RTDS and commercial distance relays.

4.1.2 Introduction

Power System quite often are exposed to major as well as minor disturbances. The large magnitude of fault current associated to short circuits can even damage equipment's like generators, transformers, transmission lines etc. unless they are protected by relays and circuit breakers to isolate such short circuit from the power system. When a fault occurs in an element of power system, protective devices must operate as quickly as possible within 2 or 3 cycles to isolate the fault and maintain the overall healthiness of the system. If a fault is not cleared within the required time then it can lead to heavy damage to the system and its components [74]. One of the main objective of Transmission System Operator (TSO) is to maintain continuity of Electricity supply, which can be achieved by the installation of protective relaying devices and circuit breakers. The protective relaying devices are responsible for the correct identification of fault, an accurate estimation of fault location and selective operation of the circuit breakers in order to eliminate the faulty elements from the power system and minimize the adverse impact of faults [75].

Nowadays ac grid, which constitutes thousands of kilometers of transmission lines (UHV, EHV and HV) also accommodates HVDC technology so as to transfer bulk amount of electrical power over long distances offering many other benefits including interconnecting major electrical grids as tie-lines and supplying offshore wind energy to onshore ac grid. These transmission lines are protected by relays, which are highly reliable, selective and sensitive in nature, for instance, distance protection that forms the backbone of the transmission level protection. However, the distance protection also comes with the major drawbacks of over-reach of distance zones and tripping during overload conditions. These drawbacks led to many major blackouts in the history of power system protection, for instance, USA 2003, Europe 2006 [76]. The incorrect operation of the distance protection was one of the reasons for these blackouts. Furthermore, a recent addition in the list of the problem encountered by the distance protection is due to the reactive current support from the VSC based renewable energy power plants and HVDC system as well as their limited fault current magnitude.

Nowadays, Voltage Source Converter (VSC) based High Voltage Direct current (HVDC) is utilized for the grid integration of offshore Wind Power Plant (WPP) and interconnection of WPPs to each other leading to Multi-Terminal HVDC (MTDC) [77]. Furthermore, one of the important benefits of VSC based HVDC or MTDC is that the onshore VSC's provide reactive current during faults as per the Network Code (NC) decided by the

Transmission System Operator (TSO) to support the network voltage [78]. Furthermore, the power system is changing day-by day by the replacement of Synchronous Generators (SG) with these VSC based renewable energy and HVDC system. This change in the power system is leading to a low Short Circuit Ratio (SCR) and reduced system inertia [79]-[80]. The short circuit current of these converter based renewable energy sources are also different from SG in terms of both magnitude and waveforms and essentially depends upon their control systems [81]. Consequently the network operator is facing challenges in handling the grid protection systems due to this exclusive behavior of VSC, which affects the current and voltage measured by the protective relays during the fault leading to an inaccurate computation of the apparent impedance and malfunction of the distance relay [82]. Hence, it is highly relevant to look into the short circuit behavior of VSC and its impact on the performance of the distance relays in the presence of VSC-HVDC system.

4.1.3 Methodology

In order to achieve the objectives of the research laid down above, a systematic approach to investigate the behavior of the distance protection in the presence of VSC-HVDC is adopted. Apart from the analytical study involving mathematical explanation of the problem, simulation in PSCAD/EMTDC and Closed-Loop test of a commercial distance relay in RTDS is done to evaluate the operation of the distance protection under different system conditions. Later on, a novel solution in the form of adaptive reach settings selection is tested in RTDS as well.

- Analytical Formulation
  - Mathematical estimation of the apparent impedance seen by the relay during single line to ground and double line faults on a transmission line connected to VSC using sequence networks diagrams.

- PSCAD/EMTDC based offline simulations
  - The impact of the reactive current injection, converter current limitation strategy, fault location and fault resistances on the impedance movement on RX plane are simulated using PSCAD electromagnetic transient program.
- RTDS based closed loop testing
  - The behavior of a commercial distance relay is tested in a closed loop using RTDS and signal amplifier to investigate its performance
- Adaptive reach solution
  - A novel adaptive reach settings selection is proposed and implemented in a commercial distance relay using closed loop test in RTDS. The relay performance with adaptive reach settings is compared with the conventional reach setting.

4.1.4 Analytical formulation

A simplified power system consisting of a VSC-HVDC system connected to a transmission line through a delta-star grounded winding transformer is presented in Figure 59. Two distance relays R1 and R2 are located at

both the ends of the transmission line connected to VSC. The grid is represented by transmission lines and Thevenin voltage sources S1 and S2. Figure 60(a) and Figure 60(b) illustrate the positive and zero sequence networks of the simplified power system for a single line to ground on a transmission line. The sequence component of the voltage at the fault point V_F^1 can be derived for the different fault types using sequence networks. Equation 7 gives the positive sequence component of the voltage at the fault location F.

$$V_F^1 = V_{R1}^1 - I_{con}^1(m \cdot Z_L^1) \qquad \textbf{Equation 7}$$

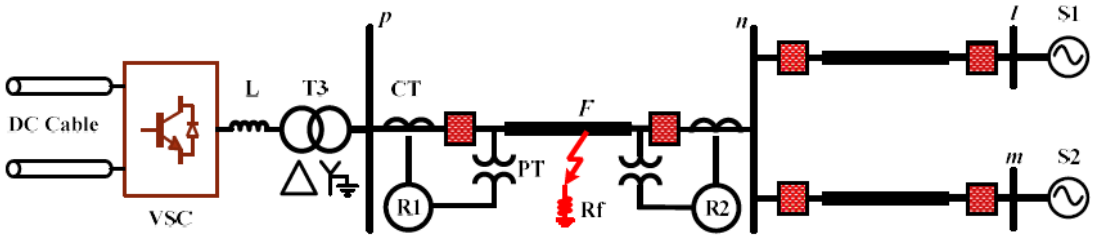

Figure 59: Simplified power system with VSC connected to transmission line

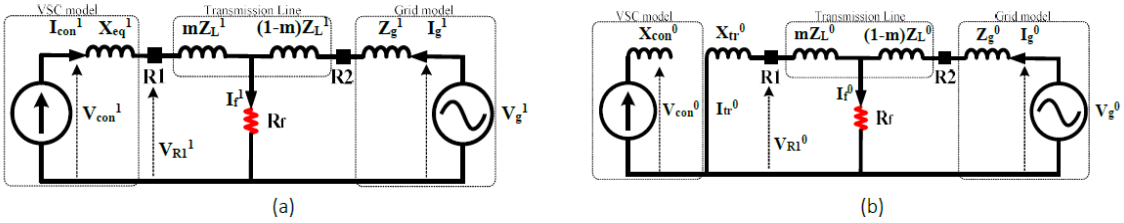

Figure 60: Sequence network diagram of the power system for single line to ground fault. (a) Positive sequence network (b). Zero sequence

The negative sequence voltage V_F^2 at the fault location is given by Equation 8 for single phase to ground. Therefore,

$$V_F^2 = V_{R1}^2 - I_{con}^2(m \cdot Z_L^2) \qquad \textbf{Equation 8}$$

For the zero sequence component of the fault voltage, the converter does not supplies the zero sequence component of the fault current because of the delta-star grounded winding of the transformer, which is evident from the Figure 60(b). The zero sequence voltage V_F^0 at the fault is given by Equation 9:

$$V_F^2 = V_{R1}^2 - I_{con}^2(m \cdot Z_L^2)$$ **Equation 9**

Using Equation 7, Equation 8 and Equation 9, the voltage seen by the distance relay *R1* at the location of the relay can be given by using Fortescue's methodology as Equation 10:

$$V_{R1}^{\alpha} = \mathrm{R_f} \cdot \left(I_{R1}^{\alpha} + I_g^{\alpha}\right) + mZ_L^1(4I_{tr}^0 + I_{con}^1 + I_{con}^2)$$ **Equation 10**

Therefore, the apparent impedance seen by the distance relay for a phase-A to ground fault is given by the Equation 11, utilizing Equation 10 as follows [83].

$$Z_{app}^{AG} = \frac{(R_f + mZ_L^1)I_{R1}^{\alpha} + R_f I_g^{\alpha} + 3mZ_L^1 I_{tr}^0}{I_{R1}^{\alpha} + 3KI_{tr}^0}$$ **Equation 11**

The expression Equation 11 clearly highlights the performance of the distance relay is directly decided by the fault current from the converter I_{R1}^{α}, current contribution from the grid I_g^{α}, zero sequence current through the transformer I_{tr}^0, and the fault resistance R_f.

Similarly, for a phase-A to phase-B fault, the phase-B to ground voltage seen by the distance relay is given by the Equation 12.

$$V_{R1}^b = V_F^b + mZ_L^1(4I_{tr}^0 + a^2 I_{con}^1 + aI_{con}^2)$$ **Equation 12**

Therefore, using Equation 10 and Equation 12, the apparent impedance seen by the distance relay during a phase A-to-phase B fault is expressed in Equation 13 as [10]:

$$Z_{app}^{AB} = mZ_L^1 + R_f\left(1 + \frac{(I_g^a - I_g^b)}{\left(I_{con}^1(1-a^2) + I_{con}^2(1-a)\right)}\right)$$ **Equation 13**

Equation 13 gives an idea about the apparent impedance dependence upon the positive and negative sequence current contribution from the converter, fault current from the grid and fault resistance.

4.1.5 Power System Model

The power system under investigation is a three phase, 50 Hz, 400 kV, modified IEEE 9-bus system with one of the transmission line is replaced by a bipolar VSC-HVDC system, as depicted in Figure 61. The transmission line next to the VSC-HVDC system i.e. Line 1 is subject to symmetrical and asymmetrical faults at different

locations and varying fault resistances. The duration of the fault is 200 ms. The VSC-HVDC system is subject to the reactive current injection during the fault depending upon the Point of Common Coupling (PCC) voltage drop, which is defined by the slope of the line, as presented in Figure 62(a). Moreover, the converter follows a limitation strategy in order to protect the converter from overcurrent during the fault.

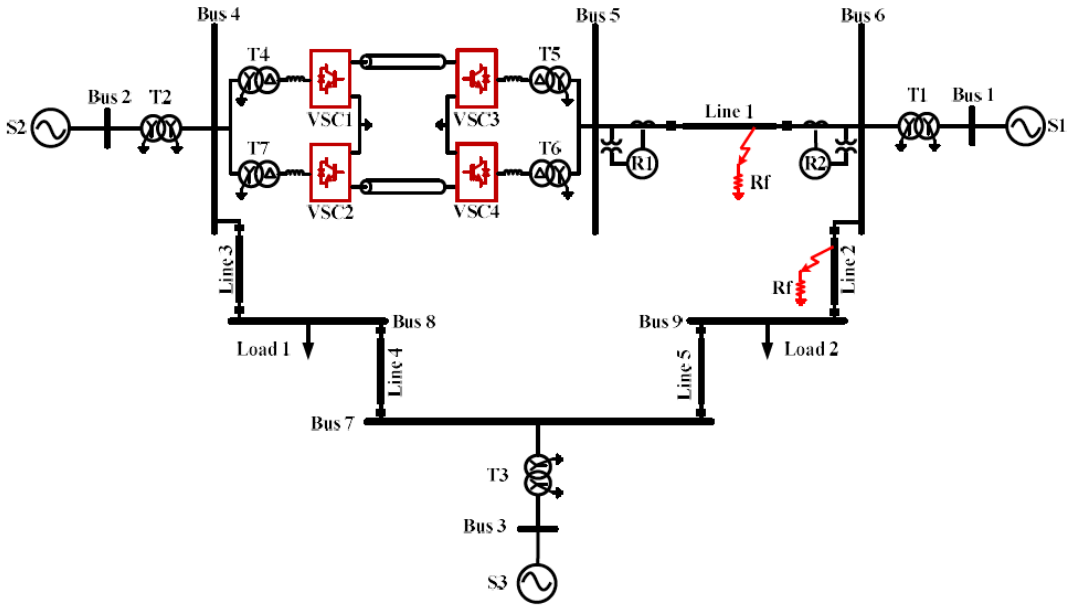

Figure 61: Modified IEEE 9-bus test system

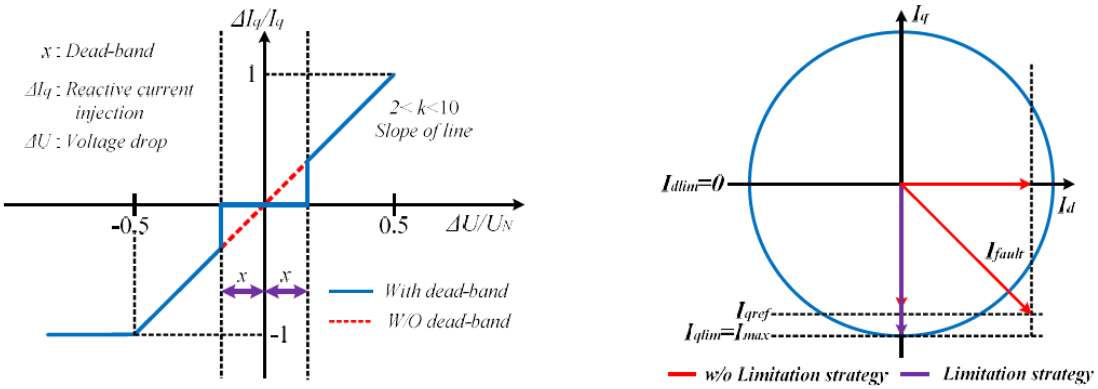

(a) (b)

Figure 62: (a) Reactive current slope for voltage support by the VSC-HVDC system. (b) Current limitation strategy

4.1.6 Voltage Source Converter

The VSC model used in the system is a Modular Multilevel Converter (MMC) in a bipolar arrangement. The rating of each converter is 700 MVA and DC voltage level of the bi-pole is +/- 320 kV. The MMC is controlled using the conventional outer voltage and inner current control. Apart from this, circulating current control and DC voltage balancing control is also implemented.

4.1.7 Reactive Current Support

Modern grid code for HVDC connections require to support the network during any disturbances by injecting the reactive current into the network, which is defined by the slope of the line given by the TSO. This slope of the line (2< k <10) is the proportional gain of the ac voltage controller, as shown in Figure 62 (a). Furthermore, the converter is also associated to current limitation strategies during the fault in order to prevent the converter from the damage. The active current blocking limitation strategy is followed where the active current limit is set equal to zero and reactive current limit is set equal to maximum current of 1.2 p.u., as indicated in Figure 62 (b).

4.1.8 Simulation and Results

Many fault scenarios have been simulated in PSCAD/EMTDC environment following the network guidelines of reactive current injection and current limitation strategy. The fault is simulated on Line 1 for a duration of 200 ms to analyze its impact on the operation of the distance protection.

4.1.8.1 Single Line to Ground Fault

A single line to ground (SLG) is simulated on Line 1 at a distance of 60 km from R1 with Rf equal to 10 Ω. The PCC voltage right after the fault inception drops. The controller shifts the priority from active power control to reactive current support during the fault. The controller of VSC station starts taking control of reactive power depending upon the voltage at PCC. The impedance locus for this single line to ground fault traverses on the impedance plane and enters into zone 1 quadrilateral characteristics.

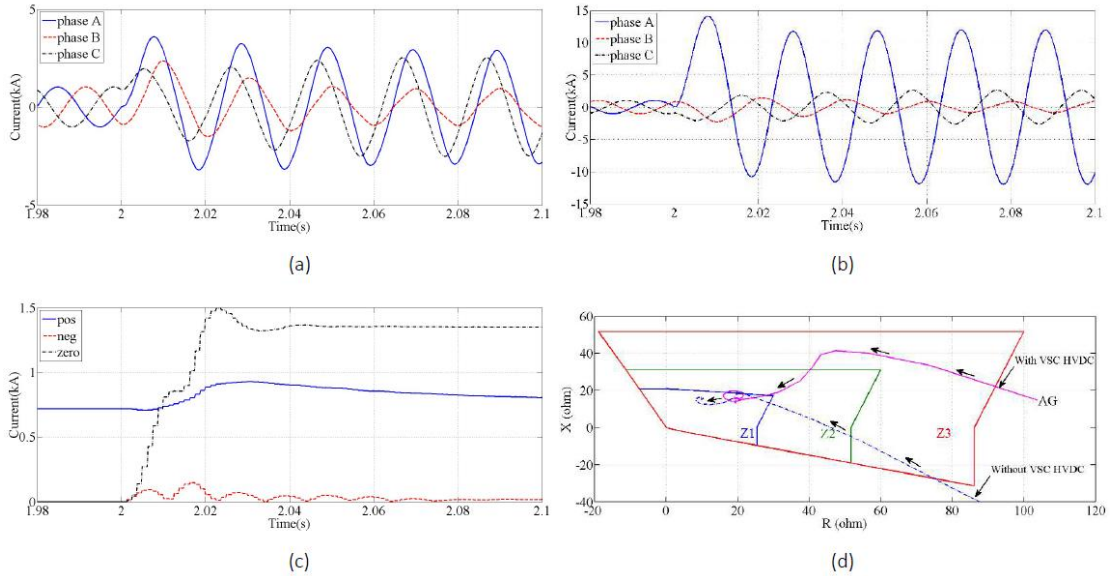

Figure 63: SLG fault on Line 1 at 60 km from R1 with Rf =10 Ω. (a) Current phasor at local relay R1. (b) Current phasor at remote relay R2. (c) Magnitude of sequence current quantities at local relay R1. (d) Impedance trajectory of ground AG element with and without VSC HVDC.

When we examine the behavior of the fault current supplied from the converter for a resistive SLG fault then we observe that the fault current is modest and limited in nature, as presented in Figure 63(a). The phase currents are approximately in the same phase with small phase differences as compared to the remote relay currents shown in Figure 63(b). The remote relay R2 fault currents have sub transient (1 cycle), transient (2-3 cycles), and steady state characteristics. Contrary to this, the local relay R1 currents are devoid of sub transient and transient periods and quickly achieve steady state after the fault. Analyzing the sequence component of the local relay fault currents lead to interesting outcomes, as depicted in Figure 63(c). The negative sequence current, which is a dominating current component in an unbalanced situation, has a highly diminished value, as reflected in Figure 63(c). The apparent impedance highlights relay under reach when compared without VSC-HVDC, as shown in Fig. 5(d) due to reactive current injection.

4.1.8.2 Phase-to-Phase Fault

At t = 2 s, a phase-to-phase fault is simulated on Line 1 at a distance of 60 km (60% reach) from R1. The fault resistance is, $R_f = 10\Omega$. The Point of Common Coupling (PCC) voltage right after the inception of phase A phase B fault drops. The controller priority shifts from active power control to reactive power support during the fault. The controller starts injecting reactive current into the network to alleviate the voltage. Fault currents flowing through the local relay R1 and the remote relay R2, are presented in Figure 64(a) and Figure 64 (b), which indicates that the fault current from the converter is modest and close to the magnitude supplied before the fault inception, and is different from the remote relay R2 current. The apparent impedance seen by the AB element of the distance relay is presented in Figure 64 (c) for a fault at 60 km with $R_f = 10\Omega$, where the locus never enters into zone 1, although, the fault takes place in zone 1 reach of the relay i.e. 60 km. The relay under-reaches during a LL fault with $R_f = 10\Omega$ due to the reactive current injection from the VSC station. Furthermore, when a LL fault is simulated at 120 km from R1 with $R_f = 10\Omega$, the impedance locus of the AB element enters into zone 3 region, as appended in Figure 64 (d).

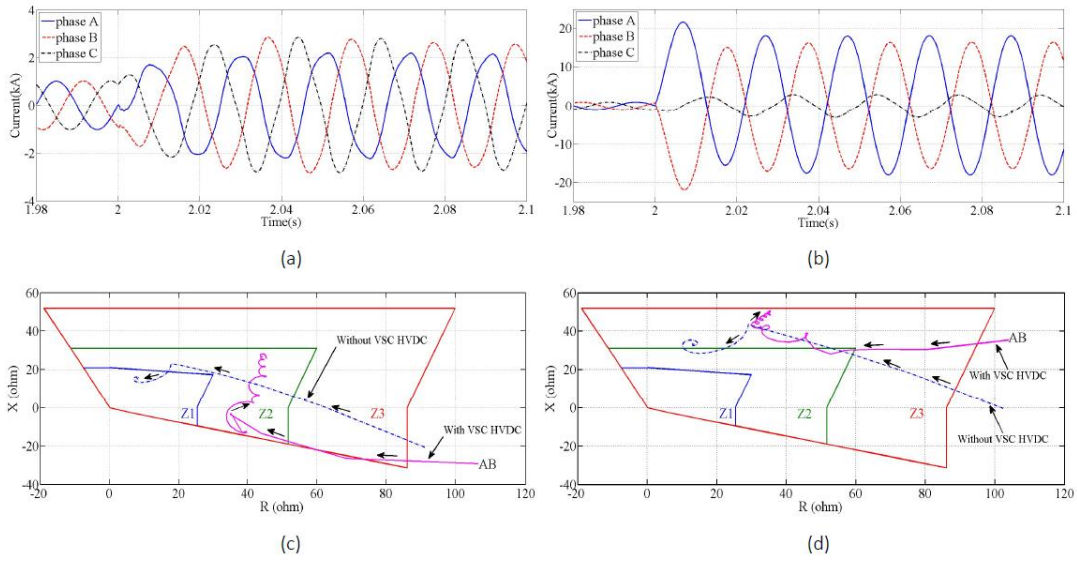

Figure 64: LL fault on Line 1 at 60 km from R1 with $R_f = 10\Omega$ (a) Current phasor at local relay R1. (b) Current phasor at remote relay R2. (c) Impedance trajectory of ground AB element for fault at 60 km. (d) Impedance trajectory of ground AG element for fault at 120 km HVDC.

4.1.9 Experimental Setup and Results

A closed-loop experimental setup has been established using RTDS, a voltage and current signal amplifier (DOBLEF 6350e), and a commercial distance relay (EFACEC TPU L500) in order to observe the performance of the distance relay, as presented in Figure 65 [84].

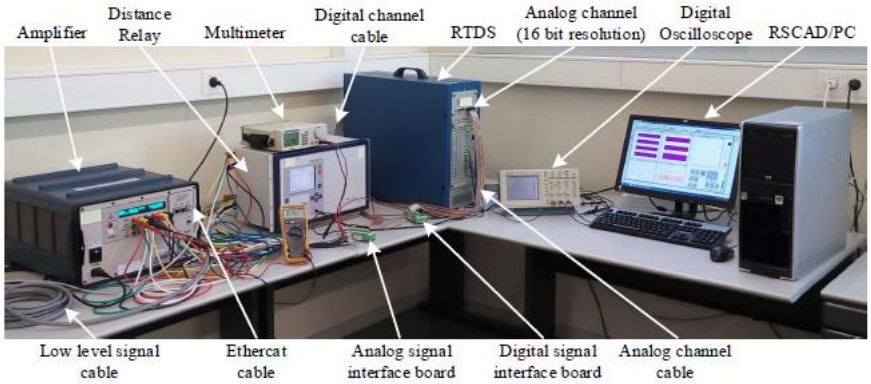

Figure 65: Experimental closed-loop test setup using RTDS, signal amplifier and distance relay

The setup of closed-loop test in RTDS involves following steps:

- Model the power system with VSC-HVDC system and its controller in RTDS.
- Configure the CT and PT and send the current and voltage signals measured by the relay at the analog output channel of RTDS.
- Amplification of the obtained current and voltage signals from the RTDS using F6350e signal amplifier.
- Pass the amplified current and voltage signal from the amplifier to the commercial distance relay TPU L500.
- The trip signals from the relay are supplied back into the RTDS to control the Circuit Breaker (CB) operation.

The distance relay performance is observed for different modes of operation of VSC, different fault types, fault locations, fault resistances and tele-protection in RTDS. Figure 66(a) presents the operation of the distance relay with and without VSC-HVDC. The commercial distance relay performs correctly with the VSC-HVDC when the fault resistance is 0.1 ohm. The reach of operation of the relay with VSC matches exactly without VSC for the forward fault in both the modes of operation (inverter and rectifier), as depicted in Figure 66(a). On the other hand, when the fault resistance increases to 10 ohms, the distance relay reach drops and it shows an under reach, depicted in Figure 66(b). It can be seen from the figures that the relay operation is limited to 0.75 p.u. of active power transfer in both the modes of operation. For the case of VSC-HVDC, the relay is not able to operate correctly for faults located at a distance more than 60 km. This gives a case that if there is a fault at 75 km from R1 with $R_f = 10\Omega$, the relay under reaches and does not operate. Similarly, many other fault scenarios have also been simulated in RTDS for communication assisted distance protection such as Permissive Under reach Transfer Trip (PUTT) and Permissive Over reach Transfer Trip (POTT) scheme, where the relay close to VSC does not function properly.

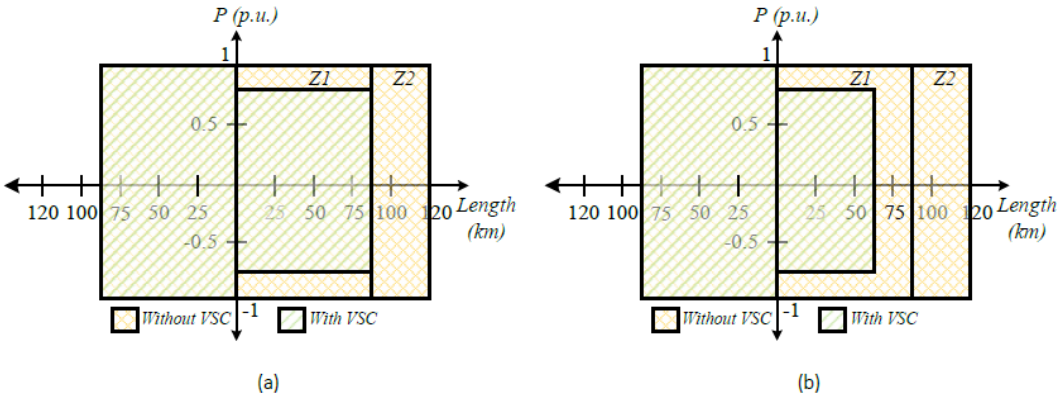

Figure 66: Distance relay operation for SLG fault (a) Fault resistance of 0 Ohm, (b) Fault resistance of 10 Ohm

4.1.10 Adaptive Reach Protection

The problem encountered by the distance protection of transmission line connected to VSC-HVDC during any symmetrical and asymmetrical faults due to the reactive current support and current limitations to protect the converter from the overcurrent scenario has been studied analytically, simulation and real time closed loop test.

In order to mitigate the impact of VSC-HVDC dynamics on the distance-relaying scheme, adaptive reach setting selection methodology has been proposed and implemented in a commercial distance relay. The adaptive reach setting takes into account the presence of VSC in the power system and computes the bus impedance matrix (ZBUS). The matrix gives the PCC pre fault voltage, which is updated when the VSC injects the reactive current into the network after the fault. The updated value of the PCC voltage and the current flowing through the relay based on the limitation strategy is utilized to calculate and select the reach setting of the distance relay. The relay will select the reach setting once a fault occurs. Table 7 and Table 8 presents the distance relay behavior during single line to ground fault at 60 km from R1 with adaptive protection at different fault location and fault resistance, respectively.

Table 7: Distance relay performance for different fault locations from R1 with fault resistance 10 Ω

Location (in km)	Zone 1	Zone 2	Zone 3
50	x	-	-
70	x	-	-
90	-	x	-

Table 8: Relay performance for phase A to ground fault for different fault resistance with location = 60 km from R1

Resistance (in km)	Zone 1	Zone 2	Zone 3
0	x	-	-
10	x	-	-
20	x	-	-

The tabular results with adaptive protection highlights the correct operation of the distance relay for different working scenarios. The relay trips for zone 1 when the fault takes place at 50 and 70 km and on the other hand, it does not trip for zone 1 when the fault is at 90 km. Similarly, for the fault situation with the different fault resistance, it also works correctly.

4.1.11 Conclusion

This work unveils that the distance protection of transmission lines connected to VSC-HVDC fails to operate during symmetrical and asymmetrical faults, when the converter provides reactive power to the network as identified by the network guidelines for HVDC connections. The relay performance is first identified analytically, which highlights the effects of the sequence components of fault currents from the VSC and the grid. Later on, simulation studies have been performed in PSCAD platform to investigate the apparent impedance seen by the relay. The relay performance is also tested in real time test bench using RTDS close loop test. An adaptive reach settings selection methodology is implemented in a commercial relay as a solution to this problem.

4.1.12 References

[74] D. Tziouvaras, "Relay Performance During Major System Disturbances," in Protective Relay Engineers, 2007. 60th Annual Conference for, 2007, pp. 251-270.

[75] D. Novosel, G. Bartok, G. Henneberg, P. Mysore, D. Tziouvaras, and S. Ward, "IEEE PSRC Report on Performance of Relaying During Wide-Area Stressed Conditions," Power Delivery, IEEE Transactions on, vol. 25, pp. 3-16, 2010.

[76] PES-PSRC. (2009). Application of Overreaching Distance Relays [online]. Available: http://www.pespsrc.org/Reports/D4_Application_of_Overreaching_Distance%20_Relays.pdf.

[77] N. Flourentzou, V. G. Agelidis, and G. D. Demetriades, "VSC-Based HVDC Power Transmission Systems: An Overview," Power Electronics, IEEE Transactions on, vol. 24, pp. 592-602, 2009.

[78] ENTSO-E. (2015, Oct.). Establishing a Network Code on Requirements for Grid Connection of High Voltage Direct Current Systems and Direct Current-Connected Power Park Modules [online]. Available:https://www.entsoe.eu/Documents/Network%20codes%20documents/NC%20HVDC/HVDC_110915_Final_Provisional_Voted.pdf.

[79] A. Egea-Alvarez, S. Fekriasl, F. Hassan, and O. Gomis-Bellmunt, "Advanced Vector Control for Voltage Source Converters Connected to Weak Grids," IEEE Transactions on Power Systems, vol. 30, pp. 3072-3081, 2015.

[80] P. Tielens and D. Van Hertem, "The relevance of inertia in power systems," Renewable and Sustainable Energy Reviews, vol. 55, pp. 999-1009, 3// 2016.

[81] A. Hooshyar, M. A. Azzouz, and E. F. El-Saadany, "Distance Protection of Lines Emanating From Full-Scale Converter-Interfaced Renewable Energy Power Plants—Part I: Problem Statement," Power Delivery, IEEE Transactions on, vol. 30, pp. 1770-1780, 2015.

[82] M. M. Alam, H. Leite, and A. S. Carvalho, "Investigating Distance Relay Behaviour on an EHV AC Lines Connected with Voltage Source Converter Based HVDC," in Proc. CIGRE Symp., Across Borders HVDC Systems And Market Integration, Lund, Sweden, 2015.

[83] M. M. Alam, H. Leite, J. Liang, and A. S. Carvalho, "Effects of VSC Based HVDC System on Distance

Protection of Transmission Lines,"International Journal of Electric Power and Energy System (revision stage), 2017.

[84] M. M. Alam, H. Leite, N. Silva, and A. S. Carvalho, "Performance Evaluation of Distance Protection of Transmission Lines Connected with VSC-HVDC System Using Closed-Loop Test in RTDS," Electric Power Systems Research (under review stage), 2017.

4.2 Solid-state HVDC circuit breakers and fault clearing in multi-terminal HVDC grid- Ataollah Mokhberdoran

4.2.1 Introduction

4.2.2 Overview

Many studies show technical and economic benefits of VSC-based MTDC grid but the main barrier against implementation of MTDC network is its high vulnerability against DC short circuit fault. Typically, power converters with better economic performance are defenseless against short circuit fault in their DC side. For instance, half bridge modular multilevel converter (MMC), which has less semiconductor switches and less power losses as compared to other types of MMC is unable to block the DC fault current. Therefore, development of fast HVDC circuit breakers (DCCBs) is strongly required to protect the power converter stations [85]-[86].

On the other hand, fault tolerant VSCs can prevent DC fault current from propagation over the grid and provides reactive power support for AC grid during a DC short circuit fault. However, these converters require higher number of semiconductor switches thus dissipate higher amount of power. Therefore, in addition to larger initial capital, they may cause higher operational costs. Moreover, the fault tolerant converters have not been yet tested practically in industrial scale. The requirement for DCCBs can be reduced by application of fault tolerant converters but it cannot be eliminated [92].

High DC current interruption has been an engineering challenge since the dawn of HVDC technology. Due to the absence of natural zero crossing point in DC current, conventional AC circuit breakers become useless for DC applications. The early research in this field led to development of mechanical HVDC circuit breakers (MCBs) in 70s. The action time of traditional MCBs lies in range of 40 to 60 ms. Although recent developments have reduced the interruption time in MCB below 10 ms, their full scale implementation cost is still unclear [86].

In last decades, attempts include research on solid-state and hybrid DCCBs. The hybrid DCCB (HCB) has low power losses and fast current interruption performance. Although the solid-state DC circuit breakers (SSCBs) have higher power losses as compared to the MCB and HCB, they are technically attractive due to their ultra-fast current interruption performance [4]. Moreover, the improvements and expectation for more advances in field of high power semiconductor switches and also wide-band gap devices can be listed as the main motivations of research on the SSCBs. Furthermore, the HCBs utilize a solid-state breaker branch to interrupt the fault current and therefore, improvements in the SSCB technology may also advance the performance of HCBs [86].

4.2.3 Objectives

SSCBs can be considered as potential solution for protection problem in MTDC grid. However, these type of DCCBs require large number of semiconductor switches in their structure, which makes their realization costly. Also, there are several other technical issues that should be investigated and addressed in design and development of SSCBs. This research work aims to perform investigations on SSCBs and short circuit fault clearing strategies in HVDC grids. This work will be carried out to study, analyze and address following issues:

- DCCB requirement reduction in MTDC grids without violating selectivity criteria of grid protection system.

- Improving SSCB topology with the aim of reducing number of requiered semiconductor switches and thus it power losses.
- Validating proposed solutions through detailed simulation models and proptotyping.

4.2.4 Methodology

4.2.5 Unidirectional Protection Strategy for MTDC

DCCBs are usually supposed to be able to interrupt the current in their forward and backward directions. On the other hand, unidirectional DCCBs (UCBs) conduct the current in their forward and backward directions whereas interrupts the current only in one direction. The main concern regarding application of UCB in the MTDC grid is its inability in interrupting fault current owing in its backward direction [90]-[93]. In this work, a protection strategy based on UCBs is suggested for MTDC grid. The suggested strategy aims to overcome the main application drawback of UCBs. Protection logics for DC bus and transmission line faults are investigated. Figure 67(a) depicts arrangement of UCBs in a three-terminal HVDC grid. The arrow in UCB symbol shows its current interruption direction.

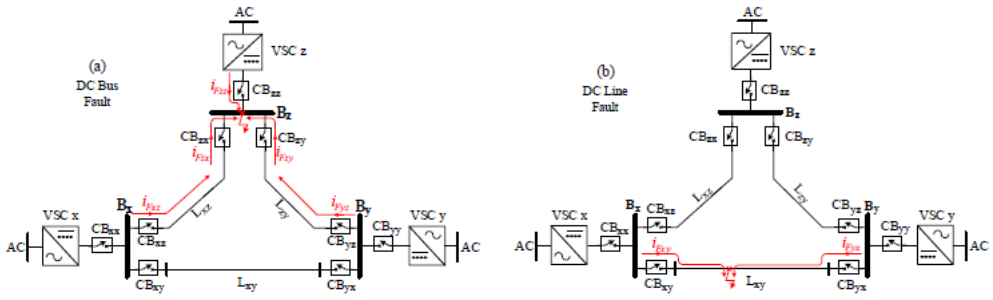

Figure 67: UHCBs arrangement and directions and fault current directions (a) Fault resistance of 0 Ohm, (b) Fault resistance of 10 Ohm

- DC Bus Fault:

Figure 67(a) shows the fault currents during a short circuit fault at DC bus B_Z. Three fault currents ow though three adjacent UCBs. Since the fault current $i_{F_{zz}}$ ows in the forward direction of the CB_{zz}, it can be interrupted by mentioned UCB. Fault currents $i_{F_{zx}}$ and $i_{F_{zy}}$ ow from the adjacent lines to the fault location and are in the backward directions of CB_{zx} and CB_{zy}. Therefore, the adjacent lines DCCBs are unable to interrupt the current. The protection logic for the DC bus fault can be given by:

$$Fault\ at\ B_x \rightarrow Trip(CB_{1x}, \dots, CB_{xx}, \dots, CB_{nx}) \qquad \textbf{Equation 14}$$

- Transmission Line fault:

Figure 67(b) shows a short circuit fault in line L_{xy}. Two fault currents ow from both ends of the transmission line into the fault location. In any line fault condition, the fault currents ow in the forward directions of corresponding UCBs. Therefore, the fault can be cleared by opening the corresponding UCBs. Unidirectional protection logic for transmission line fault can be given by:

$$Fault\ on\ L_{xy} \rightarrow Trip(CB_{xy}, CB_{yx})$$ **Equation 15**

4.2.5.1 Current Releasing Solid-State Circuit Breaker

Figure 68 shows a point-to-point HVDC connection, which is equipped by current releasing circuit breaker (CRCB) at both ends of the transmission line. The CRCB has a main breaker unit, which can be implemented by series and parallel connection of semiconductor switches. In addition to the main breaker unit two thyristor banks are also employed. Capacitor C1 and resistor R2 play the main roles in fault current interruption and overvoltage limiting process. L1 is employed to limit the rate of rise of fault current [4, 6].

Figure 68: HVDC transmission line equipped by CRCB at both ends

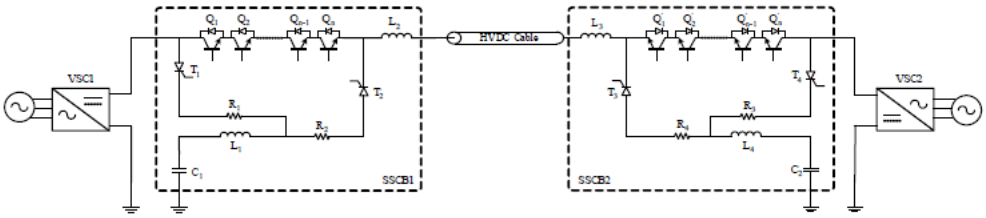

- DC Bus Fault:

In normal operation, the circuit breaker should be closed to maintain the power flow from rectifier side to inverter side of the HVDC system. Considering VSC 1 as rectifier and VSC 2 as inverter in depicted HVDC system in Figure 68, after turning on the IGBTs of SSCB 1 and SSCB 2 the current flows through the IGBTs of SSCB 1 into the DC transmission line and then via the antiparallel diodes of SSCB 2 into the inverter.

- Current Interruption:

At the initial state of the proposed circuit breaker all the thyristors and IGBTs are in off state. Charging of C1 commences after triggering the gate of T1. The next step is to close the main breaker unit. Closing main breaker unit can be done by sending turn-on signal to the IGBT drivers. Depending on voltage and current rating of system, main breaker unit may consist of a number of IGBTs in series and parallel.

Number of IGBTs in series can be defined by the rated and surge voltage of DCCB whereas the number of parallel IGBTs can be defined by maximum continuous and maximum fault current of system. Values of R2 and C1 can be calculated using Equation 16 and Equation 17.

$$R_2 = \frac{V_{C_1}}{I_{max}}$$ **Equation 16**

$$C_1 > \frac{4(L_1+L_2+L_{line})}{(R_2)^2}$$ **Equation 17**

4.2.6 Results

4.2.6.1 Simulations

Various simulation studies have been carried out for the proposed current releasing circuit breaker and unidirectional protection strategy. A part of detailed simulation results can be found in [89]-[90]. However, a part of results is presented in this section.

- Current Releasing Circuit Breaker:

CRCB voltage and cable current waveforms are simulated for PI, simple and distributed frequency dependent (FD) models of the HVDC cable and compared with the results from the equivalent circuit analysis in Figure 69. The voltage waveform from analysis is almost similar to the simulation results for the PI and simple model of the cable. The distributed frequency dependent model shows more accurate results in comparison to lumped models. Increased resistance of the cable rises overall resistance of circuit during fault interruption, which is similar to increasing the damping factor of the simplified equivalent circuit. The current waveforms from analysis and simulation are depicted in Fig. 3-3(b). The simulation of CRCB with the frequency dependent model shows better results as compared to the other models. The DC faults usually has a high rate of rise of current and thus the results from FD model is more accurate since parameters of the simple and lumped models are obtained for low frequencies. However, if the DC fault current is supposed to be constant (without high frequency components) the results from FD model might be changed.

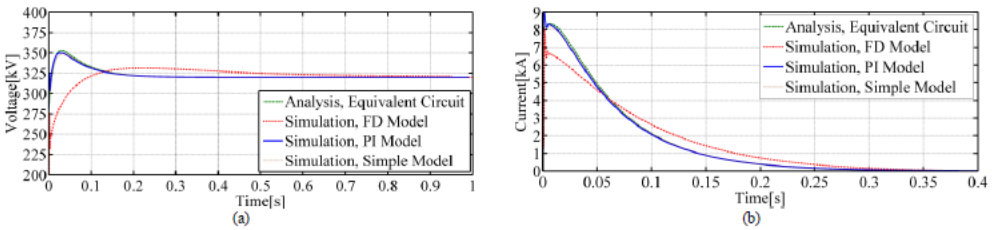

Figure 69: (a) CRCB voltage and (b) cable current waveforms, based on different cable models and analysis

- Unidirectional Protection Strategy:

A four-terminal meshed HVDC grid model, which is developed in [2] is employed in this research work. DC line pole-to-pole short circuit faults and DC bus pole-to-pole faults with 100 m resistance are studied. The DC pole-to-pole short circuit faults are applied to all transmission lines of the system in different locations at t=0 s. The fault currents for the SSCB and CRCB during the fault on lines 12, 13 and 14 are shown in Figure 69. The CRCB interrupts the fault current promptly due to its topological characteristics. Both types of DCCBs handle equal peak values of fault currents due to the identical fault identification and trip time of protection algorithm.

4.2.6.2 Experimentations

A low voltage prototype has been built up to examine the practical functionality of CRCB. The schematic of experimental set-up a photo of prototype are depicted in Figure 70. Figure 70(a) shows the experimental setup configuration. As can be seen in the Figure, CRCB is connected to a DC link, which is fed by an autotransformer through a diode rectifier. The transmission line is represented by an inductor and its equivalent series

resistance. A short circuit fault is placed using an AC mechanical circuit breaker. Fig. 3-5(b) shows a photo of main board of implemented lab-scale prototype. The line current is measured using a hall effect-based linear current sensor.

In order to carry out the experiment, the short circuit is detected by an overcurrent detector program, which is developed on a 16-bit digital signal controller. Figure 71 shows a set experimental results for interrupting 25 A of current and confirms surge-less operation of CRCB.

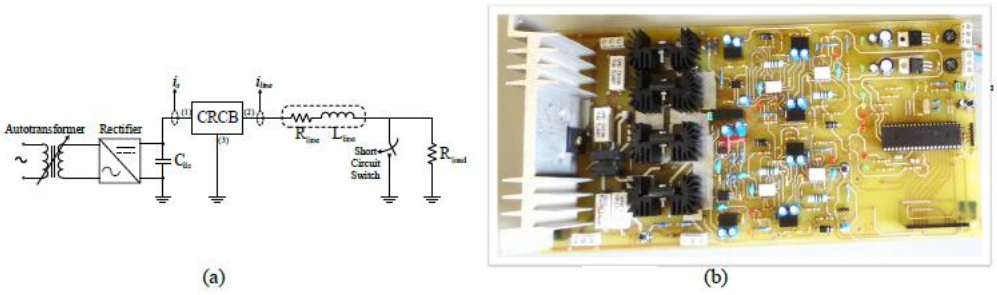

Figure 70: (a) Experimental setup configuration (b) Implemented CRCB block diagram

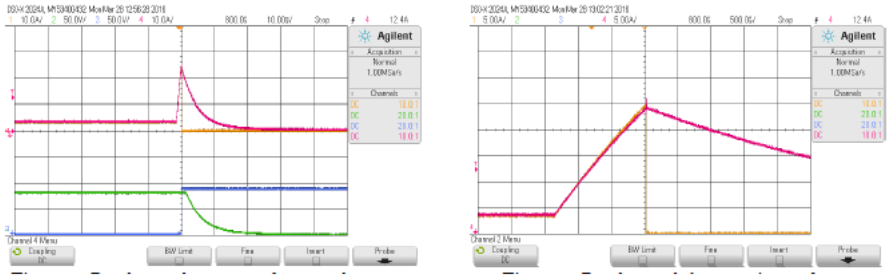

Figure 71: Experimental results

4.2.7 Summary

Unidirectional DC circuit breakers are technically and economically attractive to be applied in the meshed HVDC grids. Both bidirectional and unidirectional protection schemes show similar performances during DC transmission line faults. The current interruption requirements of UCBs are found to be similar to those of BCBs. This study suggests that UCBs can protect MTDC grids similar to the BCBs while using fewer semiconductor switches. Moreover, a different approach for DC fault current interruption namely current releasing DC circuit breaker (CRCB) is investigated through the analysis, simulations and experiments in this work. The CRCB is a solid-state type DC circuit breaker (SSCB). The results from this study show that by selecting suitable values for the internal parameters of CRCB the DC fault current can be interrupted without generating surge voltage. The CRCB can be integrated into the different HVDC system configurations including the monopole and bipolar configurations. Although this work focuses on high voltage application of CRCB, it can be utilized in medium and low level DC systems.

The CRCB has at least 60% less power loss as compared to the typical SSCB due to the less number of semiconductor switches. The functionality of CRCB is examined and validated through implementing a lab-scale prototype. The short circuit test of the prototype confirms the surge-less operation of the CRCB. Nevertheless, the high voltage implementation of CRCB might be challenging.

4.2.8 References

[85] Nilanjan Chaudhuri, Balarko Chaudhuri, Rajat Majumder, and Amirnaser Yazdani. Multi-terminal direct-current grids: Modeling, analysis, and control. John Wiley & Sons, 2014.

[86] W. Leterme, N. Ahmed, J. Beerten, L. Angquist, D. V. Hertem, and S. Norrga. A new hvdc grid test system for hvdc grid dynamics and protection studies in emt-type software. In AC and DC Power Transmission, 11th IET International conference on, pages 1-7, Feb 2015.

[87] A. Mokhberdoran, A. Carvalho, H. Leite, and N. Silva. A review on hvdc circuit breakers.

[88] In Renewable Power Generation Conference (RPG 2014), 3rd, pages 1-6, Sept 2014.

[89] A. Mokhberdoran, A. Carvalho, N. Silva, H. Leite, and A. Carrapatoso. A new topology of fast solid-state hvdc circuit breaker for offshore wind integration applications. In Power Electronics and Applications (EPE'15 ECCE-Europe), 2015 17th European Conference on, pages 1-10, Sept 2015.

[90] A. Mokhberdoran, N. Silva, H. Leite, and A. Carvalho. A directional protection strategy for multi-terminal vsc-hvdc grids. In 2016 IEEE 16th International Conference on Environment and Electrical Engineering (EEEIC), pages 1-6, June 2016.

[91] Ataollah Mokhberdoran, Adriano Carvalho, Nuno Silva, Helder Leite, and Antonio Carrapatoso. Fault current managing branch for surge-less current interruption in dc system. Filed in Portuguese National Patent Office, No. 108775, 2015.

[92] Ataollah Mokhberdoran, Adriano Carvalho, Nuno Silva, Helder Leite, and Antonio Carrapatoso. Application study of superconducting fault current limiters in meshed hvdc grids protected by fast protection relays. Electric Power Systems Research, 143:292-302, 2017.

[93] Ataollah Mokhberdoran, Nuno Silva, Helder Leite, and Adriano Carvalho. "Unidirectional protection strategy for multi-terminal hvdc grids. Transactions on Environment and Electrical Engineering, DOI: 10.22149/teee.v1i4.71, 2016.

5. Interactive AC/DC grids

5.1 Investigation of impact between AC and DC grids– Alejandro Bayo Salas

5.1.1 Introduction

In a network consisting of conventional generation, the dynamics in the power system were mainly influenced by synchronous generators. The power system oscillated in a way determined by the electromechanical interactions between rotatory components and the control loops of these power plants. Their dynamic bandwidth is located in the sub-synchronous frequencies. Therefore, electromagnetic modes of oscillation, which mainly occur at super-synchronous frequencies, were not interfering and that dynamic response of the network could be neglected. Because of this, the response of currents and voltages in the system represented by the differential equations of the variables through the LC representation of elements was reduced to algebraic equations.

For this reason, the scheme representing the different stability problems in the power system was only considering the dynamic interactions within the section of rotor angle stability because the dynamic response was influenced by the torsional rotation of shafts. Regarding voltage stability, the main problems arise from the fault response of the system and the limitations of the power flow in the system, in other words, dynamic interactions between devices due to voltage deviations did not exist.

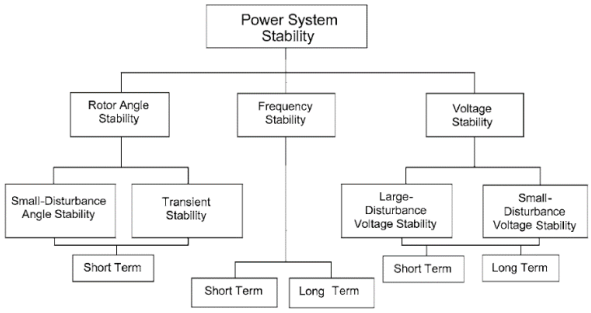

Figure 72: Classification of Power System Stability Analysis [94]

Current incentives in the energy sector promote the installation of offshore wind farms in the North Sea. At the same time, grid planning and market integration are driving the need for more interconnection between countries. High Voltage Direct Current (HVDC) connections are often considered as the preferred solution to accommodate this increase in renewable energies and additional interconnection capacity due to their controllability and suitability for long underground and undersea connections. Nowadays, the voltage source converter (VSC) is the technology used for connecting converter-based wind generators and for transferring power through HVDC lines. In the future planning for the extension to an offshore grid, an increasing number of VSCs will be closely connected at the AC side and could mutually impact each others operation. One of the

outstanding research questions is the study of possibly adverse control interactions between such converters. When a new converter is connected to the grid, it impacts the overall AC network characteristics and the corresponding dynamics as observed at other points in the system. With the number of converters increasing, this influence will increase as well. However, multi-infeed VSC HVDC connections are not commonplace yet and current VSC control design mainly considers a simplification of the grid response at the Point of Common Coupling (PCC). Hence, unanticipated interactions with other converters, either because they are not planned or built or their data is not available during the process, result in stability concerns and uncertainty during the design phase.

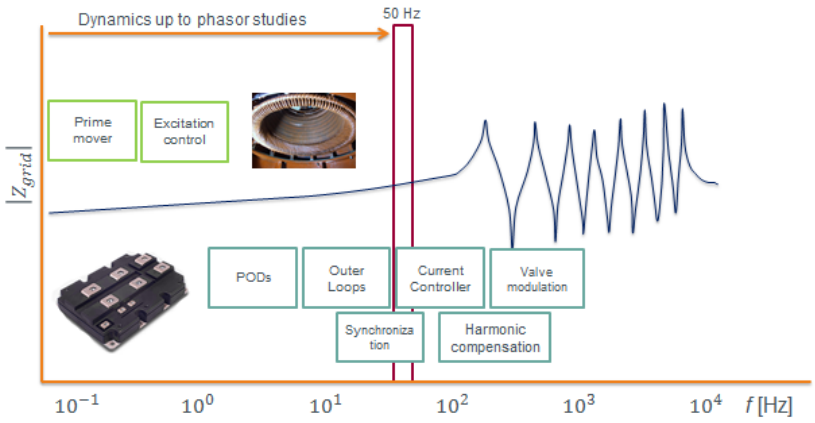

Figure 73: Interactions in the power system

Despite VSCs being considered as a reliable technology, suitable for the connection to any AC network [95], non-ideal characteristics of the power system have been detected to impose limitations. Particularly, the integration in weak grids is a concern. Such systems commonly represented by an equivalent perfect source behind the short-circuit impedance have been observed to impose limitations on the VSC control response [96].

However, in systems with controlled devices operating in a wide bandwidth of frequencies, natural resonance frequencies from the network interact with the control bandwidth of the converter. In addition, a new stability issue has emerged when fast controlled devices are connected: the harmonic stability, i.e., a small-signal voltage stability extended to a wider frequency range. These interactions might cause power quality and stability issues as well [97]-[99].

Harmonic instabilities are a well-known problem in traction networks [99]. In distribution systems, control interactions between the current controller and the LCL filter have been detected [100]. In these installations, the harmonic instability is characterized by the impact of the filter. First, the current controller uses the current feedback through the plant of the LCL filter; therefore, the plant has a resonant point. Second, low- and medium-voltage networks have more damping due to the lower X/R ratio; thus, further resonances from the network are usually inherently damped by the system. And third, the resonances from the network are usually located in higher frequencies due to the characteristics of the transmission.

Therefore, a new problem appears within the power system stability frame: small-signal voltage stability. By this, the dynamic response characterized by the differential equations of currents and voltages need to be taken into account.

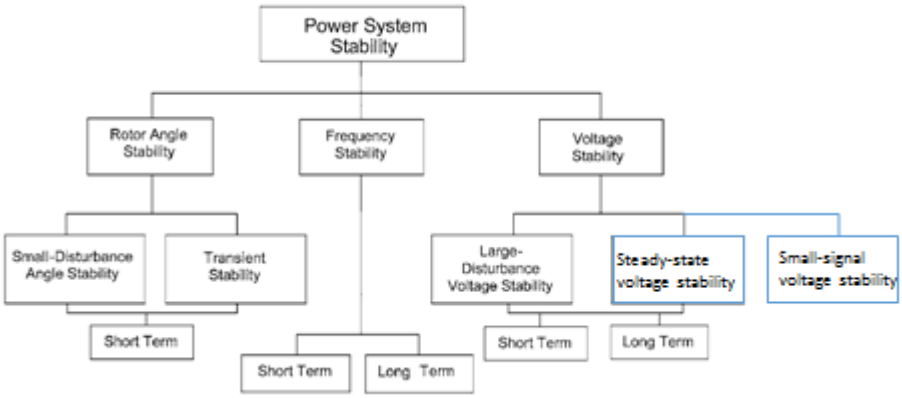

Figure 74: Interactions in the power system

Harmonic stability studies are mainly performed in the frequency domain by means of the admittance based approach [101]-[102] This method has been used to study the interaction between a VSC and a simplified AC system [103]-[106]. Extending the study to systems with multiple converters, harmonic interactions have been detected to lead to stability issues in an Offshore Wind Farm (OWF) when the number of connected turbines is increased [107], between an OWF and the collector offshore converter [14], in a parallel VSC connection composed of two VSCs [109] and between the current controllers in a converter-based distribution network composed of three converters [110]

5.1.2 Harmonic stability

The oscillations arising from the interaction between the converter and the network in the frequency bandwidth above phasor dynamics arise the following challenges:

- Understand the root of the instability issue
- How to determine/evaluate the system stability?
- Which is the bandwidth of accuracy required to model the different components?

Below, these questions are partly answered.

By the time that the first experiences in the integration of MMCs in the system are commissioned, the first harmonic stability issues are happening in the power system.

The first negative interaction was in the Borwin installation [111]. This project was one of the first experiences in connecting an offshore wind farm to the AC system by means of an HVDC link. However, the resonances in the offshore grid triggered high frequency oscillations which had destructive effects and obliged to temporarily close the link.

Also the same issues appeared in the first month of operation of the first MMC-based HVDC link in Europe, Inelfe [112]. Operations in the AC network triggered resonances which at the same time were excited by the converter control. After that, sustained oscillations at high frequencies were transferred to the AC side and lead to the trip of some protection devices and, thus, the trip of the installation. These oscillations are shown in the figure below which corresponds to the real measurements of the installation.

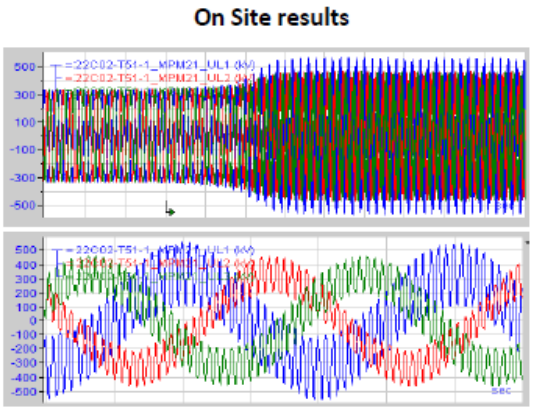

Figure 75: Real voltage measurements in INELFE [112]

In summary, harmonic instabilities are currently a new and unknown problem in the power system community and, specifically, in the power system analysis. Therefore, the study of this topic is necessary and new and opens new needs and complexity for modelling the different components, new mathematical methodologies in order to study the problem and new ways to mitigate the stability issues.

5.1.2.1 Bandwidth of interactions

The study in offshore networks with submarine cables has only focused in low-frequency resonances way below the current controller bandwidth. However, the range is still unknown and recent instabilities as the one shown in INELFE confirms it.

The required band will have an obvious impact on the modelling of components. As a practical approach, the requested range is set up to the 50th harmonic. However, there is no scientific explanation behind. In order to estimate the bandwidth of interaction, the open loop response between the converter and the network is plotted and the oscillatory behavior is determined by the 0dB crossings. Figure **76** shows this and it can be seen that after 9 kHz, there are no more zero-crossing and therefore, there is no oscillatory behavior. However, points around 4kHz already show that the phase margin is high and, hence, the oscillation is acceptably damped.

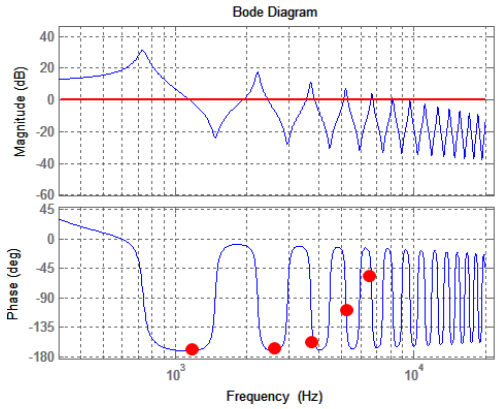

Figure 76: Bode Diagram of the loop transfer function and the oscillatory behaviour depending on the phase margin

5.1.2.2 Stability assessment

- Eigenvalue analysis:

As a common practice for the power system stability study, dynamics are represented by a system of ordinary differential equations and linearized around one operating point. The system is defined by the state space matrices A, B, C and D and the dynamic response can be determined by modal analysis. The oscillatory modes are determined by the eigenvalues calculated by the equation below, which will give the information about the frequency and damping for all the modes. Eigenvalues are the solution of the characteristic equation and one can determine the motion of the states when the system is perturbed. The state space matrices of the VSC are presented below.

The network is represented as well by the differential equations representing the electromagnetic couplings; the inputs are the currents at the nodes where the converters are connected to and the outputs are the voltages at the same nodes.

- Frequency domain:

Frequency-domain methods are based on the input/output characterization of the system. One property of transfer functions is that it only corresponds to the state space dynamics that are both reachable and observable. In other words, if there are repeated solutions of the polynomial in both numerator and denominator, the respective poles and zeros cancel each other and thus leading to a loss of dynamic information. However, the electromagnetic resonant modes of the network are both observable and controllable. In other words, series and parallel resonances cannot occur at the same frequencies and thus cancelling each other because of the inherent nature of electromagnetic systems. Therefore, at these specific frequencies, the resonant peaks in the equivalent admittance represent the eigenvalues of the dynamic system.

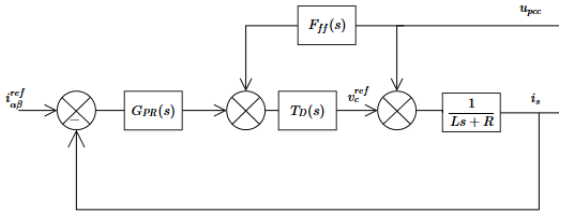

Figure 77: Typical VSC control block diagram

The converter is represented by a controlled current source with a parallel admittance Y_{VSC}. By this, VSC dynamics are represented by the transfer function between the controlled current injected to the PCC as the output and the PCC voltage *u*, regarded as the disturbance as seen in the Figure 75.

$$Y_{VSC} = \frac{\frac{1}{Ls+R}(1-T_D F_{ff})}{1+\frac{1}{Ls+R}T_D G_{PR}}$$ **Equation 18**

Different parameters such as the time delay, the feed-forward filter and the current controller bandwidth have an impact on the arising harmonic interactions.

The closed-loop response of the interconnected system is represented by the feedback system of the VSC characterized by its input/output characterization YVSC and the harmonic impedance of the network Zh as the feedback connection.

$$Y_{CL} = \frac{Y_{VSC}}{1+Y_{VSC}Z_h}$$ **Equation 19**

Therefore, system stability can be studied by common frequency domain techniques in feedback system such as the Nyquist or Bode criterion, which use the information of the denominator $1+G_{OL}(s)=0$. According to this, a feedback system is stable if and only if all roots of the characteristic equation lie to the left of the imaginary axis.

- Time-domain analysis:

Time-domain (TD) simulations are the most entrusted method for transients and stability studies in the industry. They allow to include all the non-linearities from the electric components and VSC control and thus provide

the most realistic result. However, TD analysis also presents several limitations with respect to other methods when the system stability is under study.

In the specific case for the study of control interactions between the VSC and the network, the consideration of all possible scenarios in EMT simulation tools will require the modelling of the network for the different topologies and the simulation of the latter with a highly detailed VSC. This transforms in the requirement of a very large period of time.

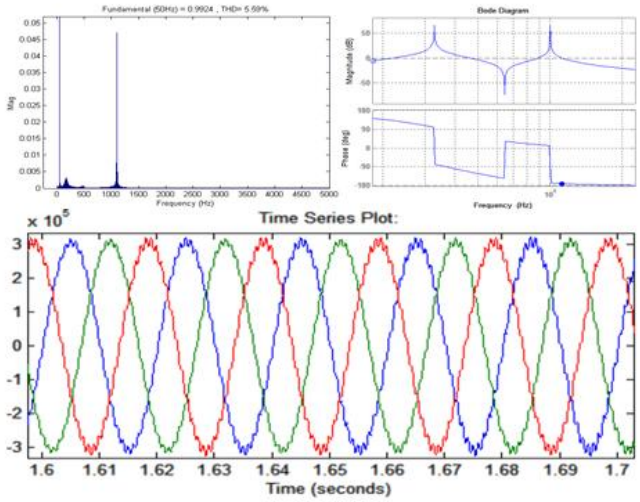

Figure 78: Stability assessment and time-domain validation of the oscillatory behaviour

5.1.3 Interaction between two converters

The system under study is shown in Figure 79. It consists of two converters connected to the AC system at different PCCs which are interconnected through a transmission line. The whole system is modelled by representing all elements by their reciprocal circuit equivalent models. The VSC is transformed into a current source with a parallel admittance, AC networks are converted into voltage sources behind an equivalent impedance and the transmission line is represented by the commonly used PI section representation of lines.

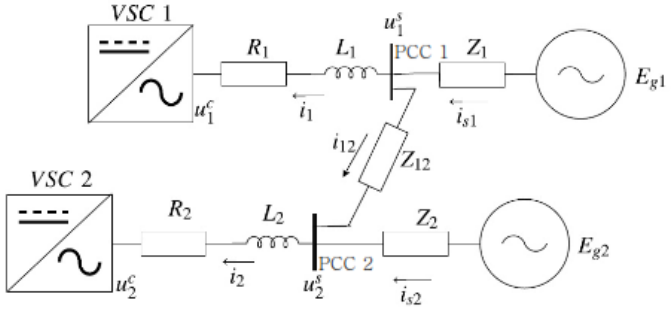

Figure 79: System for the study of interaction between two converters

The equivalent circuit of the studied system is depicted in Figure 80.

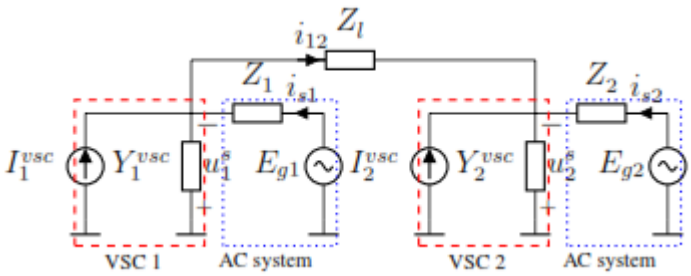

Figure 80: FD representation for the interaction study

The VSC-impedance model is obtained from building the equivalent transfer function from the input *u* to the controlled output *i*. The validation of the oscillatory behavior is done for different lengths of the transmission line as shown in Figure 81.

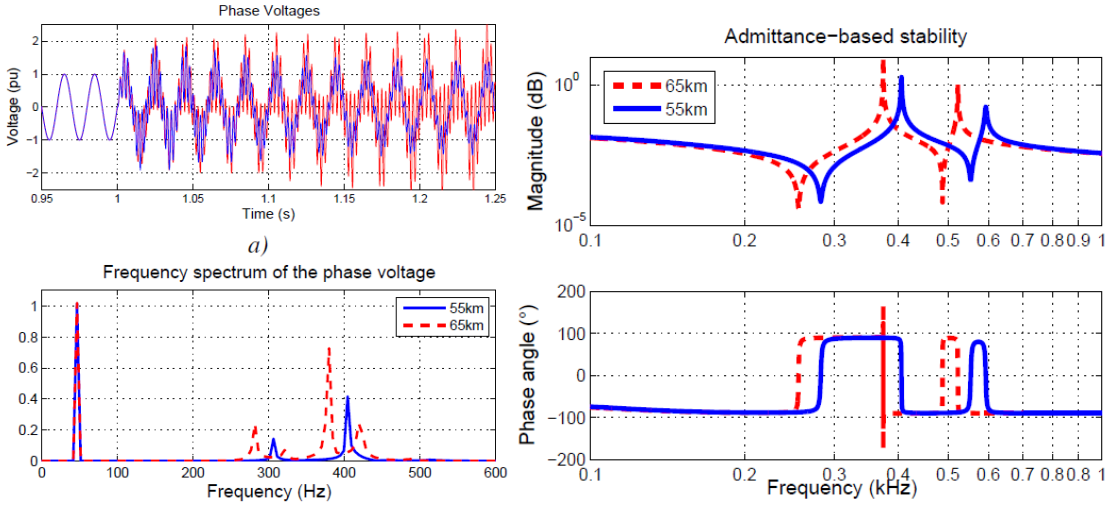

Figure 81: FD representation for the interaction study

5.1.4 Interactions in a meshed system

The different approaches are extended to a meshed system were the resulting instabilities are more complex to determine. The system in study is represented in Figure 82 and it is composed by three converters connected to a meshed network.

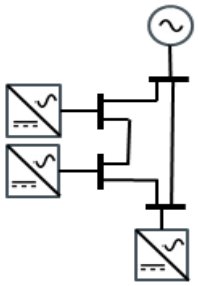

Figure 82: System for the study of the interactions in meshed network between converters

As in the previous case, the dynamic response of the system is studied by means of the state space representation as it is sketched in Figure 83.

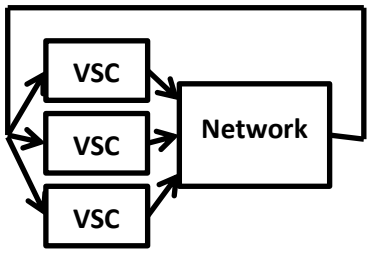

Figure 83: Interconnection of ABCD matrices for the different components

Also, the study is conducted in the frequency domain. To do this, converters are represented by current sources with their equivalent admittance in parallel. Transmission lines are represented by an equivalent impedance representation in the frequency domain. By doing this, the stability of the system is studied by means of calculating the equivalent FD impedance at the node of study and evaluating the closed-loop response as in the previous case.

The equivalent FD impedance is built by means of calculating the nodal admittance matrix in the s-domain. The different impedances of the VSCs and equivalent FD representations of transmission lines are included in the nodal matrix. The equivalent harmonic impedance is then calculated by inverting the matrix and choosing the diagonal component of the node of interest.

$$Y = \begin{bmatrix} Y_{11}(s) & \cdots & Y_{1N}(s) \\ \vdots & \ddots & \vdots \\ Y_{N1}(s) & \cdots & Y_{NN}(s) \end{bmatrix} \qquad \textbf{Equation 20}$$

$$\boldsymbol{Z_{th,nodei} = Y^{-1}(i,i)} \qquad \textbf{Equation 21}$$

The closed loop response of the interconnected system is represented in Figure 84. Also, the comparison between the dynamic response estimated by means of FD techniques and state space matrices is shown in Figure 84. Both responses show a good correlation which verifies the same dynamic estimation from both methods.

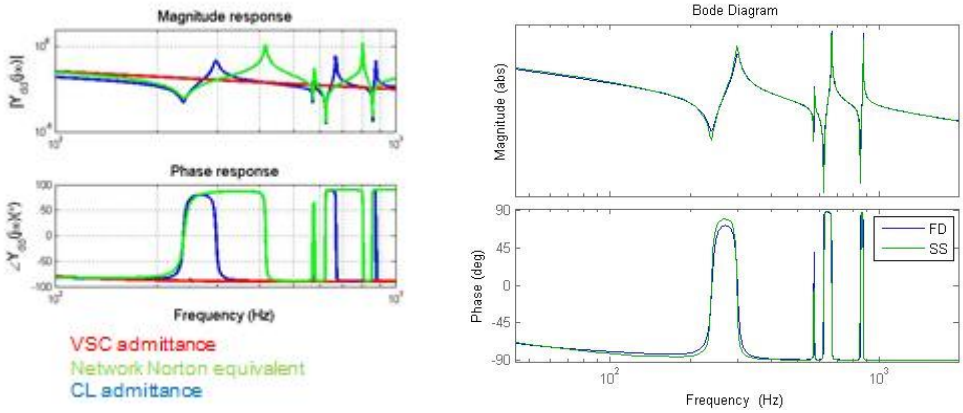

Figure 84: Interconnection of ABCD matrices for the different components

5.1.5 Resonance mitigation

Different strategies are proposed with the objective of increasing the phase margin between the converter control and the network at the resonant points. Figure 85 sketches different possibilities and control loops to do this.

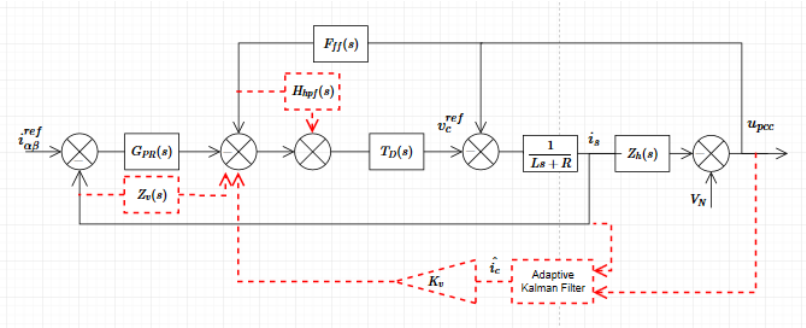

Figure 85: Active damping strategies

The different methods are based on the use of different variables for making the active damping. These variables can be the PCC voltage or the grid voltage. Also, some of the variables could be estimated. Each of the selections will have a different impact on the dynamic response of the control and their impact will need to be considered to re-tune the controllers. The main objective of active damping strategies is to shape the dynamic response in order to increase the phase margin between the VSC control and the network at the resonance points. Figure 86 shows the dynamic response of the system after adding an active damping controller.

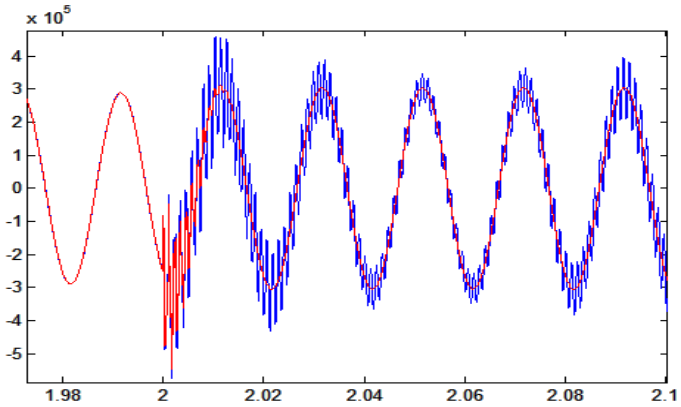

Figure 86: Dynamic response after adding active damping

5.1.6 References

[94] Kundur, J. Paserba, V. Ajjarapu, G. Andersson, A. Bose, C. Canizares, N. Hatziargyriou, D. Hill, A. Stankovic, C. Taylor, T. Van Cutsem, V. Vittal , “Definition and Classification of Power System Stability”, IEEE Transactions on Power Systems, vol. ?, pp. 1-15, 2003.

[95] Technichal Brochure 492, “Voltage Source Converter (VSC) HVDC for Power Transmission, Economic Aspects and Comparison with other AC and DC Technologies (WG B4),” Cigré, Tech. Rep., April 2012.

[96] A. Egea-Alvarez, S. Fekriasl, F. Hassan, and O. Gomis-Bellmunt, “Advanced Vector Control for Voltage Source Converters Connected to Weak Grids,” IEEE Transactions on Power Systems, vol. Early Access article, 2015, 9 pages.

[97] P. Brogan, “The stability of multiple, high power, active front end voltage sourced converters when connected to wind farm collector system,” in Proceedings in European Conference in Power Electronics and Applications, 2010, 6 pages.

[98] H. Enslin and P. J. Heskes, “Harmonic interaction between a large number of distributed power inverters and the distribution network,” IEEE Transactions on Power Electronics, vol. 19, no. 6, pp. 1586–1593, November 2004.

[99] E. Mollerstedt and B. Bernhardsson, “Out of control because of harmonics-an analysis of the harmonic response of an inverter locomotive,” IEEE Control Systems, vol. 20, no. 4, pp. 70–81, August 2000.

[100] Remus Teodorescu, Marco Liserre, Pedro Rodriguez,” Grid Converters for Photovoltaic and Wind Power Systems”. Editorial Wiley.

[101] L. Harnefors, M. Bongiorno, and S. Lundberg, “Input-admittance calculation and shaping for controlled voltage source converters,” IEEE Transactions on Industrial Electronics, vol. 54, no. 6, pp. 3323–3334, December 2007.

[102] J. Sun, “Impedance-based stability criterion for grid-connected inverters,” IEEE Transactions on Power Electronics,vol. 26, no. 11, pp. 3075–3078, November 2011.

[103] M. Cespedes and J. Sun, “Impedance modeling and analysis of grid-connected voltage-source converters,” IEEE Transactions on Power Electronics, vol. 29, no. 3, pp. 1254–1261, March 2014.

[104] K. Alawasa, Y. Abdel-Rady, and W. Xu, “Modeling, analysis and suppression of the impact of full

[105] -scale wind power converters on subsynchronous damping,” IEEE Systems Journal, vol. 7, no. 4, pp.700–712, December2013.

[106] H. Liu and J. Sun, “Voltage Stability and Control of Offshore Wind Farms With AC Collection and HVDC Transmission,” IEEE Journal of Emerging and Selected Topics in Power Electronics, vol. 2, no. 4, pp. 1181–1189, December 2014.

[107] L. H. Kocewiak, J. Hjerrild, and C. L. Bak, “Wind turbine converter control interaction with complex wind farm systems,” IET Renewable Power Generation, vol. 7, no. 4, pp. 380–389, July 2013.

[108] J. Glasdam and L. H. Kocewiak, “Control System interaction in the VSC-HVDC Grid Connected Offshore Wind Power Plant,” in Cigre B4 Simposium. Across borders - HVDC Systems and Market Integration in Lund., May 2015, 8 pages.

[109] C. Wan, M. Huang, C. Tse, and X. Ruan, “Stability of interacting grid-connected power converters,” Journal of Modern Power Systems and Clean Energy, Springer, vol. 1, no. 3, pp. 249–257, December 2013.

[110] X. Wang, F. Blaabjerg, and W. Wu, “Modeling and analysis of harmonic stability in an AC power-electronicsbased power system,” IEEE Transactions on Power Electronics, vol. 29, no. 12, pp. 6421–6432, December 2014.

[111] C. Buchhagen and C. Rauscher and A. Menze and J. Jung, “BorWin1 - First Experiences with harmonics interactions in converter dominated grids”, International ETG Congress 2015 in Bonn.

[112] Presentation from RTE about INELFE VSC control replicas. Online on: < https://sites.google.com/site/hvdcreplicaworkshop/workshop-presentations>

5.2 Interaction of HVDC grids and AC power systems: operation and control– Robert H. Renner

5.2.1 Introduction

Electricity represents the backbone of societies with a highly productive industry and it ensures all the comforts associated with modern-day living. Electricity is omnipresent in industrialised countries and it is considered such a reliable source of energy that people first check a lamp's light bulb when it fails to turn on after the switch is pressed. This reliable energy provision was achieved through continues expansion of the AC power system over the last century. Regional electricity systems were connected to their counterparties in neighbouring areas so they could rely on one another in the event of outages, which improved both their reliability and cost-effectiveness. In Europe, this expansion led to continental Europe becoming a single, synchronous area with redundant connections between countries [113]-[114]. These developments were realised by vertically integrated utilities, responsible for one control area, typically a country [115]. Each utility was responsible for generation, transmission and distribution of electrical energy in an economic and, more importantly, reliable manner. This situation changed with the deregulation, where the utilities were forced to split off generation, transmission and distribution into different independent companies and open up the newly established generation markets to new players. Regulators were moreover established to monitor and govern the efficiency of the transmission sections that represent natural monopolies. The result was that cross-border power exchanges increased due to differences in energy prices [116].

At the same time the European Union (EU) developed its 20-20-20 targets. These targets commit the EU nations to reduce energy consumption by 20%, reduce the greenhouse gas emission by 20% and to improve the energy efficiency by 20% by 2020, compared to 1990 [117]-[119]. EU member countries are expected to reach these targets by mainly using such generation technologies as photovoltaic, hydro and wind power plants. The disadvantage of these power plants is that they have to be built wherever the primary energy is available, and they produce electrical energy only when the primary energy is available. This has resulted in additional cross-border power flows due to the large availability of wind around the North and Baltic sea, hydro power in Scandinavia and the Alps and solar in the southern parts of Europe [120]-[121]. Achievement of these new targets will push the electrical grid even closer to its limits and require additional infrastructural investments, as the existing AC grid was built and optimized for short transmission distances and centralised generation so as to minimise transportation and generation losses. This was possible because transportation and storage of fossil fuels (coal, natural gas, etc.) were/are economic, safe and had/have low losses [122].

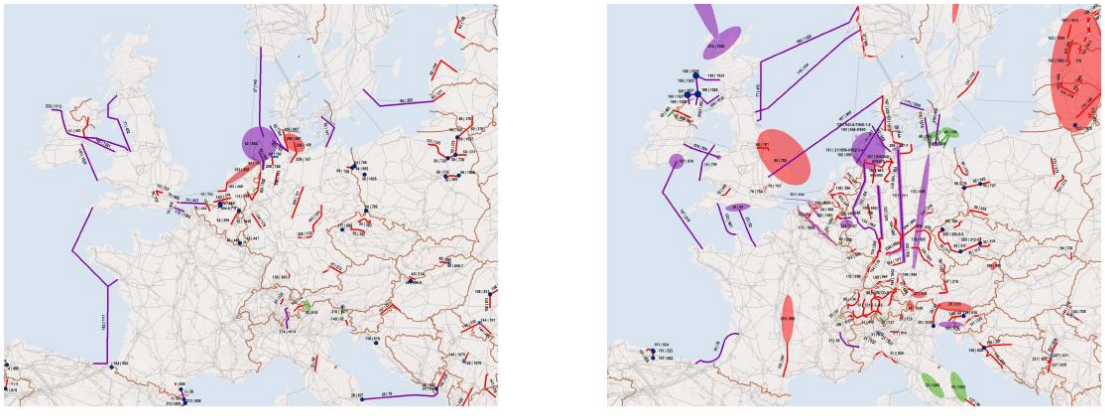

(a) Until 2018. (b) From 2019 to 2030.

Figure 87: Dynamic response after adding active damping

When renewable energy production significantly increases, as it has in Europe [6], the electrical power system needs to be retrofitted to accommodate these new requirements [123]. This problem is further compounded by the resistance of the general public, which has opposed and delayed the construction of infrastructure projects [124].

This conditions and the breakthrough of high voltage as well as high current insulated-gate bipolar transistors (IGBT) in the 1990s, makes high voltage direct current (HVDC) with voltage source converters (VSC) increasingly beneficial. Advantages are its ability to independently control active and reactive power as well as a low harmonic distortion, a smaller footprint for the same transmission power and AC black start capability. Furthermore, the technology provides the option to connect converters in parallel to build DC grids [125]. The result is a significant increase in HVDC projects.

This is illustrated in (a), which shows transmission system extensions planned until 2018 [117]. Purple connections represent HVDC lines and areas are projects which are under consideration or where routes are not yet defined. Red represents AC projects. (b) shows the time horizon from 2019 to 2030 with the same color code.

5.2.2 Methodology and Models

A switching model and average model were used to perform simulations. The switching model is a modified version of the VSC-Based HVDC link available in Matlab/SimPowerSystems [126]. The modifications include a change in AC voltage level, DC voltage level, line length, droop control, AC voltage control, etc. The VSC models are the IGBT-Diode bridge from the SimPowerSystems library [127].

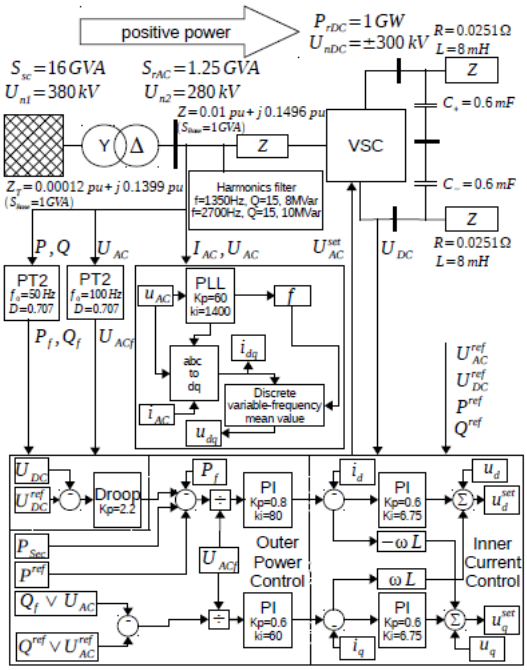

Figure 88: VSC station model and control with a sinusoidal PWM switching frequency of 1350 Hz

They have a symmetrical monopole configuration and a two-level topology. Because the model is highly detailed, the simulations were limited to a few converter stations so as to have an acceptable simulation time. To simulate larger systems with up to 24 converter stations, the provided average model of DIgSILENT PowerFactory was used. A description of the computation times is give at the end of this section. The controller concept as described in this section was used to obtain a similar behaviour for both models. The general converter station layout and control concept is shown in Figure 88. The nominal AC voltage of the AC grid equivalent is defined as 380 kV with a short circuit power (SCP) of S_{SC} = 16 GVA. The transformer has an apparent power of 1.25 GVA, a short circuit voltage of 14 % and a ratio of $\frac{380}{280}$. The nominal converter AC voltage is defined as 280 kV and its DC voltages as 600 kV pole to pole. The positive power direction is from AC to DC, with a nominal value of 1 GW. The AC reactor has a short circuit voltage of 15 % and the DC capacitance is 0.3 mF, which is implemented by two capacitors of 0.6 mF in series. The direct current is smoothed with a DC reactor of H=8 mH and R=0.0251 W. To get steady signals for active and reactive power, the measured signals are filtered by a low pass with a damping of 0.707 and a cut-off frequency of 50 and 100 Hz respectively. In addition, the dq-voltages are smoothed by computing the mean value over a running window of one cycle of the measured frequency.

5.2.3 VSC control concept and control parameters

The controller parameters for the controller concept, depicted in the Figure 88, are shown in the Table 9. The controller concept is common in academia [128]-[129] and consists of an inner current controller (ICC) and an outer active/reactive power controller. Due to the cascaded control structure, the controller can limit the current. The control is implemented in the dq0 frame, in which time varying sinusoidal three-phase signals are converted to phasors, so that controllers can be designed by common methods in linear time invariant systems. In order to achieve the correct synchronization of dq0 signals to the three-phase AC grid voltage, a phase-locked loop (PLL) is used. Moreover, AC voltage control instead of reactive power control can be used. The power exchange balance is guaranteed with droop control, which uses the local DC voltage to identify energy imbalances [130]. Each controller has control parameters that each influence the stability of the VSC and the remaining AC power system. To establish a stable VSC control, common methods for controller design are selected.

The inner current control parameters are defined with the modulus optimum method. The controller is thus tuned to compensate for the dominant time constant, resulting in Equation 22 to calculate proportional gain and Equation 23 to determine integral gain [131].

Table 9: Overview of stability.

Control concept	**Control parameter (concept-dependent)**	**External parameter (concept-dependent)**
ICC	K_{pICC}, K_{ilCC}	Short Circuit Ratio (SCR)
PLL	K_{pPLL}, K_{iPLL}	R/X Ratio
Active Power	K_{pP}, K_{iP}	Voltage Angle
Reactive Power	K_{pQ}, K_{iQ}	U_{DC} , U_{AC}

Energy Balance	K_{pDROOP}	$P(x)$, $Q(x)$

$$K_{pICC} = \frac{R \cdot \tau}{4\zeta_{ICC}^2 \tau_\sigma}$$ **Equation 22**

Where R is the resistance of Z in Figure 88, τ is $\frac{L}{R}$, τ_σ the inverse of the switching frequency and ζ_{ICC} the desired damping of the ICC.

$$K_{iICC} = \frac{K_{pICC}}{\tau} = \frac{R}{2\tau_\sigma}$$ **Equation 23**

The active and reactive power controller should be approximately 10 times slower than the ICC to ensure that there is no interaction between both loops and makes a trade-off between speed and stability. The bandwidth f_p of the power controller should consequently be 10 times smaller than the bandwidth f_{ICC} of the ICC, which is

$$f_{ICC} = \frac{\omega_{ICC}}{2\pi} = \frac{\frac{K_{pICC}}{L}}{2\pi} = \frac{1}{\tau_{ICC}}$$ **Equation 24**

From the closed-loop transfer function

$$\frac{P}{p_{ref}} = \frac{(K_{pP}.s + K_{ip})\frac{u_d}{\tau_{ICC}}}{s^2 + s\left(\frac{K_{pP}.u_d}{\tau_{ICC}}\right) + \frac{K_{iP}.u_d}{\tau_{ICC}}}$$ **Equation 25**

Follows

$$K_{iP} = \frac{\omega_P^2 . \tau_{ICC}}{u_d}$$ **Equation 26**

$$K_{pP} = \frac{2\zeta_p \omega_P \tau_{ICC}}{u_d}$$ **Equation 27**

Where $\omega_P = 2\pi f_p \zeta_p$, the desired damping of the power controller and u_d the d-part of the voltage. For the PLL a method is described in [132] and it results in:

$$K_{pPLL} = \frac{2\zeta_{PLL}\omega_{PLL}}{\hat{U}}$$ **Equation 28**

$$K_{iPLL} = \frac{\omega_{PLL}^2}{\hat{U}}$$ **Equation 29**

Where ζ_{PLL} is the damping, $\hat{U}$ is the peak voltage at the point of common coupling (PCC) and ω_{PLL} the chosen closed-loop bandwidth.

In this thesis the droop for all converters is set at the same value and it is implemented with a deadband for DC grids with more than 10 converter stations and without a deadband for DC grids with less than 10 converter stations. The maximum acceptable DC voltage deviation is used as the limitation to define the droop setting. This, in return, results in the minimum acceptable proportional gain. The controller proportional gain of the DC grid $K_{ConDCVCR}$ is calculated using:

$$K_{ConDCVCR} = \frac{\Delta P_{Max}}{\Delta U_{DCMax}}$$ **Equation 30**

This proportional gain for the entire DC grid is distributed equally between the participating converters, i.e.

$$K_{ConDCVCR} = \frac{K_{TotDCVCR}}{n-1}$$ **Equation 31**

With $n-1$ being the number of participating converter stations considering the outage of a $DCVCR$ controlling converter. More advanced gain calculations methods exist [133]-[134], but this simple, fast and comprehensible method was used since this work is not focused on droop control.

After all the controller parameters are tuned, a small signal analysis shows interactions with the remaining AC power system. Small signal stability with VSC is described in [135]. In addition, a large disturbance analysis indicates the stability after events such as short circuits. If one of these tests reveals instabilities, the control parameter or concept needs adaptation.

5.2.4 Simulations and results

5.2.4.1 Switching and RMS model comparison

In order to validate the models and their parameters, a point-to-point connection with droop control is used, and a reactive and active power set point change is compared. The reactive power set point is changed at 1 second from $Q_1^{ref} = Q_2^{ref} = 0$ pu to $-Q_1{}^{ref} = Q_2{}^{ref} = 0.05$ pu, and the active power set point is changed at 1.5 seconds from $P_1^{ref} = P_2^{ref} = 0$ pu to $-P_1{}^{ref} = P_2{}^{ref} = 0.8$ pu. The switching model is shown in light green solid lines and the average model is shown in blue dashed lines. The behavior for DC voltage, AC voltage, active power and reactive power are nearly the same (Figure 89a). The exception is the dynamic peak deviation, which is somewhat higher for the switching model due to the simplification of filters in the averaged model. The averaged model generally does not need filters as it already uses phasors for the simulation. However, additional second-order filters were implemented in the averaged model for active power, reactive power and AC voltage so as to obtain similar time delays. A comparison of the inner current controller parameters shows similar results Figure 89b.

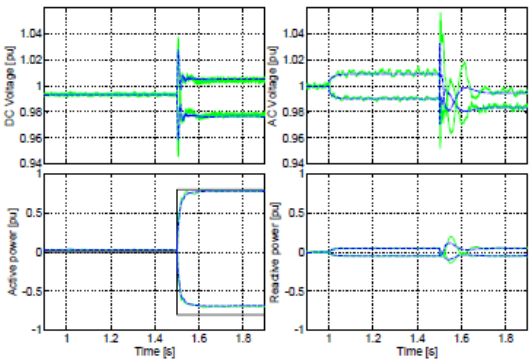

(a) Active power and reactive power.

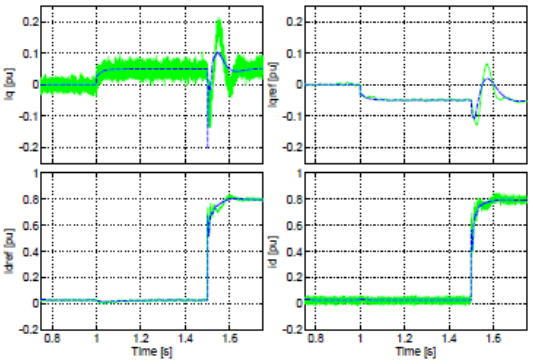

(b) Current reference and measurement in dq-frame.

Figure 89: RMS and switching model comparison. Blue dashed lines represent the averaged model and light green solid lines represent the switching model.

5.2.5 Ancillary services in power system with DC grids

Integration of a DC grid into an existing power system will influence existing ancillary services [136].

The reasons are that new users will be added to the existing power system, new sources of ancillary services will become available, and new services will be needed. This section provides a high-level overview of the required ancillary services, taking into account different possible responsibility models for the hybrid AC/DC system. To analyze the changes related to ancillary services, the power system was simplified into three parts: control area, equipment and interface between AC and DC.

Each of these elements can exist for an AC or DC grid. This resulted in 15 independent combinations that spanned the entire spectrum from an AC power system to a combined AC/DC power system. Analyzing the combinations revealed that four combinations for ancillary services exist in a power system with AC and DC grids, shown in Figure 90. The first combination, ancillary services from AC equipment for AC grids, are those that are defined and in use today.

Figure 90: Overview of the four ancillary services in a power system in a single control area and with an both AC and DC grid (the grey arrows are responsibility-dependent and thus belong to AC or DC equipment).

The second one, ancillary services from DC equipment for AC grids, is being discussed at the moment and used on a case-by-case basis in the field. For this combination, two additional ancillary services were introduced to handle the AC/DC interactions; these were called transmission reserve and power flow control. The last two combinations, ancillary services from AC equipment for DC grids and ancillary services from DC equipment for DC grids, had not yet been defined. The Eurelectric definition and existing definitions for ancillary services for AC systems were used as a starting point to define ancillary services of these combinations. The result is a basic set of ancillary services that maintain the integrity and stability of a combined AC and DC power system.

5.2.5.1 DC grid scheduling

A DC grid needs a scheduled operation point [137]. One option is to maximize the overall buffer energy. From Figure 91 follows that this is reached when ΔU_{Up} and ΔU_{Down} are equal. The behavior of two DC voltages for a given power flow can be approximated as a linear function with a gradient equal to 1. The DC voltage difference between two nodes is then defined by the power flow equation and can thus be assumed to be constant for the energy balance equations. This results in:

$$U_{max} = mU_{Min} + d$$

Equation 32

With U_{max} the highest DC voltage, U_{Min} the lowest DC voltage, m the gradient equal to 1 and $d = U_{Max} - U_{Min}$ the DC voltage band. With the constraint:

$$\Delta U_{U_p} = \Delta U_{Down}$$

Equation 33

The results are

$$U_{Min}^{ref} = \frac{U_{LimUp} - d + U_{LimDow}}{m+1}$$

Equation 34

$$U_{Max}^{ref} = \frac{U_{LimUp} + d + U_{LimDow}}{m+1}$$

Equation 35

This results are the DC reference voltage at the node with either lowest or highest DC voltage. Asymmetrical limits need to be defined to achieve an asymmetrical upper and lower buffer energy.

To show that this optimization is valid, a case study was implemented, with the optimal DC reference voltages calculated. These results were also compared to a dynamic simulation in DIgSILENT, in which a DC voltage controller was implemented to shift the DC voltages to the defined DC reference voltage. All these tests offered sufficient results and demonstrated that this method is capable of calculating the optimal DC reference voltages. A drawback of this method is that the power flow has to be known to perform the calculation. Its application is thus limited to scheduling tasks since changes to the DC grid topology or converter power output will change the optimal DC reference voltage. This algorithm can easily be extended with a security state calculation (e.g. N-1), which makes it a complete DC grid scheduling tool. Its integration in DC SCADA/EMS is moreover also an option, as it requires limited communication.

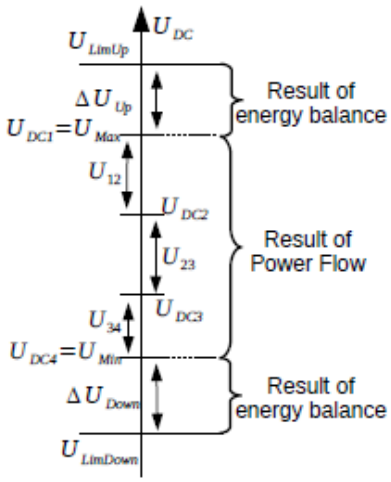

Figure 91: Used DC voltage band and available distance to the upper and lower limit

5.2.5.2 DC grid reserve

This part defines reserves for DC grids, which were named in analogy to the reserves in the European AC power system: DC Voltage Containment Reserve (DCVCR) or DC Primary Reserve; DC Voltage Restoration Reserve (DCVRR) or DC Secondary Reserve; and DC Replacement Reserve (DCRR) or DC Tertiary Reserve. The DCVCR control was furthermore described and it was shown that the DCVRR control can be arranged in a similar fashion to the FRR control in AC systems provided that the DC grid reaches a certain dimension and accepts a DC voltage band of around ±10 %, or that it is damped with inertia from the AC grid. In this case, the DCVRR control has the same functionality as FRR control. This means that it is capable of defining different control areas, that it can compensate for continuous small and slow fluctuations, that it can have similar pre-qualifications for reserve providing power plants and that it can automatically establish pre-fault conditions for DC voltage and power transmission [138].

An example shows the response of a DC grid with 24 converters, when one converter with maximum power injection is disconnected. Figure **92**(a) shows the DC voltages at all nodes. After initialization (first 100 s), the power set-points are constant Figure **92**(b) and the DCVRR maintains the pre-defined DC voltage. A converter with an infeed of 1 pu, is disconnected at 150 s. The result is a strong and immediate decrease in the DC voltage, stopped by the DCVCR.

The DCVRR first compensates for the DCVCR and then re-establishes the DC voltage at node 14 (blue line). The DC voltages after the converter outage differ from the former DC voltages due to the power flow change in the DC grid. Figure **92**(b) shows the power through the converters. The converter stations responsible for the DCVRR (blue lines) are not exactly on their set-points as they are compensating for the unconsidered losses. At 150 s, converter 2 is switched off. As a result, all converters participating in the DCVCR (blue and green lines) change their set-points to compensate for the power imbalance. All DCVRR converters (blue line) subsequently change their power to re-establish the pre-defined DC voltage at node 14, and bring back the scheduled power of the other converter stations (green lines) and between the control areas. It can be seen that the DCVRR converters of control area 2 (blue solid lines) change their power albeit not responsible. This constitutes a difference between AC and DC restoration reserves. DCVCR is not activated identically to K_{DCArea} due to the tendency to solve deficits locally [139]. The change in power over the tie lines is consequently not equal to $K_{DCArea} \cdot \Delta U_{DC}$. At simulation time 450 s, the power exchange between the control areas is re-established and the DCVRR converters from control area 1 (blue dashed lines) have compensated for the complete imbalance since the control area with the outage has to compensate for this. The DCVRR control parameters Figure **92**(c) display the same type of behaviour. At first, all parameters are close to their set-points (dashed lines) or zero. The DC voltage (green solid line) and the power exchange between the control areas (blue lines) are different after the outage. This is compensated after 300 s.

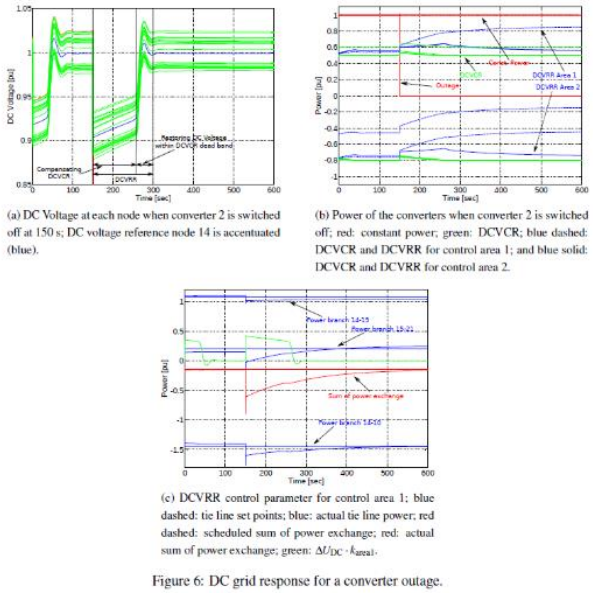

(a) DC Voltage at each node when converter 2 is switched off at 150 s; DC voltage reference node 14 is accentuated (blue).

(b) Power of the converters when converter 2 is switched off; red: constant power; green: DCVCR; blue dashed: DCVCR and DCVRR for control area 1; and blue solid: DCVCR and DCVRR for control area 2.

(c) DCVRR control parameter for control area 1; blue dashed: tie line set points; blue: actual tie line power; red dashed: scheduled sum of power exchange; red: actual sum of power exchange; green: $\Delta U_{DC} \cdot k_{area1}$.

Figure 6: DC grid response for a converter outage.

Figure 92: DC grid response for a converter outage.

5.2.5.3 Low AC voltage ride-through of DC grids

Using simulations, this part demonstrates that DC choppers are capable of providing AC fault ride-through capabilities in accordance with grid code requirements [140]. This remains the case when point-to-point connections are extended to MTDC grids. The utilized DC choppers affect the DC voltage in a similar manner as in point-to-point connections, although a dynamic analysis should be performed to obtain a detailed picture of possible harmonic oscillations. Single DC chopper placements feasible in limited grid configurations and the integration of DC voltage droop control complements voltage containment. This paves the way for smaller DC chopper capacities in future grids with a higher DC voltage droop availability.

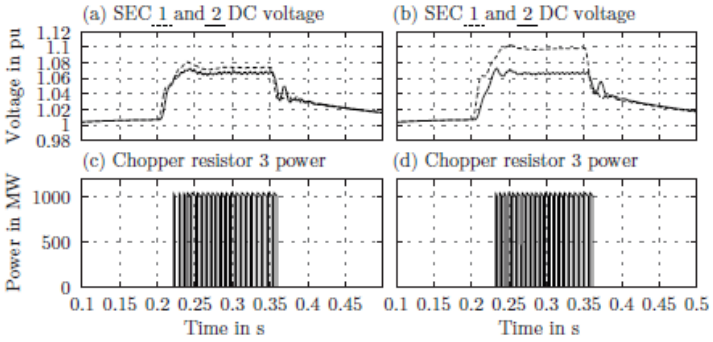

Figure 93: FRT with a varying DC link connection length between the OWFs. Left: 100km, right: 500km.

As an example, Figure 93 shows the simulation results for offshore wind farm (OWF) distances of 100 and 500 km. It can be seen that the DC voltage difference between SEC 1 and SEC 2 increases due to higher line resistances. Furthermore, the DC link voltage at SEC 1 tends to rise in a delayed fashion, with the result that the chopper controller activates the valves at a later point. This can be seen when comparing Figure 93(c) and Figure 93(d), and it can be attributed to the higher resistance between the nodes. Excess energy dissipation is initiated at a later point, and the DC link connecting sending end converter (SEC) 1 and receiving end converter (REC) 4 is charged for a longer time. The maximum DC voltage value consequently exceeds 1.1 pu. In addition, a configuration with one DC chopper can result in over-currents if the DC chopper and its corresponding REC are simultaneously activated. Although the over-currents are active for a maximum of 150 ms, which may not result in a thermal problem, this should be considered in the protection scheme.

5.2.6 Sources of ancillary services for DC grids

Wind power plants have limited capabilities to procure DC ancillary services due to their slow reaction time compared to DC grid time constants for energy buffer services. However, if the DC grid is sufficiently damped by AC inertia or DC storage, the wind power plants can provide DC primary reserve. This can be achieved through a combined de-loading/de-rating control, which uses the fast de-loading reaction time and the de-rating capability of a permanent power change. Furthermore, DC secondary reserve is technically feasible if the WPP is operated in de-rating mode. A problem could be a reliable forecast for the defined provision time. However, in both cases the available primary energy is not optimally used.

This research topic also defined a coordination factor for generation and VSC, as well as describing the behavior of AC and DC grids at the level of buffer energy, primary reserve and secondary reserve.

This work also illustrates how synchronous generators and WPPs with a coordination factor of HC = 1 can provide energy services to DC grids. A method was presented to calculate the maximum instantaneous power a synchronous generator can provide and how this is related to the proportional gain of the connected VSC. In addition, it was discussed how adequate storage for WPPs could be defined to handle the same instantaneous power change. The results were validated with simulations that compared the ability of synchronous generators and WPPs to provide DC primary and DC secondary reserve.

As a final remark, it has to be mentioned that economic criteria will ultimately decide whether wind power plans will contribute to DC reserves or whether another source might be more beneficial.

5.2.7 Summary

More and more HVDC point-to-point connections are planned, are today being constructed or are already being put in operation to connect offshore wind farms or to increase transmission capacity. If point-to-point connections are operated in parallel, it may be more economic and reliable to connect them to form a DC grid. This calls for new operation and control strategies to handle uncertainties and maintain a certain power quality in the DC grid. The limits and boundaries of the connected AC grids furthermore have to be respected so as not to jeopardize the stability of the electrical power system in its entirety. This work consequently focused on operation and control of DC grids that simultaneously respect AC grid limits and boundaries. Such a research focus suggested a description of voltage source converters and how they influence the different categories of AC grid stability: angle stability, AC voltage stability and frequency stability. This work also analyzed how procurement of ancillary services is affected when DC grids are operated in parallel to the existing AC grids, because the development of DC grids will require new definitions for these services. This work consequently analyzed these requirements and proposes ancillary services for DC grids, in addition to presenting a new implementation to manage imbalances in DC grids. The management of imbalances implies scheduling to minimize uncertainties, DC primary reserve to guarantee the stability of a DC grid after a major outage of power infeed or withdraw, as well as DC secondary reserve to re-establish DC voltage and power exchanges between DC control areas. This work also explored the possible function that DC choppers could serve in a DC grid. In addition, it was analyzed which power services synchronous generators and wind power plants can provide to DC grids. This was achieved through theoretical descriptions of the problems and validation of the results using simulations.

5.2.8 References

[113] S. Henry, O. Despouys, et al. Influence of Embedded HVDC Transmission on System Security AC Network Performance. Technical report, Cigré, 2013.

[114] Elia Grid Data.

[115] ENTSO-E.

[116] D. Kirschen and G. Strbac. Fundamentals of Power System Economics . John Wiley & Sons Ltd, 2004.

[117] Ten-Year Network Development Plan 2014. Technical report, ENTSO-E, 2014.

[118] Directive 2009/28/EC, April 2009.

[119] Directive 406/2009/EC, April 2009.

[120] Europe’s onshore and offshore wind energy potential, 2009.

[121] Photovoltaic Geographical Information System.

[122] D. Oeding and B.R. Oswald. Elektrische Kraftwerke und Netze. Springer-Verlag, 6. edition, 2004.

[123] A.J. Schwab. Elektroenergiesysteme. Springer-Verlag, 2. edition, 2009.

[124] P. Buijs, D. Bekaert, S. Cole, D. Van Hertem, and R. Belmans. Transmission investment problems in Europe: Going beyond standard solutions. Energy Policy, 39(3):1794–1801, March 2011.

[125] D. Van Hertem and M. Ghandhari. Multi-terminal VSC HVDC for the European supergrid:

[126] Obstacles. Renewable and Sustainable Energy Reviews, 14(9):3156–3163, December 2010.

[127] VSC-Based HVDC Link, 2014.

[128] Universal Bridge, 2016.

[129] Dragan Jovcic and Khaled Ahmed. High Voltage Direct Current Transmission: Converters, Systems and DC Grids. John Wiley & Sons, 2015.

[130] A. Egea. Multiterminal HVDC transmissions systems for offshore wind. PhD thesis, Universitat Politècnica de Catalunya, Sep 2014.

[131] Til Kristian Vrana. System Design and Balancing Control of the North Sea Super Grid. PhD thesis, 2013.

[132] Gerd Terörde. Electrical drives and control techniques. ACCO, Belgium, 2004.

[133] Agustí Egea-Alvarez, Adria Junyent-Ferré, and Oriol Gomis-Bellmunt. Active and reactive power control of grid connected distributed generation systems. In Modeling and control of sustainable power systems, pages 47–81. Springer, 2012.

[134] Fernando D. Bianchi and Oriol Gomis-Bellmunt. Droop control design for multi-terminal VSCHVDC grids based on LMI optimization . In 2011 50th IEEE Conference on Decision and Control and European Control Conference (CDC-ECC) . IEEE, 2011.

[135] Robert Eriksson, Jef Beerten, Mehrdad Ghandhari, and Ronnie Belmans. Optimizing DC Voltage Droop Settings for AC/DC System Interactions . IEEE Transactions on Power Delivery, 29(1):362–369, February 2014.

[136] Alejandro Bayo Salas, Jef Beerten, Johan Rimez, and Dirk Van Hertem. Analysis of control interactions in multi-infeed VSC HVDC connections. IET Generation, Transmission & Distribution, 2016.

[137] Robert H. Renner and Dirk Van Hertem. Ancillary Services in Electric Power Systems with HVDC Grids. IET Generation Transmission & Distribution, 9(11):1179–1185, 2015.

[138] Robert H. Renner, Jef Beerten, and Dirk Van Hertem. Optimal DC Reference Voltage in HVDC Grids . In ACDC 2015. IET, 2015.

[139] Robert H Renner and Dirk Van Hertem. Potential of using DC voltage restoration reserve for HVDC grids. Electric Power Systems Research, 134:167–175, 2016.

[140] Jef Beerten and Ronnie Belmans. Analysis of Power Sharing and Voltage Deviations in Droop-Controlled DC Grids . IEEE Transactions on Power Systems, 28(4):4588–4597, November 2013.

[141] Christoph Nentwig, Robert H Renner, Dirk Van Hertem, and Jens Haubrock. Application of DC Choppers in HVDC Grids. In Energy Conference (ENERGYCON). IEEE, 2016.

5.3 Control of DC grids to improve stability of AC Grids- Tibin Joseph

5.3.1 Wind-Thermal Generation Coordination in Multi-Terminal HVDC-Connected AC systems for Improved Frequency Support

5.3.1.1 Introduction

It is estimated that 20% of the world's electricity will be supplied from wind generation by 2020 [142]. In order to meet this goal, a substantial integration of onshore and offshore wind power has been planned globally. In Europe, offshore wind farms are preferred due to the high quality of the offshore resource; however, in countries like China, USA and India onshore wind farms have been widely deployed and are the preferred installations [142]. A good example of the scale and pace of wind integration can be seen in China, where the total installed capacity has increased by 45% from 31 GW in 2010 to 45 GW in 2011 [142]-[143]. It is expected that by 2020 the wind penetration in China alone will be of 150-200 GW, out of which more than three quarters will be provided by onshore installations [143]-[144]. As the power generation mix becomes more diverse and further distanced from the main load centres, the interconnection of HVDC links to interface generation and consumption becomes more attractive in a multi-terminal DC grid (MTDC) configuration. Such a scenario facilitates power flow management and operational reliability [149]-[150]. Nonetheless, as thermal generation still satisfies the base load in current power systems, the large integration of wind presents an operational challenge for the coordination of these two sources of generation. As large-scale wind integration progresses, significant power mismatches and frequency deviations may occur due to the wind intermittency and the comparatively slower primary frequency control from synchronous generators of thermal power plants [151]-[152].

5.3.1.2 Operational Scenario and Frequency Regulation

The system under investigation is shown in Figure 1. This system has been modelled to resemble China's future power grid with proposed transmission reinforcements [144]-[146]. The system consists of three AC grids (Grids 1, 2 and 3) connected through a three-terminal MTDC grid. A ratio of wind to thermal generation of 1:2 has been used, which implies that thermal power generation is two times larger than wind generation [150]-[153]. The synchronous generator production is 500 MW and the wind farm generates 250 MW at nominal wind speed. Grids 2 and 3 represent load centres located in Eastern China [153]. Power (750 MW) is transmitted form Grid 1 to Grids 2 and 3 through the three-terminal VSC-based MTDC grid. The MTDC grid has a nominal voltage of 400 kV and each DC transmission line has a length of 500 km. Given that HVDC systems have the advantage of a fast controllability, the active power modulation of the HVDC transmission system is employed to retain system stability. The power absorbed by VSC 1 is injected into the MTDC grid, binding AC and DC power balances; *i.e.*, AC power fluctuations are routed to the MTDC grid, exploiting the fast power routing capabilities of VSCs to balance AC grid power. Frequency deviation ω can be expressed as a function of system inertia and the injected and absorbed powers for grids 1 to 3 (see Figure 95(a) and Figure 95(b)).

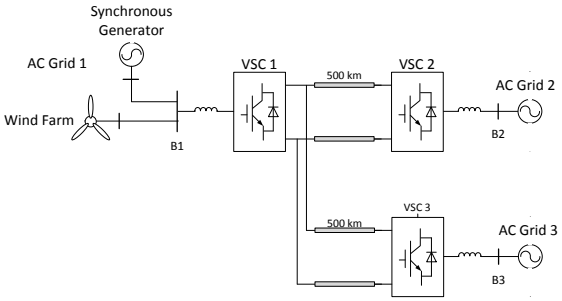

Figure 94: Single-line diagram of the system under study

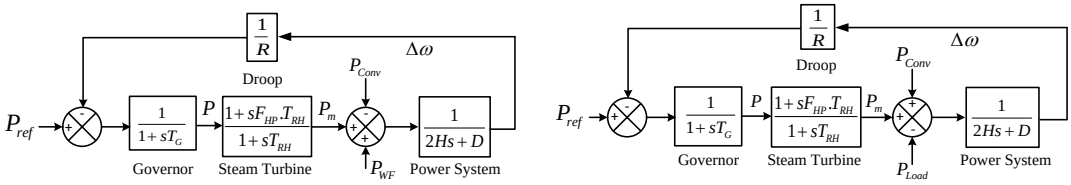

(a) (b)

Figure 95: Primary frequency regulation including a speed governor and a steam turbine: (a) Grid 1; (b) Grids 2 and 3

5.3.1.3 MTDC Grid Operation

Droop (or distributed) control has been widely studied in the literature [147]-[149]. It is employed to regulate the DC voltage in systems that have more than one VSC terminal. Its application for MTDC grids is borrowed from AC power systems, where frequency-power droop schemes are used [147]-[149]. Droop control is considered to be more reliable than the master-slave or the improved voltage margin methods, mainly due to its simplicity and the ease of power sharing between different terminals [149]. Nonetheless, unlike frequency in traditional AC systems, voltage is not a universal measurement in a DC network. A DC voltage droop control may cause deviations from the desired DC voltage, resulting in power losses in the transmission line. Such a scenario is detrimental to the seamless integration of HVDC grids, and, to avoid it, droop settings should be carefully designed to prevent mismatches [156]-[157]. Consider an MTDC grid with three terminals as shown in Figure 94. VSC 1, the sending-end converter, is assumed to work in constant power injection mode as shown in Figure 96(a). VSCs 2 and 3 work in droop control mode, as depicted in Figure 96(b). The control law for VSCs 2 and 3 can be written as:

$$V_{DC}^{ref} = V_{DC}^{ref\,0} + k_{V_{DC}-P}\left(P_{Inj}^{ref} - P_{Inj}\right) \qquad \textbf{Equation 36}$$

where V_{DC}^{ref} is the DC voltage reference order, and $V_{DC}^{ref\,0}$ is the DC voltage reference when there is no power deviation between the injected power P_{Inj} and its reference value P_{Inj}^{ref}. The droop coefficient $k_{V_{DC}-P}$ binds the power deviations in the MTDC grid to the DC voltage reference.

5.3.1.4 Conventional Frequency Support Methods and Dual Droop Control

Since active power injection at VSC 1 is directly related with the power balance in Grid 1 as shown by Equation 36, the converter power absorption can be used for frequency regulation [154]. A system similar to the one presented in Figure 94 but employing an LCC-HVDC link was studied in [152], where a coordinated control scheme to integrate wind and thermal generation was proposed. The coordination of wind farms and LCC-HVDC links for inertia and primary frequency response has been discussed in the literature. In [153]-[155], frequency derivative and frequency deviation measurements were used to provide inertia support and frequency control see Figure 96(a) and Figure 96(b). In order to overcome the limitations of the previous methods, a novel dual droop control scheme is proposed here [156]. This uses the system frequency deviation and the DC voltage as feedback signals. Consider that it is desired to provide frequency regulation to the wind-thermal integrated system of Grid 1 (see Figure 94). If the frequency deviation and the DC voltage act as input signals to the rectifier converter station (*i.e.* VSC 1), the following control law can be defined, see Figure 96(c):

$$P_{Conv}^{ref} = P_{Conv}^{ref\,0} + k_{DC} \cdot (V_{DC} - V_{DC}^{L})(f_0 - f)$$

Equation 37

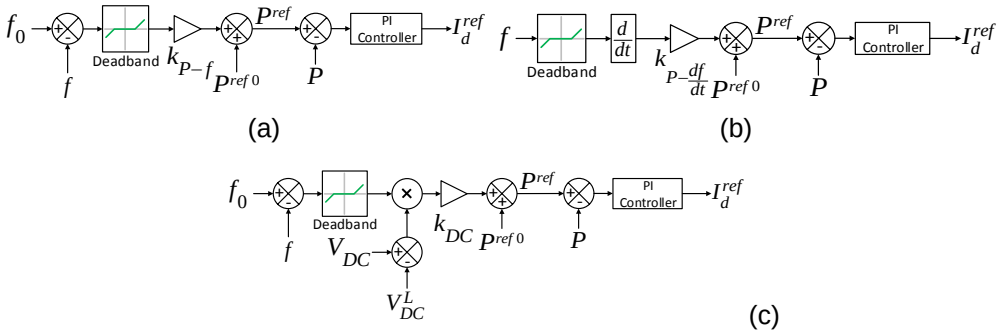

Figure 96: Active power modulation strategies in response to power imbalances: (a) frequency deviation; (b) frequency derivative; (c) dual droop.

Simulation results with the different control methods are provided in Figure 97. The frequency of Grid 1, to which VSC 2 is connected, and its injected power are shown in Figure 97(b) and Figure 97(c), respectively. The DC voltage at the terminals of VSC 1 is given in Figure 97(d). The notable benefit of the proposed control method can be observed in Figure 97(b) and Figure 97(c): as the power injected by VSC 1 responds to frequency and DC voltage deviations, the power injection is changed at significantly higher magnitudes than in all other methods. This in turn leads to a very small frequency deviation of about 0.1 Hz in Grid 1. This demonstrates that the primary frequency regulation of the integrated system has been significantly improved when the dual droop control scheme is employed. It should be highlighted that this has been achieved without considerably modulating the DC voltage: its deviation is very small (less than 0.5%) [156].

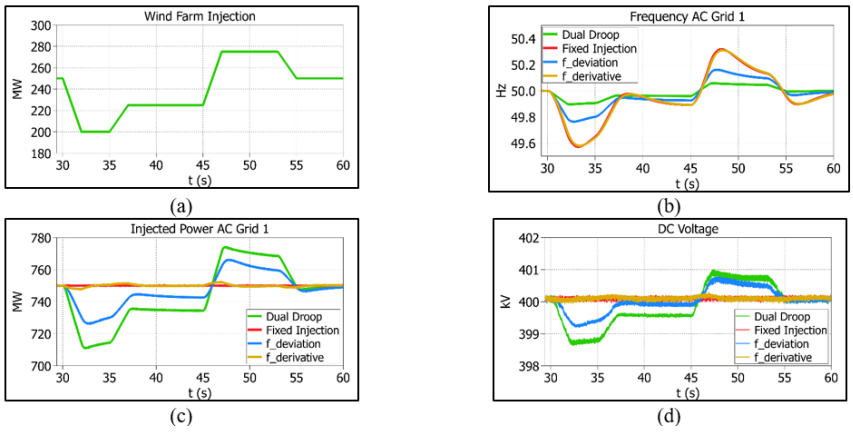

Figure 97: Simulation results of the case study. Comparison between the proposed dual droop scheme and conventional methods: (a) Wind farm power injection; (b) frequency in Grid 1; (c) VSC 1 injected power from Grid 1; (d) DC voltage at the terminals of VSC 1

5.3.1.5 Summary

A VSC-based MTDC grid is a prominent alternative to conventional HVAC transmission due to its inherent advantages of fast and independent active and reactive power control, ability to connect weak grids and seamless power flow reversal capability. Thus, this paper has proposed an effective utilisation of this technology for the further integration of wind power by providing additional frequency regulation support, generation balancing and reduction of wind power curtailment.

The stability problems caused by large-scale wind power fluctuations and primary frequency response in a wind-thermal-MTDC grid integrated system have been analysed. A novel control method, entitled dual droop control, has been proposed to mitigate these issues. The control scheme has been tested in a system resembling a future power grid in China which considers transmission reinforcements. Simulation results have shown that frequency stability issues caused by wind power fluctuations can be addressed and mitigated when the proposed method is employed. Furthermore, the DC voltage is kept within a narrow range regardless of significant power flow changes. This way, the operational performance of the wind-thermal bundled AC system can be enhanced without compromising DC grid operational constraints.

5.3.2 Asset management strategies for Power Converters in Transmission Network

5.3.2.1 Introduction

The increased deployment of power electronic converters into transmission grids has raised the need of managing these assets optimally and in an efficient way. In line with this, the existing methods for evaluating the value of AC system assets have to be redefined. To this end this work examines the business needs on which future power converter assets can be quantified. The main areas that have been covered include trends in condition monitoring, asset maintenance policies and the estimation of ageing and failure mechanisms. The use of a physics-of-failure based assessment for power converter assets life-cycle management has been introduced and discussed. Research directions and roadmaps for effective management of power electronic assets have significantly evolved. Recently, focus has been placed on the monitoring, maintenance, andageing and failure mechanisms as reported in [157]-[159] and references therein. In this context, research efforts concentrate on the development of methodologies for assessing asset condition

and estimation of the risk of failure through state of the art models, optimisation of maintenance practices, development of cost analysis modules, and investigation into decision-making practices. Following this line, power electronic assets can be mainly characterised by the following business needs (see Figure 98):

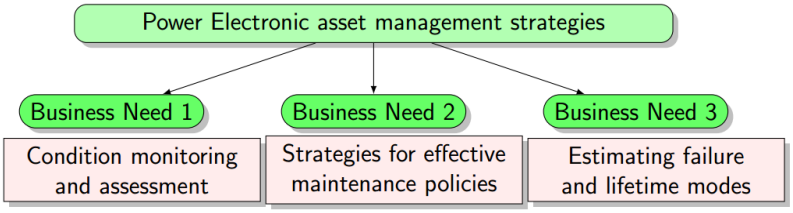

Figure 98: Business need for power electronic asset management

5.3.2.2 Condition Monitoring

The technique or process for monitoring the operating characteristics of a component or an equipment, in such a way as to predict the need for maintenance before serious deterioration or breakdown, is known as condition monitoring (CM) [161]-[162]. Current CM systems are mainly focussed on AC substations; however, the monitoring function is single and completely independent, protocols are not compatible and the interface is not unified [159]-[165]. To address these shortcomings and better satisfy the needs of monitoring levels in power electronic substations, the design and implementation of CM and decision support systems in HVdc and FACTS converter stations are required [165]. Therefore, in this section the CM and assessment approaches used in power converter based assets are categorised (see Figure 99).

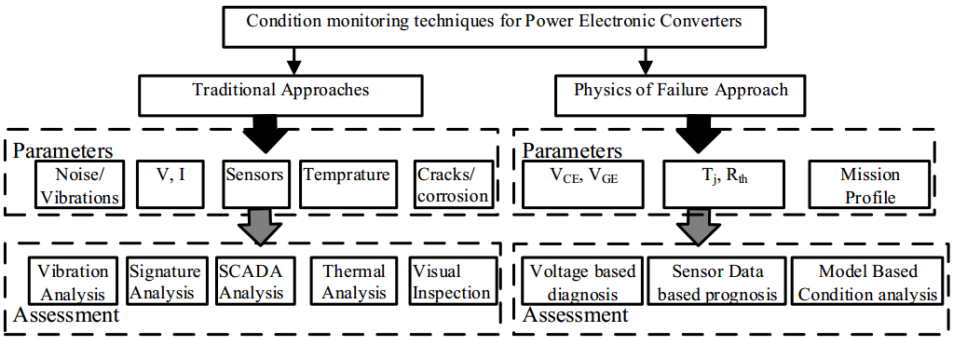

Figure 99: CM and assessment methods for power electronic assets

- **Traditional approach:** The traditional CM approach applied to combined AC and DC substation components can be divided into five main categories: visual inspection; monitoring the hot spot temperature; assessment of the vibration of wall and winding; sensor analysis for examining dissolved gases and partial discharges; and the voltage and current signature measurement. To obtain meaningful information from these monitored parameters, data should be analysed to assess the state of

the components [165]. Each CM data category can be evaluated using condition assessment (CA) techniques, as illustrated in Figure 99.

- **Physics-of-Failure Based CM:** Ensuring a high availability and reliability is the top priority for transmission network operators. To achieve this through power electronic assets, a physics-of-failure (PoF) based assessment during the design stages has been widely accepted. The combination of degradation calculation with root cause failure analyses and probabilistic methods forms the basis of PoF [24]. Surveys indicate that IGBTs have been the most frequently used devices (42%) among power semiconductors, followed by metal-oxide semiconductor field-effect transistors (MOSFETs) (27%), thyristors (14%) and PiN diodes (10%) [167].

In contrast with traditional CM approaches, PoF based CM focusses on the lifetime estimation of new generation power semiconductor devices such as IGBTs, IGCTs, MOSFETs, SiCs, among others. A threefold process is employed to monitor the strength of power electronic components; this involves diagnosis, prognosis and condition analysis.

5.3.2.3 Maintenance methodologies

One of the main driving forces behind the transition from mercury arc to thyristor valves and later onto IGBTs for power conversion in the high voltage power electronic industry was the burden on maintenance requirements [167]-[169]. However, many of the existing and new power electronic assets are equipped with CM systems along with SCADA for operation. This provision provides a platform for the development of intelligent and device dependent maintenance policies. Therefore, CM leads to the next business need: developing of a proper maintenance strategy which includes corrective, preventive, reliability and PoF centred maintenance. This is shown schematically in Figure 100. The use of PoF as the new indicator for developing maintenance policy for power electronic assets is in its early stages compared to other strategies.

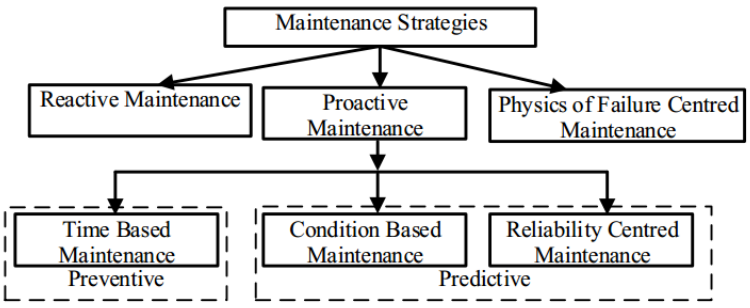

Figure 100: Maintenance strategies

5.3.2.4 Estimating Failure and Lifetime Modes

Since their appearance in the transmission regime, manufacturers have claimed an infinite lifespan of semiconductor devices as they have no moving parts and thus no wear and tear. Even CIGRE reported that *"semiconductor devices do not wear out" [171]*. Refurbishment and replacement strategies for HVdc and FACTS controllers have reached a level in which utilities and manufactures alongside are looking for options to extend their lifespan through upgrades,

renovations and extension methods [171]-[173]. The three different concepts of lifetime mechanisms for power system assets can be applied to power semiconductors as well. These are physical lifetime, technical lifetime and economic lifetime [172] and are illustrated in Figure 101.

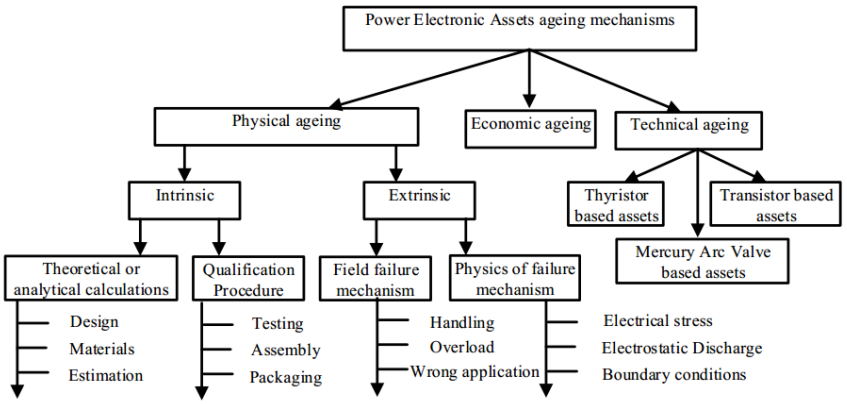

Figure 101: Classification of ageing mechanism for power semiconductor assets

5.3.2.5 Roadmap in Power Electronic Asset Management Research

While the aforementioned procedures provide a systematic way for the selection of power converter assets while considering an optimised cost, size and lifetime, their high complexity and the need for further research may restrict their application. This is highlighted in Figure 102. The review of industrial experience documented in this work, together with recent developments in power electronic assets, has allowed the identification of a range of needs and gaps faced by power transmission utilities [173]. The primary gaps have been grouped into three categories—in line with the present industry asset management needs.

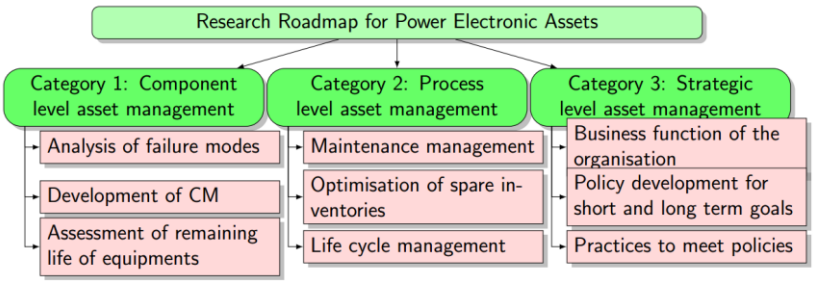

Figure 102: Research roadmaps in terms of power electronic asset management

5.3.2.6 Summary

The large-scale deployment of power converter assets into transmission networks has reached a level of parity with AC system assets. Their management and maintenance has thus become an extremely difficult job for asset managers and engineers. To tackle these difficulties, this paper has characterised power electronic assets into three business trends. In particular, the different aspects that need to be considered for the development of an effective asset management framework for HVdc and FACTS devices have been illustrated. It has been concluded that an imminent change in the

monitoring and assessment methods (ranging from traditional, reliability, or PoF-based approaches) is needed due to the inherent design of power electronic components. Moreover, the incorporation of DC substations into AC grids will pose the challenge of maintaining them in a reliable and optimal way, thus making of PoF a potential new philosophy for maintenance practice.

5.3.3 Sub-synchronous Oscillatory Stability Analysis and Control in an AC/DC Transmission system

5.3.3.1 Introduction

The rapid expansion in power transmission for the integration of large-scale renewables complemented by infrastructure reinforcements in the form of series compensation poses the threat of subsynchronous resonance (SSR) [174]-[176]. However, existing and future high-voltage direct current (HVDC) links can be effectively used to mitigate this undesirable phenomenon [174]-[176]. In this line, this chapter presents a formal analysis of torsional interactions (TI) -a form SSR in series-compensated systems featuring voltage source converter (VSC) based HVDC links. Further an auxiliary control loop embedded in the VSC-HVDC system to damp torsional interactions has been introduced [175]. The proposed damping scheme employs modal filters to identify SSR upon occurrence and then injects currents at sub-synchronous frequency to damp it. The SSR damper has been tested in the three machine GB model (see Figure 103(a)), which has been upgraded with a VSC-HVDC link to form an integrated AC/DC system [177]-[178]. Simulations have been performed in PSCAD, with eigenvalue analysis carried out in MATLAB for the small-signal stability assessment of the AC/DC system. Results show that the proposed scheme effectively damps SSR irrespectively of the torsional mode being excited.

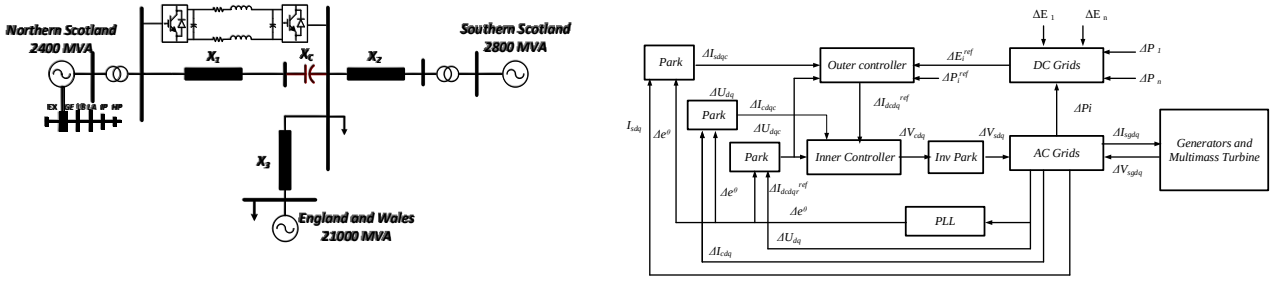

(a) Adapted three machine GB model (b) State Space model

Figure 103: Schematic of AC/DC network

5.3.3.2 Mathematical modelling of AC/VSC-HVDC Link

The test system resembles a simplified GB mainland system splitting into three major generation areas: England and Wales, Southern Scotland and Northern Scotland, with respective ratings of 21000, 2800 and 2400 MVA [178]. The Northern Scotland generator has been modelled to include a multi-mass shaft with four turbine masses. The remaining two machines were modelled as single mass turbo generators. The detailed state-space model of the system (see Figure 103(b)) includes the dynamic equations of the synchronous machines, transmission lines and the HVDC link with its controllers has been performed. This is a system of 77 differential equations linearized around an operating point, given by

$$\Delta\dot{\mathbf{X}}_{sys} = \mathbf{A}_{t,sys}\Delta\boldsymbol{X}_{sys}$$

Equation 38

$$\Delta\boldsymbol{X}_{sys} = [\boldsymbol{X}_{NSG}\ \boldsymbol{X}_{NSM\omega}\ \boldsymbol{X}_{NSM\theta}\ \boldsymbol{X}_{SSG}\ \boldsymbol{X}_{SSM}\boldsymbol{X}_{EWG}\ \boldsymbol{X}_{EWM}\boldsymbol{X}_{Tr}\ \boldsymbol{X}_{VSC}\ ]$$

Equation 39

Where $\mathbf{X}_{NSG}, \mathbf{X}_{NSM\omega}, \mathbf{X}_{NSM\theta}$, constitute the states associated with the Northern Scotland synchronous generator; $\mathbf{X}_{Tr}$ the series compensated transmission line; $\mathbf{X}_{SSG}$, $\mathbf{X}_{SSM}$, $\mathbf{X}_{EWG}$, $\mathbf{X}_{EWM}$ the Southern Scotland and England and Wales generators; and $\mathbf{X}_{VSC}$ the VSC-HVDC link. The real part of relevant eigenvalues (TM*x*) and their relation with the subsynchronous mode of the AC transmission line (SUB) are plotted in Figure 104. As it can be seen, mode SUB changes with the percentage of series compensation. It can be observed that the system features four critical conditions arsing when SUB is in the neighborhood of TM1-TM4. For specific values of series compensation, the interaction with specific modes is maximum –coincidental with the frequencies of TM1-TM4. Figure 104 also shows the behaviour of modes TM*x* and SUB. It is worth noting that the dynamics of the VSC-HVDC link do not contribute any negative damping; instead it provides a positive effect, as discussed in [174]-[178].

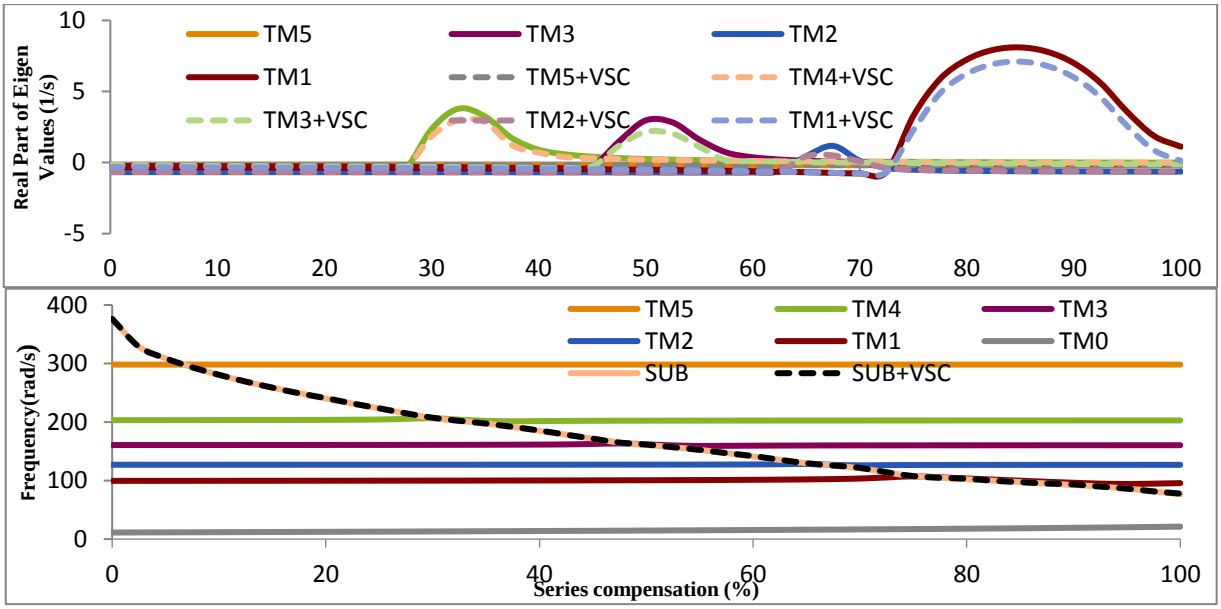

Figure 104: Stability of the TMs in terms of series compensation level

5.3.3.3 Control of Multi-Modal SSR Damping in an AC/DC system

In addition to the provision of bulk power transfer, an auxiliary control loop embedded in the VSC rectifier station has been designed to damp SSR. The SSR controller is a real-time system that injects subsynchronous currents at the point of connection to the AC system (in this case, near the stator terminals of the synchronous generator) to mitigate SSR upon occurrence. The structure of the SSR damping loop is shown in Figure 105 [174]. As it can be seen, the line current of the network is used as the input signal, which after an adequate conditioning is transformed into a *dq* frame reference. The resulting current is filtered through low & high-pass filters to eliminate DC, supersynchronous (>50 Hz) and low frequency components (<10 Hz). This process isolates subsynchronous components of interest only. The filtered signals then follow separate paths (in this case four), each of which targets different subsynchronous modes along the frequency range of interest and comprises an additional band-pass modal filter, a gain, and a phase-shifter. The outputs are then summed to form the SSR damping signal, which is injected in anti-phase (i.e., with a 180 degree phase shift) to the inner control loops of the VSCs. The idea and effectiveness of targeted filters to damp subsynchronous components has been recently studied and implemented as in [179]-[181].

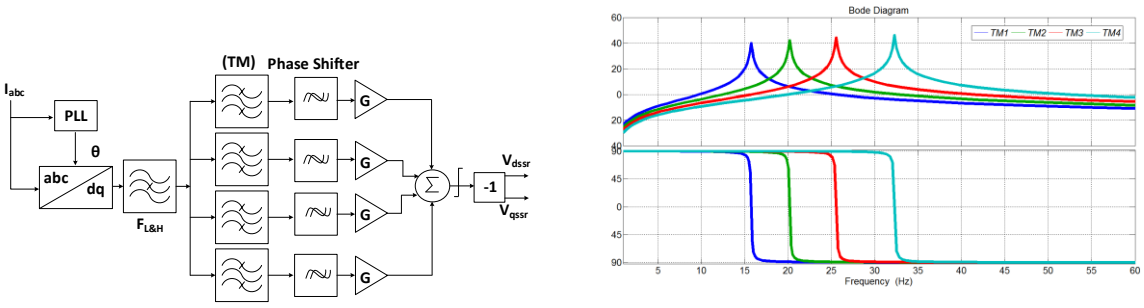

(a

Proposed injection method using modal filters

Frequency response of band-pass filters

Figure 105: Controller and its response

To validate the results from the eigenvalue analysis and subsequent design of the SSR damping filter, time domain simulations of the system have been carried out in PSCAD/EMTDC. These have been performed with and without the SSR damping controller being active. Relevant results are plotted in Figure 106. The simulation starts in steady state with 20% series compensation. This condition does not produce SSR, as evidenced by Figure 105. At 2 s the value of series compensation is modified to 40%.

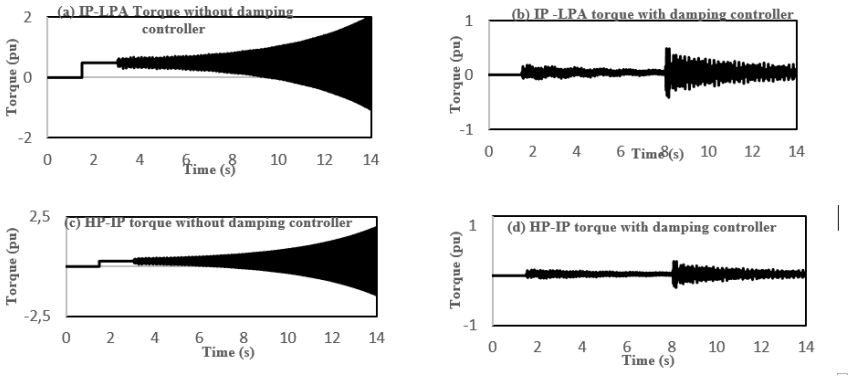

Figure 106: Simulation results featuring test system with and without damping controller

5.3.3.4 Hardware in the Loop Damping of SSR in an AC/DC Network

This SSR damping is tested in an experimental rig. The experiment considers an AC grid connected through a HVDC link in parallel as shown in Figure 103(a). VSC based converters for the sole purpose of damping SSR has been discussed and implemented in [39-41]. To take this research beyond the state of art we tested parallel AC/DC operation with SSR damping provision. In [35] a similar experiment is presented for a three terminal system using the same experimental rig, but the test was focus on the operation of converter as STATCOM, with damping provided for only one mode. Figure 107, shows the general diagram of the hardware-in-the-loop (HIL) set-up. The main components are: VSC test rig, DC Network cabinet, real time simulator and grid simulator. These components represents the scaled-down elements of a real system. The real time simulator represents a model of the three machine AC system with turbine generators and series compensated transmission line, which is interfaced to the VSC test rig with a grid simulator. The main objective of performing the HIL is to evaluate the risk of SSR in an AC/DC network without risking the real generators and converters.

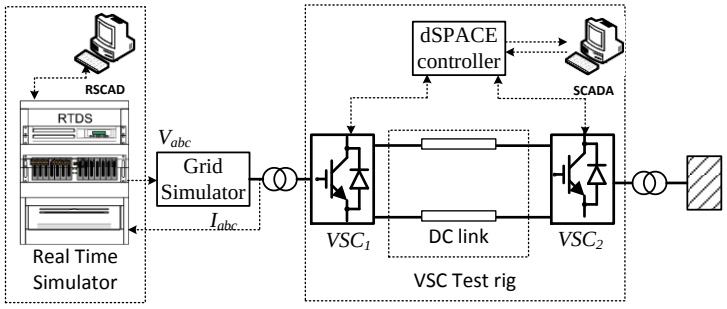

Figure 107: General diagram of the Hardware in the Loop (HIL) set-up

5.3.3.5 Experimental Results

To evaluate the flexibility of VSC HVdc links in providing SSR damping, the generic diagram shown in Figure 107 has been tested and the key results are discussed here. Figure 108 shows the air gap torques responses with and without damping controller compared in simulation and real time platform. Case-1, as in Figure 108(a) series compensation is modified from 20 % to 40% at 2s without proposed controller, as depicted the torque oscillations grows in magnitude indicating TI as tested in previous sections. In case 2 series compensation is modified from 20 % to 40% at 2s and from 40 % to 60 % at 5s with damping controller (see Figure 108(b)). As

compared to case 1 the reduction in the torque oscillations are evident with the controller in operation and the oscillations dies out in seconds.

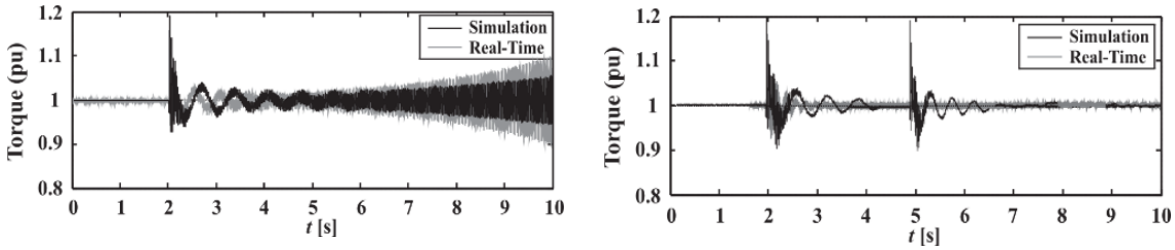

(a) Airgap torque without controller

(b) Airgap torque with controller

Figure 108: Experimental Results

5.3.3.6 Summary

A method for extracting subsynchronous components of the current flowing in a transmission line at different series compensation levels has been presented in this chapter. This has been embedded in a VSC-HVDC station as an auxiliary control loop to damp SSR upon occurrence. As it has been shown, if the torsional modes of the shaft of a synchronous generator are known, the design of the proposed damping scheme can be easily carried out. This can be extended to any transmission topology. The effectiveness of the scheme has been assessed in the three machine GB model, which has been upgraded with a point-to-point VSC-HVDC link. This AC-DC system has been assessed through eigenvalue analysis following the state-space modelling of the system. The test system, together with the SSR damping controller, have been implemented in PSCAD/EMTDC to perform time domain simulations. The eigenvalue analysis and the results obtained through simulations agree on well. More importantly, the SSR damping controller proposed in this work is effective for a broad series compensation range. Experimental validation of the proposed method is also presented in order to evaluate the real time operation of the AC/DC grid while providing SSR control. The HIL tests presented here can act as a frame work for future testing of different control of AC/DC grids, thee by reducing the risk on the real network components.

5.3.4 References

[142] L. Jiang, et al., “Wind Energy in China”, IEEE Power and Energy Magazine, 9, pp. 36-46, (2011).

[143] L. Yao, “Large Wind Power Outage & Defense Strategies. Workshop on Large Disturbances August”, CIGRE Session, Paris, (2012).

[144] W. Pei, et al., “Temporal-spatial analysis and improvement measures of Chinese power system for wind power curtailment problem”, Renewable and Sustainable Energy Reviews, 49, pp. 148-168, (2015).

[145] L. Xu, L. Yao, and C. Sasse, “Grid Integration of Large DFIG-Based Wind Farms Using VSC Transmission”, IEEE Transactions on Power Systems, 22, pp. 976-984, (2007).

[146] S. Lauria, S. Maddalena, P. Francesco and M. Marco, “Very long distance connection of gigawatt-size

offshore wind farms: extra high-voltage AC versus high-voltage DC cost comparison", IET Renewable Power Generation, 10, pp. 713-720, (2016).

[147] J. Liang, T. Jing, O. Gomis-Bellmunt, J. Ekanayake and N. Jenkins, "Operation and Control of Multiterminal HVDC Transmission for Offshore Wind Farms", IEEE Transactions on Power Delivery, 26, pp. 2596–2604, (2011).

[148] K. Xie, J. Dong, H. M. Tai, B. Hu and H. He, "Optimal planning of HVDC-based bundled wind–thermal generation and transmission system", Energy Conversion and Management, 115, pp. 71–79, (2016).

[149] C. Luo and B. T. Ooi, "Frequency Deviation of Thermal Power Plants Due to Wind Farms", IEEE Transactions on Energy Conversion, 21, pp. 708-716, (2006).

[150] W. X. Lin, et al., "A Three–Terminal HVDC System to Bundle Wind Farms With Conventional Power Plants", IEEE Transactions on Power Systems, 28, pp. 2292–3000, (2013).

[151] [X Zhao, S. Zhang, R. Yang and M. Wang, "Constraints on the effective utilization of wind power in China: An illustration from the northeast China grid", Renewable and Sustainable Energy Reviews, 16, pp. 4508-4514, (2012).

[152] P. Kundur, Power System Stability and Control. New York, NY, USA: McGraw-Hill, (1994).

[153] Z. Miao, L. Fan, D. Osborn and S. Yuvarajan, "Wind Farms With HVDC Delivery in Inertial Response and Primary Frequency Control", IEEE Transactions on Energy Conversion , 25, pp. 1171–1177, (2010).

[154] H. Yin, L. Fan and Z. Miao, "Fast Power Routing Through HVDC", IEEE Transactions on Power Delivery, 27, pp. 1432-1441, (2012).

[155] H. Liu and Z. Chen, "Contribution of VSC-HVDC to Frequency Regulation of Power Systems With Offshore Wind Generation", IEEE Transactions on Energy Conversion, 30, pp. 918-926, (2015).

[156] T Joseph, J. Goncalves, C. E. Ugalde-Loo and J. Liang "Wind-Thermal Generation Coordination in Multi-Terminal HVDC Connected AC Systems for Improved Frequency Support", in IET AC/DC 2017.

[157] W. Qiao et al., Condition Monitoring, Diagnosis, Prognosis, and Health Management for Wind Energy Conversion Systems, IEEE Trans. Ind. Electron. 62 (10) (2015) 6533-6535.

[158] S. Bahramirad et al., Guest Editorial: Special Section on Asset Management in Smart Grid, IEEE Trans. Smart Grid. 6 (2) (2015) 953-954.

[159] F. Blaabjerg et al., Special Issue on Robust Design and Reliability of Power Electronics, IEEE Trans.

[160] Power Electron. 30 (5) (2015) 2373-2374

[161] Asset management of transmission systems and associated CIGRE activities, CIGRE Technical Brochure 309 (2006).

[162] Y. Han et al., Condition monitoring techniques for electrical equipment-A literature survey, IEEE Trans. Power Del. 18 (1) (2003) 4-13.

[163] J. L. Velasquez-Contreras et al., General asset management model in the context of an electric utility: Application to power transformers, Electr. Power Syst. Res. 81 (11) (2011) 2015-2037.

[164] A. E. B. Abu-Elanien et al., Asset management techniques for transformer, Electr. Power Syst. Res.

80 (1) (2010) 456-464

[165] N. M. Kirby et al., Optimizing the availability of HVDC systems via effective Asset Management, CIGRE Canada Conference (2015)

[166] E. E. Kostandyan et al., Physics of failure as a basis for solder elements reliability assessment in wind turbines, Rel Eng. Syst. Safety. 108 (2012) 100-107

[167] S. Yang et al., An industry-based survey of reliability in power electronic converters, IEEE Trans. Ind. Appl. 47 (3) (2011) 1441-1451.

[168] W. Litzenberger et al., When It's Time to Upgrade: HVdc and FACTS Renovation in the Western Power System, IEEE Power Energy Mag. 14 (2) (2016) 32-41.

[169] H. Bilodeau et al., Making Old New Again: HVdc and FACTS in the North eastern United States and Canada, IEEE Power Energy Mag. 14 (2) (2016) 42-56

[170] N. M. Kirby et al., Extending Their Lifetimes : Keeping HVdc and FACTS Installations in Service Longer, IEEE Power Energy Mag. 14 (2) (2016) 57-65

[171] Semiconductor Power Devices for use in HVDC and FACTS Controllers, CIGRE Technical Brochure 112 Working Group 14.17, (DC Links and Power Electronic Equipment, (1997).

[172] W. Li et al., Power system equipment ageing, IEEE Power Energy Mag. 4 (3) (2006) 52-58.

[173] T. Joseph et al., Asset management strategies for power electronic converters in transmission networks: Application to HVdc and FACTS devices, Electr. Power Syst. Res. (Under Review)

[174] T. Joseph, C. E. Ugalde-Loo, J. Liang and P. Coventry, "Active filtering based current injection method for multi modal SSR damping in an AC/DC system," Power Electronics and Applications (EPE'15 ECCE-Europe), 2015 17th European Conference on, Geneva, 2015, pp. 1-10.

[175] T. Joseph, C. E. Ugalde-Loo and J. Liang, "Subsynchronous oscillatory stability analysis of an AC/DC transmission system," 2015 IEEE Eindhoven PowerTech, Eindhoven, 2015, pp. 1-6.

[176] Zhang, Jian, et al. "Suppressing intermittent subsynchronous oscillation via subsynchronous modulation of reactive current." IEEE Transactions on Power Delivery 30.5 (2015): 2321-2330.

[177] L. Livermore, et al, "Damping of subsynchronous resonance using a voltage source converter-based high-voltage direct-current link in a series-compensated Great Britain transmission network," Generation, Transmission & Distribution, IET , vol.8, no.3, pp.542,551, January 2014

[178] C.E. Ugalde-Loo, J.B. Ekanayake, N. Jenkins, "Subsynchronous resonance on series compensated transmission lines with quadrature boosters", IEEE PowerTech Trondheim, pp. 1 – 7, 2011.

[179] L. Wang, et al "Mitigation of Multimodal Subsynchronous Resonance Via Controlled Injection of Supersynchronous and Subsynchronous Currents," IEEE Trans. Power Syst., vol. 29, no. 3, pp. 1335–1344, 2014.

[180] Xie, Xiaorong, Liang Wang, and Yingduo Han. "Combined Application of SEDC and GTSDC for SSR Mitigation and Its Field Tests." IEEE Transactions on Power Systems 31.1 (2016): 769-776.

[181] Xie, Xiaorong, et al. "Development and field experiments of a generator terminal subsynchronous damper." IEEE Transactions on Power Electronics29.4 (2014): 1693-1701.

[182] A. K. Mohammad, and Y A I. Mohamed. "A Simple Approach to Damp SSR in Series-Compensated Systems via Reshaping the Output Admittance of a Nearby VSC-Based System." IEEE Transactions on Industrial Electronics 62.5 (2015): 2673-2682.

[183] A. K. Mohammad, Y A I. Mohamed and Wilsun Xu. "Active mitigation of subsynchronous interactions between PWM voltage-source converters and power networks." IEEE Transactions on Power Electronics 29.1 (2014): 121-134.

5.4 Analysis and protection of HVDC systems subject to AC and DC faults– Gen Li

5.4.1 Introduction

The voltage source converter-based (VSC) high voltage direct current (HVDC) technology has experienced a great development over the last decade due to the following features: 1) compact and flexible station layouts, with low space requirements, and a scalable system design; 2) a high dynamic performance and stable operation with AC networks; 3) supply of passive networks and black-start capability; 4) an independent control of active and reactive power; and 5) STATCOM features [184]-[188].

In a VSC multi-terminal high voltage direct current (MTDC) grid, the resistances dominate the impedances of the DC transmission system. The inductances tend to have a small impact on the propagation of a DC fault. This means that all parts of an MTDC grid will be affected if a DC fault cannot be isolated quickly. Additionally, an AC side connected system will feed currents to the fault through anti-parallel diodes, which can be seen as a three-phase fault on the AC side of a converter. Therefore, a DC fault can be seen as “multi-point” AC faults on its connected AC system.

DC circuit breakers (DCCBs), AC circuit breakers (ACCBs) and Full-Bridge Modular Multi-Level Converters (FB-MMCs) can be used to block DC fault current in VSC MTDC grids. However, the DC fault transient characteristics of AC/DC networks will be different depending on the type of devices used to protect the DC grid.

In this project, the DC fault clearance and post-fault restoration processes using DCCBs and ACCBs are analysed. The transient responses of the AC/DC system during DC faults are also assessed considering the analysed approaches. The studies are conducted in PSCAD/EMTDC, where an integrated AC/DC transmission system has been modelled. Simulation results indicate that a different transient behaviour arises when different fault isolation and post-fault restoration schemes are employed. The work of this project provides an understanding of the dynamic behaviour in AC/DC systems, in turn contributing to a deeper comprehension of system operation and control system design.

The transient characteristics of an AC/DC network using DCCBs to isolate a DC fault are studied. The influence of different operating times and sizes of DC reactors are considered. For completeness, the power angle and AC voltage stability of the AC connected systems are examined. The input impedance of the VSC is defined to analyse the “multi-point” faults. In addition to providing a further understanding on the dynamic behaviour of AC/DC systems during DC fault conditions, the studies in this paper show that an increase in the operating speed of the DCCBs provides better results to mitigate the impacts of “multi-point” faults than by increasing the size of the DC reactor. A balance between these two aspects may contribute to the risk-managed deployment of DCCBs –which is essential to design effective protection strategies for combined AC/DC systems.

5.4.2 Methodology and system modelling

5.4.2.1 Methodology

If a short-circuit occurs in an AC system, the voltage will drop and current will increase at the fault location. The impedance at this point will decrease near to zero. However, other places in the AC system far from the fault may not be affected by this impedance change. The distance protection method is based on this principle, which considers the ratio of measured voltages to measured currents [189].

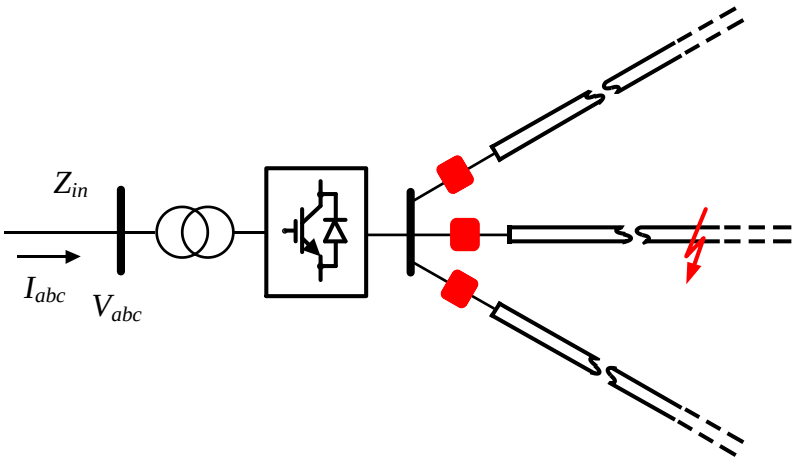

Figure 109: Measurements of the input impedance of a VSC

In order to show that a DC fault in an MTDC grid can be seen as “multi-point” faults by its connected AC system, the concept of impedance measurement is borrowed from distance relaying in AC systems. The input impedance of a VSC during a DC fault is defined as the equivalent impedance as seen from the AC side of a converter into the DC system.

The concept of input impedance (Z_{in}) is illustrated in Figure 109 As it can be seen, currents and voltages are measured at the AC side of a converter. Equation 40 and Equation 42 are used to calculate the magnitude of Z_{in} :

$$V_{rms} = \sqrt{\frac{V_a^2 + V_b^2 + V_c^2}{3}}$$

Equation 40

$$I_{rms} = \sqrt{\frac{I_a^2 + I_b^2 + I_c^2}{3}}$$

Equation 41

$$Z_{in} = \frac{V_{rms}}{I_{rms}}$$

Equation 42

The input impedance can be used to describe the electrical distances within an MTDC grid during a DC fault. If the value of Zin of different converters drops to a similar value, this implies that the DC fault is equivalent to “multi-point” faults from the viewpoint of the connected AC system.

The studies presented focus on the impact that DC faults have on AC system stability. To achieve this, the phase angles of synchronous generators and AC bus voltages in the AC system are used. Different DCCB operating times and values of the DC reactor will be examined to investigate the effect on the value of Zin.

Fault isolation and post-fault restoration schemes using DCCBs (both through the fully selective and the “Open Grid” approaches) and ACCBs are analysed.

5.4.2.2 Test System Modelling

An integrated AC/DC power transmission system, shown in Figure 110, has been developed in PSCAD/EMTDC. The system consists of the four-machine two-area AC system reported in [189] which has been upgraded to include a four-terminal meshed HVDC grid.

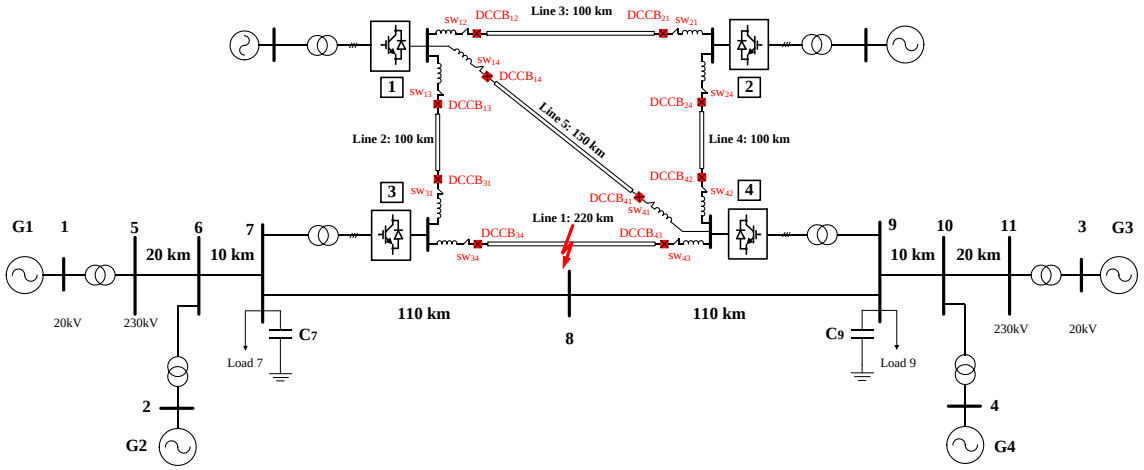

Figure 110: Integrated AC/DC transmission test system with DCCBs

The MTDC grid can represent offshore DC systems connecting offshore wind farms to onshore AC grids. Every DC cable has a DCCB at each end. Converters 1 and 2 are connected to equivalent AC systems (which are not of special interest in this investigation). Converters 3 and 4 are connected to buses 7 and 9 of the AC system. Each synchronous generator is modelled together with an exciter, a turbine and a governor. The converters are two-level VSCs with a symmetrical monopole configuration.

Although half-bridge MMCs are now widely adopted, a two-level VSC has a very similar DC fault behaviour [190]. As it will provide a reasonably similar impact on the connected AC systems it is thus adopted in this work. The parameters of the DC grid are given in Table I. The data for HVDC cables has been taken from [191]. The cable lengths are indicated in Figure 110.

The IGBTs from the converters cannot withstand large fault currents; therefore, the converter internal protection systems will block the IGBTs to prevent damage.

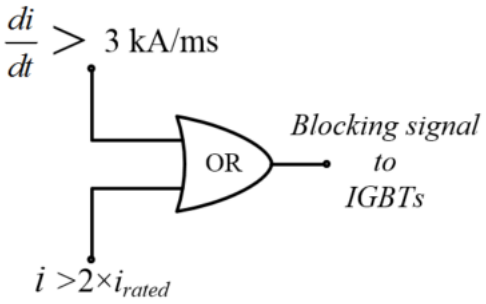

Figure 111: **Logic of converter local protection**

The converter local protection is based on an overcurrent and rate-of-rise of current criterion. Once the rate-of-rise of the current flowing through the converter is higher than 3 kA/ms or if the current exceeds twice the value of rated DC current, tripping signals will be sent to block the IGBTs. The converter local protection logic is shown in Figure 111.

5.4.3 Simulation results and analysis

5.4.3.1 Influence of DCCB operating times

Simulations are performed to assess the effect of different DCCB operating times, with results shown in Figure 112 DCCB34 and DCCB43 trip at 5, 20 and 60 ms. As it can be seen, a decrease in the operating times enables a faster system recovery to steady state. When the DCCBs operate 60 ms after the fault (for instance, due to a long decision making algorithm time or to the use of mechanical DCCBs), the phase angle between synchronous generators 1 and 3 experiences large oscillations, which means that the AC system is severely impacted.

It can be observed that the AC voltages of both buses are affected at almost the same time. When the DCCBs trip 5 ms after the fault, the system will recover to steady state, leading to a voltage increase in bus 7 and a voltage decrease in bus 9.

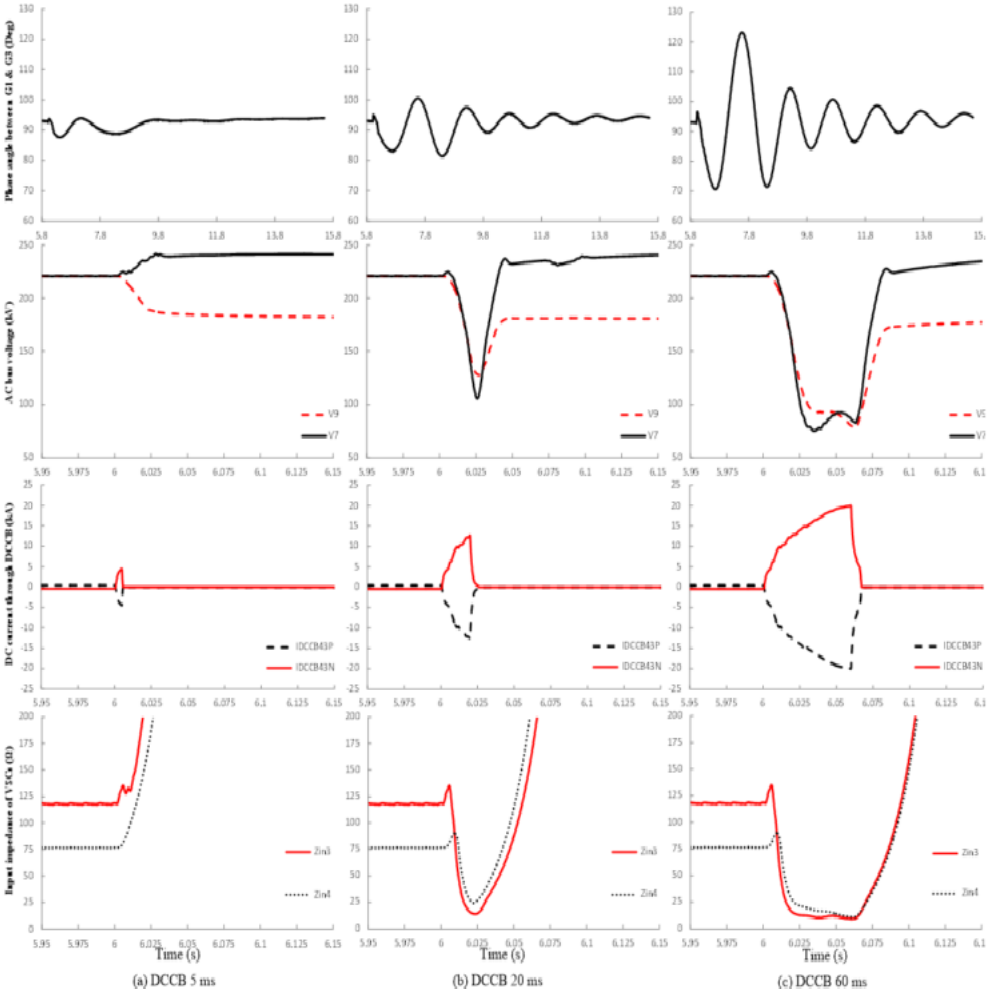

Figure 112: System responses during a DC fault with different DCCBs operating time

If the DC fault is not isolated quickly, the DC voltage will continue to drop and AC currents will start to feed into the DC side once the DC voltage is lower than the AC line-to-line voltages. Following this, AC voltages will drop considerably.

As it can be seen in Figure 112(c), the DC fault current increases to more than 20 kA when a 60 ms operating time is employed. This value goes beyond the current interrupting capabilities of any available DCCB. In practical applications, a DC reactor would be used to limit the rate-of-rise of fault current so that the DCCBs can interrupt the fault within its rated current.

Figure 112 also shows the input impedance Z_{in} of converters 3 and 4. During normal operation, Z_{in3} and Z_{in4} have different values since each converter has different set points. However, both drop quickly and reach a similar value if the DC fault is not isolated fast enough. As discussed previously, this implies that the fault in the MTDC grid could be interpreted as “multi-point” faults in the adjacent AC system. In this case, the stability of the overall system may have been compromised. It should be highlighted that the input impedances cannot become zero due to the impedance contribution of the AC transformer, AC and DC reactors and DC cables.

5.4.3.2 Influence of DC protection approaches

Case 1 – Fully Selective Approach

When the fully selective scheme is used, 5 ms are considered for fault detection, discrimination and location. It is assumed that operating time of the DCCB is 5 ms.

Simulation results are shown in Figure 113(a). $DCCB_{34}$ and $DCCB_{43}$ trip 10 ms after the fault. Within this time the DC fault current flowing through $DCCB_{34}$ rises to about 10 kA. The converter terminal voltages drop to around 100 kV. The DC voltages start to recover as long as the converters are de-blocked.

The voltages of both AC buses 7 and 9 are impacted by the fault at almost the same time. The reason for this behavior is that unlike their AC counterparts, MTDC grids are “low-inertia” systems and thus the DC voltage drop propagates very quickly within the MTDC grid once a DC fault occurs. The AC system will be affected multiple times through the AC/DC connecting points. From the viewpoint of AC systems, a DC fault within the DC grid can be seen as “multiple faults”.

The power angle difference between generators 1 and 3 reaches steady state following some oscillations. Although the faulted DC line is isolated, the power in this line shifts to other routes within the DC grid. The converter is capable of operating at the pre-fault power. For this reason, the power transferred in the AC corridor recovers to the original value after the fault.

Case 2 – ‘Open Grid’ Approach

In this case, the “Open Grid” method is utilized. The DCCBs will be tripped depending on the local measurements without fault discrimination and location. A DCCB will be tripped if the current flowing through it is higher than 5 kA or if the DC voltage is lower than 80% of the DC voltage reference. A time of 5 ms has been considered for the DCCB to measure the residual voltages and currents of the remaining circuits in order to detect the fault location. The converter local protection algorithm is similar to that of the last section.

In this case, only converters 3 and 4 are blocked. $DCCB_{31}$, $DCCB_{42}$ and $DCCB_{41}$, which are connected to the same DC busbar of $DCCB_{34}$ and $DCCB_{43}$, are also tripped. After 5 ms these DCCBs reclose base on post-fault signals. This occurs since only the DCCBs “seeing” the fault operate immediately when their fault detection criteria is satisfied. The faulted line is isolated rapidly so that the voltage collapse (which drops to about 240 kV) stops quickly. This in turn prevents converters 1 and 2 from seeing the fault. Figure 113(b) shows that the current flowing through $DCCB_{34}$ is interrupted at 5 kA. In other words, $DCCB_{34}$ is tripped due to the overcurrent criteria.

Due to the short fault isolation and post-fault restoration times, the host AC system is impacted less severely than when the fully selective approach is employed. The overall system can restore to a satisfactory steady state faster.

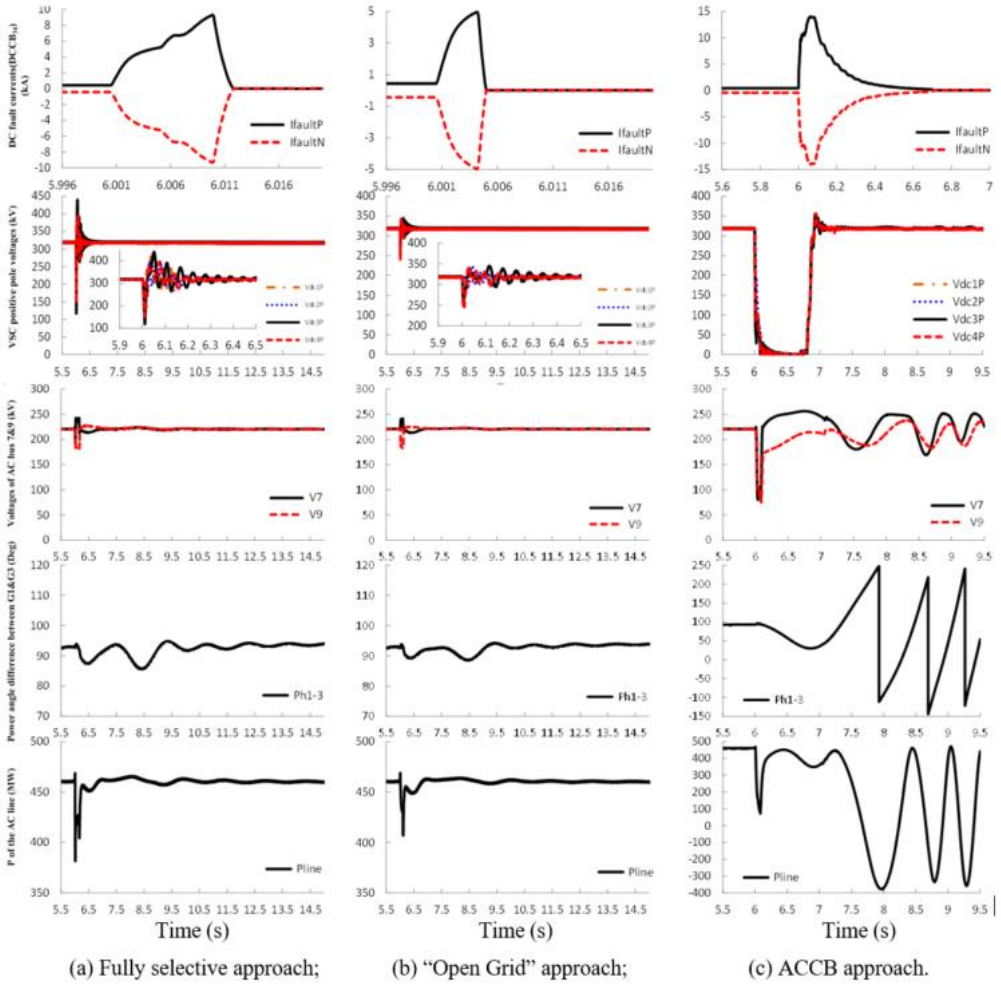

Figure 113: Simulation results for the fault at the middle of line 3

Case 3 - ACCBs

Figure 113(c) shows the transient response of the test AC/DC system when ACCBs are used as fault isolation and post-fault restoration devices.

The converters are blocked firstly by the converter local protection. A waiting time of 80 ms is used to simulate the operating time of ACCBs. The entire DC grid starts to de-energize and the fault discrimination and location completes during this period. Therefore, the DC fault current increases to about 15 kA. This large fault current is in-fed from the AC side of the VSC, which draws a large amount of reactive power. Thus, AC voltage drop at buses 7 and 9 is much larger than in the previous cases. As previously pointed out, from its viewpoint the AC system suffers "two faults" at buses 7 and 9. Moreover, the fault isolation and post-fault restoration time

would not be acceptable for the AC system and therefore becomes unstable. As it can be observed, the power angle of the generators oscillates and the power transferred in the AC corridor experiences large unwanted oscillations.

5.4.4 Summary

In an MTDC grid, a DC fault will propagate to all converters quickly due to the small impedance of the transmission circuits. If a DC fault occurs within an MTDC grid which is connecting to an AC system with multiple converters, all the AC sides of converters will sense this fault. Therefore, a DC fault within an MTDC grid can be seen as “multi-point” faults on its connected AC system.

In this project, the impacts of DCCB and DC grid protection on AC/DC system stability subjects to DC faults are analysed and assessed. The input impedance of VSC is defined to analyse the influence of a DC fault on the stability of AC system.

The studies show that the impacts of a DC fault on the stability of AC system are nearly the same regardless of the fault locations within the DC grid. The magnitudes of the input impedances at VSCs in AC/DC systems move towards a similar value if the DC fault cannot be isolated quickly. This indicates that a DC fault produces multiple impacts on its connected AC system which can be seen as “multi-point” faults on its connected AC system. As a consequence, voltage and power angle stability of the system will be reduced.

The dynamic interactions between a DC grid and an AC system during DC faults are analysed and assessed when the DCCBs and ACCBs are employed. In a DC grid using DCCBs to provide fast clearance of a DC fault, two main solutions appear possible. One is the fully selective approach to apply the same protection philosophy and principles used in AC systems. The second is the “Open Grid” concept. Both of the two approaches can reduce the impacts on the stability of the AC/DC systems. An increase in the size of the DC reactor to mitigate “multi-point” faults provides limited benefits compared to enhancing operating speeds of the DCCBs.

The use of ACCBs will lead to the de-energization of the entire DC grid. The long fault isolation and restoration time can lead to the instability of integrated AC

5.4.5 References

[184] J. Liang, T. J. Jing, O. Gomis, J.B. Ekanayake, N. Jenkins, “Operation and Control of Multiterminal HVDC Transmission for Offshore Wind Farms,” IEEE Transactions on Power Delivery, vol. 26, no.4, pp. 2596-2604, Oct. 2011.

[185] X. Hu, J. Liang, D. J. Rogers and Y. Li, “Power Flow and Power Reduction Control Using Variable Frequency of Offshore AC Grids,” IEEE Transactions on Power Systems, vol. 28, no. 4, pp. 3897-3905, Nov. 2013.

[186] D. van Hertem, O. Gomis, J. Liang, HVDC Grids: For Offshore and Supergrid of the Future, Wiley-IEEE Press, 2016.

[187] S. Debnath, J. Qin, B. Bahrani, M. Saeedifard and P. Barbosa, "Operation, Control, and Applications of the Modular Multilevel Converter: A Review," IEEE Transactions on Power Electronics, vol. 30, no. 1, pp. 37-53, Jan. 2015.

[188] J. Liang, O. Gomis-Bellmunt, J. Ekanayake and N. Jenkins, "Control of multi-terminal VSC-HVDC transmission for offshore wind power," in 13th European Conference on Power Electronics and Applications EPE '09, Barcelona, Spain, 2009, pp. 1-10.

[189] P. Kundur, Power System Stability and Control, EPRI Power System Engineering Series. New York: McGraw-Hill, 1994, p.904.

[190] M. Hajian, L. Zhang and D. Jovcic, "DC Transmission Grid With Low-Speed Protection Using Mechanical DC Circuit Breakers," in IEEE Transactions on Power Delivery, vol. 30, no. 3, pp. 1383-1391, June 2015.

[191] M. K. Bucher and C. M. Franck, “Contribution of Fault Current Sources in Multiterminal HVDC Cable Networks,” IEEE Transactions on Power Delivery, vol. 28, no. 3, pp. 1796-1803, July 2013.

DTU Wind Energy is a department of the Technical University of Denmark with a unique integration of research, education, innovation and public/private sector consulting in the field of wind energy. Our activities develop new opportunities and technology for the global and Danish exploitation of wind energy. Research focuses on key technical-scientific fields, which are central for the development, innovation and use of wind energy and provides the basis for advanced education at the education.

We have more than 240 staff members of which approximately 60 are PhD students. Research is conducted within nine research programmes organized into three main topics: Wind energy systems, Wind turbine technology and Basics for wind energy.

Technical University of Denmark
Department of Wind Energy
Frederiksborgvej 399
Building 118
4000 Roskilde
Denmark
Telephone 46 77 50 85

info@vindenergi.dtu.dk
www.vindenergi.dtu.dk